

Differential glycomics of epithelial membrane glycoproteins
from urinary exovesicles reveals shifts towards complex-type
N-glycosylation in classical galactosemia

Inaugural-Dissertation
zur
Erlangung des Doktorgrades
der Mathematisch-Naturwissenschaftlichen Fakultät
der Universität zu Köln

vorgelegt von
Simon Staubach
aus Bergisch Gladbach

Differential glycomics of epithelial membrane glycoproteins
from urinary exovesicles reveals shifts towards complex-type
N-glycosylation in classical galactosemia

Inaugural-Dissertation
zur
Erlangung des Doktorgrades
der Mathematisch-Naturwissenschaftlichen Fakultät
der Universität zu Köln



vorgelegt von
Simon Staubach
aus Bergisch Gladbach

Berichterstatter: Prof. Dr. Franz-Georg Hanisch
(Gutachter)

Prof. Dr. Marcel Bucher

Tag der mündlichen Prüfung: 14. Mai 2012

The present research work was carried out under the

supervision and the direction of

Prof. Dr. Franz-Georg Hanisch

Institute of Biochemistry II

Medical Faculty, University of Cologne

Cologne, Germany,

February 1st, 2009 to Mai 14th, 2012

The second supervisor was

Prof. Dr. Marcel Bucher

1. Directory

1. Directory	4
1.2 Tables of figures	6
1.2.1 Table of figures	6
1.2.2 Table of supplements	7
1.2.3 Table of Excel-Tabs	7
1.3 Abbreviation.....	8
1.4 Synopsis	10
2. Introduction	12
2.1.1 Galactose-1-phosphate uridylyltransferase (GALT)	12
2.1.1.1 GALT 3D structure	12
2.1.1.2 The GALT mutation Q188R	13
2.1.1.3 Ping-Pong double displacement reaction of GALT	13
2.1.2 Galactose and the Leloir pathway	14
2.1.3 Dysglycosylation of secreted glycoproteins in classical galactosemia	16
2.1.4 Clinical picture of classical galactosemia	16
2.1.5 Exosomes	17
2.1.5.1 Characteristics of exosomes	17
2.1.5.2 Epithelial origin of exosomes.....	18
2.1.5.3 Exosomes are enriched in subpopulations of lipid rafts.....	18
2.1.6 Lipid rafts	19
2.1.6.1 Lipid raft endocytosis.....	19
2.1.6.2 Glycoprotein trafficking via multivesicular bodies (MVB's) to exosomes	20
2.1.7 The Tamm-Horsfall glycoprotein (THP)	21
2.1.8 N-glycan processing	22
2.1.9 Reabsorption of proteins in the kidney	23
2.1.9.1 Megalin cubilin receptor complex.....	23
2.2 The aims of the study	25
3. Materials & Methods	25
3.1 Materials.....	25
3.1.1 Samples from GALT deficient patients	25
3.1.2 SDS-Polyacrylamide-gel electrophoresis buffers	26
3.1.3 Transfer buffer for Wet blot	26
3.1.4 Other buffers	26
3.1.5 SDS-polyacrylamide gels.....	27
3.1.6 Inhibitors	27
3.1.7 Staining solutions and dye.....	27
3.1.8 N-glycan detachment / methylation	28
3.2 Methods.....	28
3.2.1 BioRad DC protein assay for high concentration.....	28
3.2.2 Preparation of urinary exovesicles	28
3.2.3 Electron microscopy of exovesicular preparations	29
3.2.4 Isolation of Tamm-Horsfall protein	29
3.2.5 Release and purification of N-linked glycans	30
3.2.6 Derivatization of N-linked glycans	30
3.2.7 MALDI-TOF-TOF mass spectrometry of methylated glycans.....	30
3.3 Differential proteomics by application of the i-TRAQ-technology	31
3.3.1 Preparation of lipid rafts out of urinary exovesicles	31
3.3.2 Protein quantitation in the context of i-TRAQ experiments	31
3.3.3 Chloroform / methanol-precipitation	32

3.3.4 Filter assisted sample preparation (FASP)	32
3.3.5 iTRAQ labeling	33
3.3.6 MALDI Spotting	33
3.3.7 LC-MALDI MS/MS analysis.....	34
3.3.8 Database Searches	34
3.4 Identification of exosomal vesicles by detection of marker proteins in density gradient fractions.....	35
3.4.1 Preparative gradient centrifugation of urinary vesicles.....	35
3.4.2 Detection of exosomal marker proteins by Western blot.....	35
3.4.3 Antibodies	36
4. Results	37
4.1. Vesicle classification by electron microscopy and exosomal marker proteins	37
4.2 N-glycosylation of exosomes	38
4.2.1 Differential N-glycomics of the urinary exovesicles from galactosemia patients and healthy controls	38
4.2.2 High-mannose and complex-type N-glycans	40
4.2.3 Bi-antennary complex-type glycan, the most abundant structure	42
4.3 The GPI-anchored transmembrane Tamm-Horsfall Protein	44
4.3.1 N-Glycosylation of urinary Tamm-Horsfall Protein (THP).....	44
4.3.2 Validation of predominant high-mannose-type N-glycosylation of exosomal lipid raft associated THP	45
4.4 Differential proteomics of exosomal membranes	46
4.4.1. Isobaric tags for relative and absolute quantitation.....	46
4.4.2 Proteins found increased	47
4.4.2.1 Serum proteins.....	47
4.4.2.2 ECM-related proteins	48
4.4.3 Identification of exosomal raft proteins by LC-ESI of SDS-gel fractions.....	49
5. Discussion	50
5.1 A multitude of N-glycosylated proteins	50
5.2 Disglycosylation and targeting of glycoproteins.....	51
5.3 Secreted high-mannose-type glycoproteins probably do not recycle through the Golgi compartment.....	52
5.4 Criteria for Tamm-Horsfall Protein being membrane integrated or associated.....	53
5.5 Galactosemia - a secondary dual congenital disorder of glycosylation (CDG)	53
6. Conclusion.....	54
6.1 N-Glycan remodelling of high-mannose to complex-type.....	54
6.2 Clinical pictures of renal failure.....	55
6.3 Reasons for detecting serum proteins in urine	55
6.4 Hypergalactosylation in samples from galactosemia patients.....	56
6.5 Hypertension in combination with renal failure is dangerous in galactosemia.....	57
7. Future experiments	58
7.1 Glycolipids analyzation of urinary exosomes	58
8. References	59
9. Legends to attached figures.....	62
10. Legends to supplements	67
11. Attachment.....	67
12. Kurzzusammenfassung.....	97
13. Erklärung.....	99

1.2 Tables of figures

1.2.1 Table of figures

Fig. 1: GALT 3D / Source: PDB (Protein Data Bank). GALT complexed with UDP-galactose	12
Fig. 2: Mislinkage of Arginin 188 / Attm.	68
Fig. 3: Bulky residue of arginine disturbs dimeric close up of subunits and active sites / Attm	69
Fig. 4: Ping-Pong double displacement reaction of GALT / Attm.	70
Fig. 5: Leloir Pathway	15
Fig. 6: Affected organs in galactosemia	17
Fig. 7: Origin of exosomes	19
Fig. 8: Glycoprotein travelling via lipid rafts / Attm.	71
Fig. 9: Tamm-Horsfall protein	22
Fig. 10: N-glycan processing	23
Fig. 11: Megalin cubilin reabsorption complex	24
Fig. 12: N-glycosylation of exosomes / Attm.	72
Fig. 13: Electron micrograph of exovesicular preparations	37
Fig. 14: Western blot of marker proteins separated by continuous gradient centrifugation / Attm.	73
Fig. 15: Tamm-Horsfall protein contamination of urinary exosomal vesicles / Attm.	74
Fig. 16: Electron microscopy of 0.1µm filtered exosomes / Attm.	75
Fig. 17: MALDI mass spectrum exosome derived N-glycans of a galactosemic patient	39
Fig. 18: MALDI mass spectrum exosome derived N-glycans of a healthy persons	39
Fig. 19: High-mannose versus complex-type species / Attm.	76
Fig. 20: Relative amounts of high-mannose-type vs. complex-type N-glycans	42
Fig. 21: MS2 spectrum of the monosialyl bi-antennary complex-type N-glycan m/z 2377	43
Fig. 22: MS2 spectrum of the high-mannose-type N-glycan M6 m/z 1730	44
Fig. 23: THP removal from urinary-exosomes using DTT / Attm.	77
Fig. 24: N-glycans electrophoretically purified THP exovesicular origin galactosemic patient	

/ Attm.	78
Fig. 25: N-glycans electrophoretically purified THP exovesicular origin healthy person / Attm.	79
Fig. 26: One dimensional gelelectrophoreses of exosomal lipid rafts prior to iTraQ experiment/ Attm.	80
Fig. 27: Validation of regulated proteins (iTRAQ) by Western blot / Attm.	81
Fig. 28: THP-identification / Attm.	82
Fig. 29: Mascot Search results (LC-ESI) of four gel slices / Attm.	83
Fig. 30: EGFR expression in healthy and diseased fibroblasts / Attm.	84
Fig. 31: Glycosylation shift of MUC1 / Attm .	85
Fig. 32: THP (Uromodelin) identified by top Score (LC-ESI/Mascot Search) / Attm .	86
Fig. 33: One dimensional gel electrophoreses of exosomal lipid rafts for LC-ESI-MS-MS analysis / Attm.	87
Fig. 34: Perlecan involvement in basement membrane assembly	52

1.2.2 Table of supplements

Suppl. Tab1: Ration of complex- to high-mannose-type glycans in exosome samples with high or low THP content	88
Suppl. Tab2: Variation between independent protein samples urine samples from one healthy control	89

1.2.3 Table of Excel-Tabs

Tab. 4a: Genuine exosomal proteins	90
Tab. 4b: Exosome associated proteins	91
Tab. 4c: Disease associated proteins	92
Tab. 4d: ECM / Basement membrane assembly	93
Tab. 4e: Multivesicular body proteins	94
Tab. 4f: Lysosomal proteins	95
Tab. 4g: Unsorted proteins	96

1.3 Abbreviation

1D	one - dimensional
AA-solution	acrylamid-solution
AB	apoptic blebs
ACN	acetonitril
AKI	acute kidney injury
AMBP	alpha-1-microglobulin protein
AP2	adapter protein 2
APS	ammonium persulfate
ARF1	ADP-ribosylation factor 1
Attm	attachment
CAP	adenylate cyclase associated protein
CD13	cluster of designation 13
CDC42	cell division control protein 42 homolog / invoved in endocytoses
CDG	congenital disorder of glycosylation
CHAPS	3-[(3-cholamidopropyl)dimethylammonio]-1-propanesulfonate / detergent for lysis buffer
CHM2A	charged multivesicular body protein 2A
CNS	central nervous system
ddH ₂ O	aqua bidest.
DTT	dithiothreitol
ECM	extracellular matrix
EDTA	ethylenediaminetetraacetic acid
EGF	epidermal growth factor
EGFR	epidermal growth factor receptor
EN	endemic nephropathy
ESCRT	endosomal sorting complexes required for transport
FASP	filter-aided sample preparation
FibH	healthy fibroblasts
FibQ	GALT deficient fibroblasts Q188R
Fig	figure
Fuc	fucoese
Gal	galactose
gal-1-P	galactose-1-phosphate
GALT	galactose-1-phosphate uridyltransferase
Gal-T	galactose-transferase
GlcNAc	N-Acetylglucosamin
GlcNAc-T	GlcNAc-Transferase
GM3	third monoganglioside
GPI-anchor	glycosylphosphatidyinositol-anchor
g-proteins	guanine nucleotide-binding proteins / interact with gpcr g-protein coupled receptors
GTPase	hydrolyzes guanosine triphosphate
Hex	hexose

HexNAc	N-Acetylhexosamine
HPLC	high-performance liquid chromatography
HRP	horse radish peroxidase
Hsp	heat shock protein
HSPG2	heparan sulfate proteoglycan core protein 2 / perlecan
Ig	immunoglobulin
IgAN	immunoglobulin A nephropathy
ILV	intraluminal vesicles
iTRAQ	isobaric tags for relative and absolute quantitation
kD	kilo Dalton
LC-ESI-MS	liquid chromatography-electrospray-ionisation-mass spectrometry
LDL receptor	low density lipoprotein receptor
LRG1	leucine-rich alpha-2-glycoprotein
MALDI	matrix-assisted laser desorption ionization mass spectrometry
Man	mannose
MCF-7	Michigan Cancer Foundation - 7 / breast cancer cell line
MHC	major histocompatibility complex
microRNA	micro ribonucleinsäure
MPs	microparticles
mRNA	messenger ribonucleinsäure
MS2	MS/MS, multistage mass spectrometry
MUC1	mucin 1
MVB	multi-vesicular body
MVs	microvesicles
nanoLC	nano liquid chromatography
NeuAc	neuramic acid / sialic acid
NeuAc	neuraminic acid, sialic acid
NSCLC	non-small cell lung cancer
PBS	phosphate buffered saline
PDB	Protein Data Bank
PNGaseF	peptide N-Glycosidase F - cleaves between the innermost GlcNAc and asparagine of N-linked glycoproteins
RAC1	ras-related C3 botulinum toxin substrate 1
RAP1A	ras-related protein Rap-1A
ROBO4	roundabout homolog 4
RT	room temperature
SDS-PAGE	sodium dodecyl sulfate polyacrylamide gel electrophoresis
SGP	stacking gel buffer
sialyl-T	sialyltransferase
SPFH-domain	stomatin/prohibitin/flotillin/ HflK/C-domain
Src kinase	sarcoma (virus) kinase
SW41	swing rotor 41
TALH	thick ascending limb of Henle's loop
TBMN	thin basement membrane nephropathy
TBST	tris buffered saline with Tween

TEABC	triethylammonium bicarbonate
TEMED	tetramethylethylenediamine
TFA	trifluoroacetic acid
TGP	resolving gel buffer
THP	Tamm-Horsfall protein
TSG101	tumor susceptibility gene 101
Tyr	tyrosin
U	units
UDP	uridine-diphosphate
UMP	uridine-monophosphate
VP37B	vacuolar sorting protein 37B
Vps	vacuolar protein sorting-proteins

1.4 Abstract

Classical galactosemia is caused by deficiency of the enzyme galactose-1-phosphate uridylyltransferase (GALT). The reason for the deficiency is a specific gene mutation causing an amino acid exchange near the active site of the enzyme. The turnover rate of the enzyme is therefore more than thousand-fold decreased. Dietary galactose uptake, for instance drinking milk, is followed by an intracellular stress response. The co-substrate of the GALT galactose-1-phosphate accumulates intracellularly and disturbs carbohydrate-dependent metabolic pathways and presumably the Leloir pathway. The Leloir pathway supplies UDP-galactose and UDP-glucose for glycosylation of proteins and lipids. UDP-galactose incorporation is necessary, for example, to build up complex-type antennae of N-glycans on glycoproteins. It was supposed that, if the Leloir pathway is affected, the N-glycosylation, especially galactosylation in complex-type chains, will be affected. For examination of changes in glycosylation patterns mass spectrometric glycomics methods were chosen as most suitable. The N-linked carbohydrate branches were detached by PNGaseF digestion and analyzed applying matrix-assisted laser ionization mass spectrometry after glycan methylation. For examination of glycan pattern changes we isolated vesicles, mainly exosomes from urine of galactosemia patients as easily accessible source of epithelial membranes, and compared the N-glycome with the corresponding samples of healthy controls. The comparison of the mass spectra reveals a dramatic glycosylation shift from prevalent high-mannose-type N-glycans found in healthy controls towards complex-type glycosylation in patients. The estimated ratio of the amounts of high-mannose-type *versus* complex-type was about 3:1 respecting the healthy control samples. Especially the N-glycans that either carry five or six mannoses were

detected as most abundant. In contrast the ratio for patients shifted to nearly 1:1 towards complex-type glycosylation. The most abundant complex-type glycans from exovesicular membranes of GALT-deficient patients were of bi-antennary structure, terminal disialylated and without core fucosylation. Glycans with higher antennary branching were found in marginal amounts, only. The observed glycosylation shift can be regarded as a new finding and it may be assumed that not only secreted proteins like transferrin become dysglycosylated in galactosemia. Furthermore, cell surface located glycoproteins, especially receptors, were affected. Changes in glycosylation patterns were suspected to be responsible for missorting of glycoproteins especially for glyco-receptors like the EGFR (epidermal growth factor receptor) which is regularly expressed at apical membranes of epithelial cells.

Quantitative and qualitative alterations of membranous exosomal glycoproteins indirectly provide information of alterations at the cell membrane. To study alterations of glycoproteins, especially glyco-receptors, in exosomal lipid rafts, an iTRAQ (isobaric tags for relative and absolute quantitation) labeling was chosen as suitable for a quantitative in vitro experiment based on urinary exosomes. Four different individual samples were selected: two galactosemic samples (from patients showing drastic shifts from high-mannose to complex-type N-glycosylation) and two healthy controls. The samples were labeled with the isobaric tags, mixed and analyzed by offline nano-LC MALDI-MS/MS (liquid chromatography-matrix-assisted laser desorption-ionization-mass spectrometry). Although EGFR was not detected in the experiment we found strongly increased amounts of N-glycoproteins and some receptors associated with galactosemic exosomes: tyrosine-protein kinase receptor UFO, zinc-alpha-2-glycoprotein (ZA2G, MHC I -family) and aminopeptidase N (CD13), to name some. The cubilin receptor and megalin were also found. They dimerize to form the megalin-cubilin-complex and are responsible for protein reabsorption at the proximal tubulus of the nephritic kidney. This cubilin receptor was detected in a further experiment to be one of the major differences between samples of galactosemia patients and control persons.

Finally, the iTRAQ experiment revealed another unexpected result. The samples of the galactosemia patients contained increased amounts of serum proteins, in particular N-glycoproteins. A large variety of immunoglobulins were found increased; further albumin, fetuin, transferrin and many more. All together these results strongly suggest renal failure for these examined galactosemic patients.

Biopsy is usually the most common method to detect renal diseases. The examination of urinary exosomal samples therefore possibly represents a new diagnostic method to detect renal failure without surgical intervention.

2. Introduction

2.1.1 Galactose-1-phosphate uridylyltransferase (GALT)

2.1.1.1 GALT 3D structure

Classical galactosemia is caused by a profound deficiency of galactose-1-phosphate uridylyltransferase (GALT; EC 2.7.712).

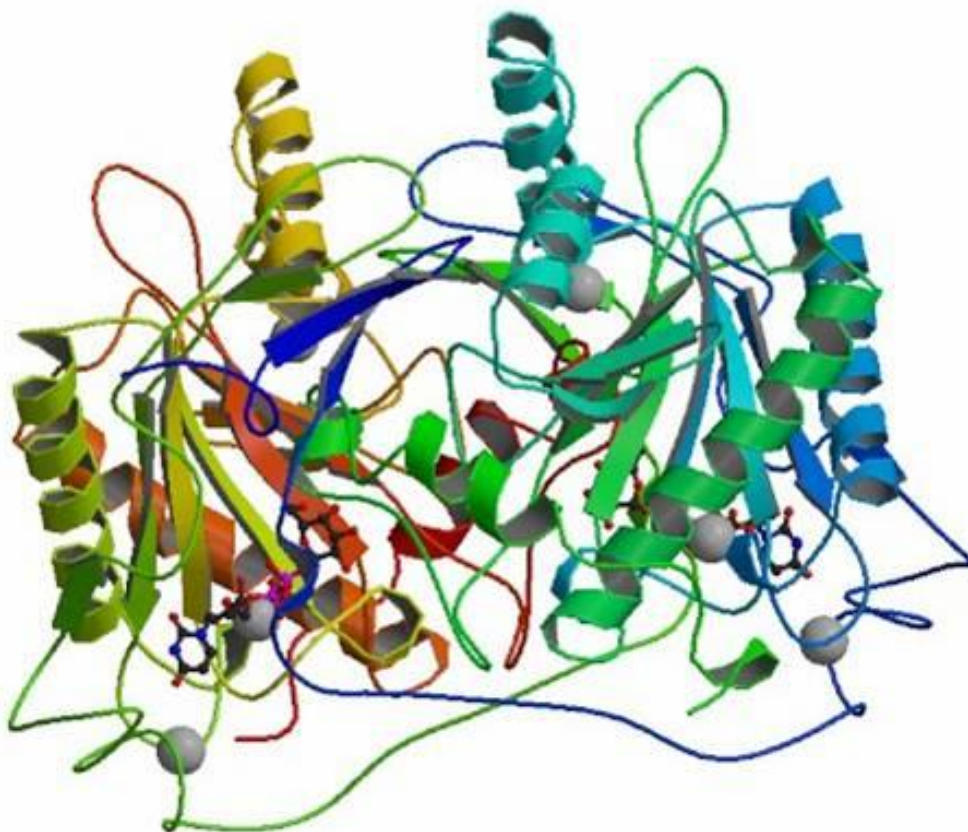


Fig. 1: GALT 3D / Source: PDB (Protein Data Bank). GALT complexed with UDP-galactose.

GALT is a homodimer. Each subunit is characterized by a nine-stranded antiparallel β -pleated sheet flanked on either side by two α -helices [1]. Three different ions are incorporated in each subunit to stabilize the enzyme, the dimerization, and the substrate binding. An iron ion is

located near the subunit interface it serves as a bridge between two β -strands and an α -helix. A further zinc ion is located near the active site of the substrate binding position of uridine and at the opposite side to the surface loops of the enzyme. The third metal ion, a potassium ion, stabilizes two phosphoryl groups of UDP after binding of the first substrate (UDP-glucose) at the active site. Each loop of the dimer forms a component part to the active site of the opposite subunit.

2.1.1.2 The GALT mutation Q188R

A gene mutation causes the amino acid exchange from glutamine to arginine at position 188 of the amino acid sequence of the enzyme (Q188R). The peptide site p188 is located at the active site. As a result for this exchange a mislinkage of the hydrogen bond from the upper phosphoryl groups (O2A/O1B) to the lower situated hydrogen bond types (O5'/O2B) rearrange (Fig. 2/Attm. p.68)[2]. This mislinkage is accompanied by a loose fitting of the second GALT substrate the cosubstrate gal-1-phosphate. The loose fitting causes the reduction of the enzymatic turnover rate by a factor greater than 1000.

In addition, another destabilization effect is caused by the bulky arginine residue that exhibits a longer side chain in comparison to glutamine (Fig. 3/Attm. p.69)[2]. Moreover, the bulky arginine residue disturbs the dimeric close up of the subunits and negatively influences the substrate fitting to the surrounding hydrophobic pocket of the active site.

2.1.1.3 Ping-Pong double displacement reaction of GALT

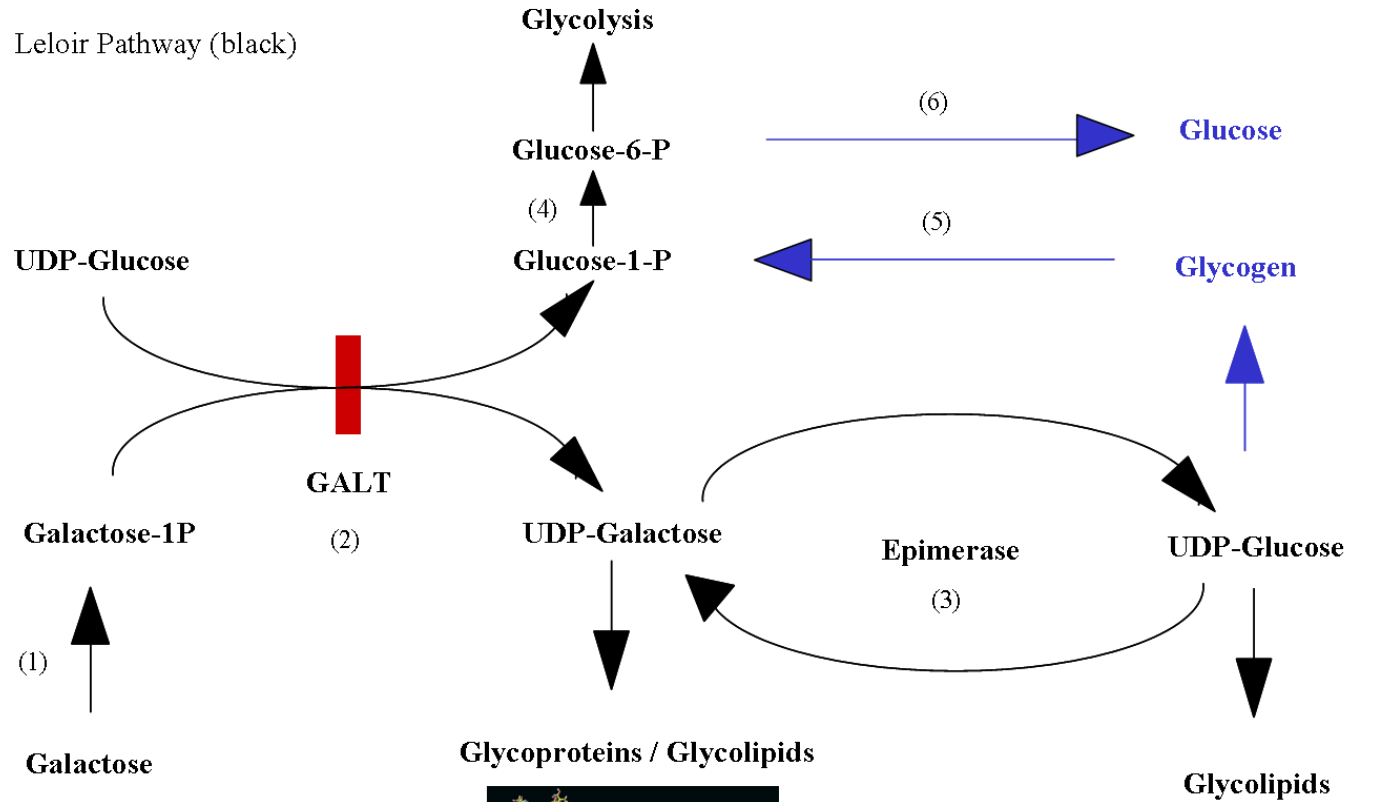
GALT acts on two substrates in a ping-pong double displacement reaction (Fig. 4/Attm. p.70) [3]. Primarily, the first substrate UDP-glucose in composition with GALT binds to the active site that forms the intermediate complex GALT-UDP-glucose. It is subsequently cleaved to GALT-UMP. It remains attached to the enzyme in complex. Glucose-1-phosphate the first product that is released (“ping-reaction”). The second (co-)substrate added is galactose-1-phosphate that forms the second intermediate complex GALT-UDP-galactose with GALT-UMP. During the final step the second product UDP-Galactose is released by the enzyme (“pong-reaction”) and the GALT is ready to take part in another turnover cycle.

2.1.2 Galactose and the Leloir pathway

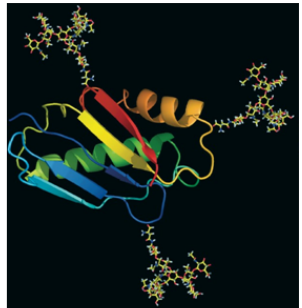
Lactose, one of the major sources of galactose, is cleaved by lactase, a transmembrane enzyme that is located at the epithelial surface of the small intestine. More precisely, the enzyme is exposed on villi to the intestinal lumen. These villi carry active transporters as well, which are able to take up galactose in the way of a galactose-proton symport. The galactose subsequently enters the Leloir pathway (Fig. 5 see next p.), is phosphorylated by galactokinase and then serves as a cosubstrate of the GALT. GALT is the second enzyme in the Leloir pathway of galactose metabolism that converts galactose-1-phosphate to glucose-1-phosphate which is metabolized in the glycolytic pathway. Alternatively, galactose-1-phosphate may instead be activated to UDP-galactose, the cosubstrate involved in enzymatic galactosylation of glycoproteins and glycolipids. In this study we focused on the alternative pyrophosphorylase pathway correspondent to galactosylation of glycoproteins. UDP-galactose and UDP-glucose are balanced by UDP-galactose-4-epimerase which is able to convert one activated sugar into the other, dependent on the substrate concentration.

Deficiency of GALT should expectedly lead to an imbalance between UDP-galactose and UDP-glucose. The maladjustment might result in disglycosylation of glycoproteins and glycolipids. Deficiency of GALT results in a severely impaired galactose metabolism. The intracellular metabolite concentration of Gal-1-P was shown to accumulate more than five-fold under galactose-stress and this has an effect on at least three enzymes of galactose metabolism: phosphoglucomutase, glucose-6-P-phosphatase and phosphorylase (three enzymes shown in Fig. 5 see next p.).

Fig. 5 Leloir Pathway (black)



 Defect transferase (GALT)



Source of picture: Glykostrukturfabrik

- (1) galactokinase
- (2) galactose-1-phosphate uridylyltransferase
- (3) UDP-galactose-4-epimerase
- (4) phosphoglucomutase
- (5) glycogen phosphorylase
- (6) glucose-6-phosphatase

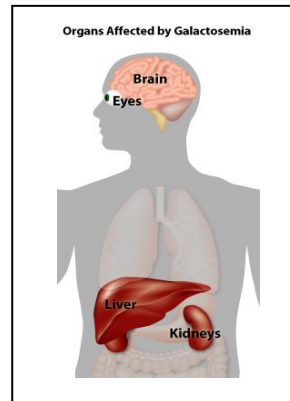
2.1.3 Dysglycosylation of secreted glycoproteins in classical galactosemia

Reports on glycosylation abnormalities in galactosemic patients so far exclusively refer to secreted proteins, in particular to plasma glycoproteins such as transferrin and glycopeptide hormones such as follicle-stimulating hormone (FSH) [4-5]. Transferrin of galactosemic patients prior to dietary galactose restriction was shown to have large proportions of truncated glycans lacking terminal sialic acid and galactose residues in N-glycan antennae [6]. The distinct glycosylation abnormalities of transferrin prior to dietary galactose restriction were the consequence of the acute hepatotoxic status caused by exogenous galactose. These abnormalities should be distinguished from aberrant glycosylation which might be related to cell or tissue dysfunction responsible for the development of long-term complications. Rather, for such a harmful event abnormally glycosylated cellular glycoproteins come into consideration, since proper N- and O-glycosylation of glycoproteins is a precondition for proper sorting and trafficking of membrane glycoproteins, so that they can reach their correct destination and function [7]. Likewise, a defective synthesis of glycoproteins and galactolipids can have a strong impact on normal myelin formation [8]. Thus, in search for the role that aberrant glycosylation may play for the development of long-term complications in galactosemia the glycosylation of cellular glycoproteins should be studied.

2.1.4 Clinical picture of classical galactosemia

Newborn infants affected with severe GALT deficiency develop a potentially lethal hepatotoxic syndrome induced by dietary (exogenous) galactose, which usually resolves rapidly after institution of a galactose-restricted diet. In contrast to rapid recovery of liver disease, long term outcome in classical galactosemia is disappointing. Despite strict adherence to the galactose-restricted diet, a great percentage of patients develop long-term complications which may result from deleterious perturbations in cell biology caused by endogenously synthesized galactose. The long-term complications comprising cognitive impairment, speech defects, motor function disturbances and in most female patients hypergonadotropic hypogonadism are related to the CNS and ovary as target tissues. Their origin is prenatal. They worsen, if at all, only slightly with time [9-10]. The possible mechanisms underlying long-term complications comprise the individual or combined effects of excess galactose-1-phosphate, galactitol or other galactose metabolites, or defective

glycosylation of proteins and lipids leading to direct and / or indirect cell or tissue dysfunction [4]. A number of reports have demonstrated that GALT deficiency leads to aberrant protein glycosylation especially prior to dietary galactose restriction, but also in a diminished form under a galactose-restricted diet [5-6,11].



<http://learn.genetics.utah.edu>

Fig. 6: Affected organs in galactosemia: Primary effect on liver; secondary effect on kidney, brain and eyes. In the eye a characteristic grey deposit of galactitol could be recognized.

2.1.5 Exosomes

2.1.5.1 Characteristics of exosomes

Exosomes are found in almost all body fluids that are exposed to epithelial surfaces: blood, urine, amniotic fluid, malignant ascites, bronchoalveolar lavage fluid, synovial fluid and mother's milk [12]. They are able to communicate with the immune system *via* major histocompatibility complexes (MHC). Inside the lumen they carry mRNA and microRNA and can therefore influence protein expression if transferred to another cell. Typical exosomal marker proteins are: alix, TSG101, CD81 (tetraspanin), Hsp70, MUC1, GPI-anchored proteins like RhoA, G-proteins, receptor CD24, flotillin and caveolin. Exosomes exhibit a density of about 1.15-1.18 g/ml, consist of a double layer membrane and are highly enriched in sphingomyelin, cholesterol and the glycolipid GM3 [13]. Exosome-like vesicles were also found in the hemolymph of *D. melanogaster* and in supernatant of Schneider 2 cells [14] which characterizes them for an evolutionary conserved function.

2.1.5.2 Epithelial origin of exosomes

Human urine has been reported to contain exosomes [15], with sizes ranging between 30 and 100nm. They originate from internal vesicles that are called intra luminal vesicles (ILV), accumulate in endosomal multi-vesicular bodies (MVB) and are then released after fusion of the MVBs with the cell membrane. The membrane of these nanovesicles exhibits a close relationship to the protein composition of the respective plasma membranes and hence these exovesicles can reveal insight into the proteome and glycome of the exosome forming cell [16-17]. In case of urinary exosomes, each renal epithelial cell facing the urinary tract contributes to the pool of exosomes.

2.1.5.3 Exosomes are enriched in subpopulations of lipid rafts

Transmembrane and membrane integrated proteins are often found in particular subdomains of the plasma membrane, called lipid rafts (see also below under 2.1.6.1). The transmembranous glycoprotein MUC1, for example, is sorted for trafficking *via* lipid raft platforms (Fig. 7 next p). Each of these lipid rafts is structurally stabilized by either caveolin-1 or flotillins. The arrangement of these scaffolding proteins close to the cell surface induces an inward budding of the plasma membrane and the formation of vesicles. These vesicles are then transported to the early endosomes that mature to multivesicular bodies (MVBs) by a second inward budding. Inside the MVBs, proteins are sorted through ESCRTs (endosomal sorting complexes required for transport) and Vps-proteins (vacuolar protein sorting-proteins) into the membrane of the intra luminal vesicles (ILVs). Protein-ubiquitination therefore provides the targeting signal to these vesicles. During the second inward budding the proteins regain the same orientation that they previously exhibited at the cell surface. Thus the extracellular part of the protein is exposed at the outside of the exosome. Finally, MVBs fuse with the membrane and release their content, now called exosomes, into the extracellular space (Fig. 7 next p).

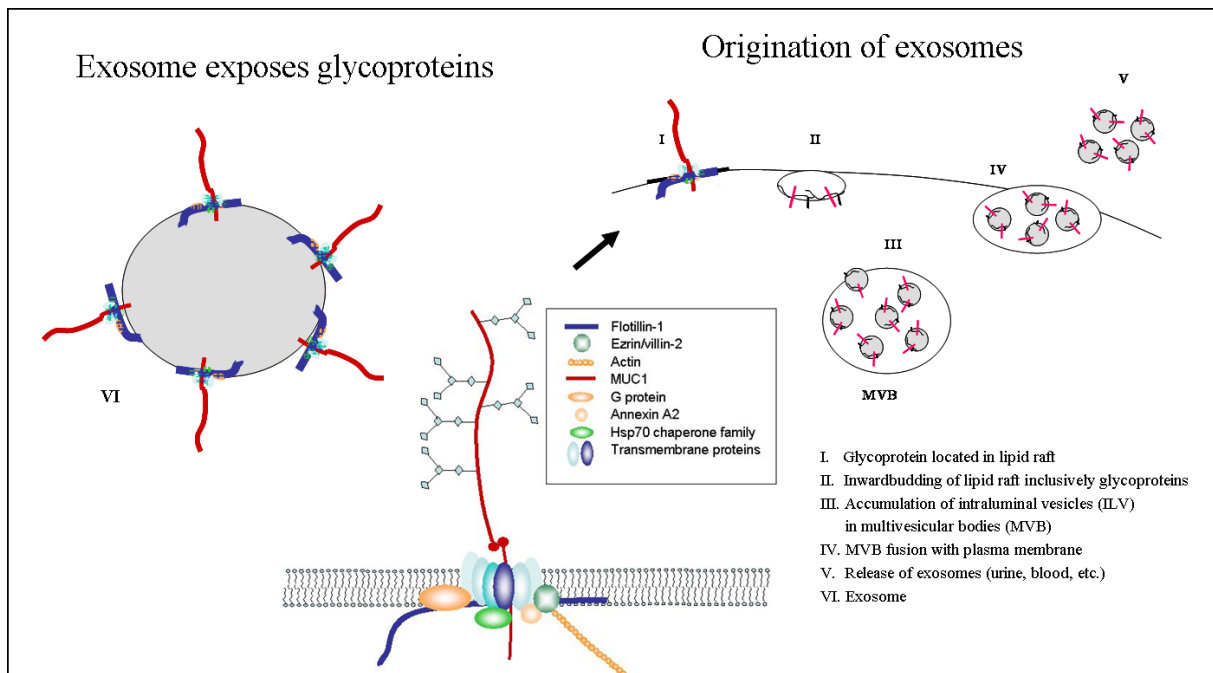


Fig. 7: Origin of exosomes. Glycoprotein trafficking from lipid raft to exosome.

The surface of the exosomes thus represents a section of the plasma membrane, which is reflected in results of comparative proteomic analyzes [18].

2.1.6 Lipid rafts

2.1.6.1 Lipid raft endocytosis

Lipid rafts are enriched in sphingolipids, cholesterol and gangliosides their composition is distinct from the surrounding less ordered membrane. This lipid composition, in particular the high content of cholesterol, makes lipid rafts less soluble in the presence of neutral detergents, like Triton-X100 at 4°C, a feature, which is used during their preparation. The cholesterol reduces the lipid raft density a property that enables to fractionate them by gradient ultracentrifugation.

Two types of lipid rafts can be distinguished: “planar lipid rafts” which are also referred to as “non-caveolar”, and a subset of rafts known as “caveolae”. Planar rafts are defined as non-invaginated microdomains lacking specific morphological features. Caveolae, on the other hand, are tube-like invaginations of the plasma membrane characterized by specific scaffolding proteins, the caveolins. Functionally, lipid rafts can be regarded as sorting platforms for targeted transport of transmembrane and GPI-anchored proteins and hence their

protein compositions are highly fluctuating. Some proteins however are key components for membrane raft formation and function and can be found as constitutive components of rafts. One of the essential proteins serving scaffolding functions in caveolar raft formation is caveolin-1, a classical hairpin protein that plays a key role in caveolae-mediated endocytosis and transport.

However, caveolin-1 is not the only protein involved in raft formation, as other proteins may be substituted for its scaffolding functions in caveolin-independent rafts. Reggie/flotillins, members of the SPFH-domain containing protein family (stomatin/prohibitin/flotillin/HflK/C), are also an indispensable prerequisite for raft formation in non-caveolar or so-called reggie microdomains [19]. Reggie 1/flotillin-2 and reggie 2/flotillin-1 promote the co-assembly of activated and specific GPI-anchored proteins in plasma membrane microdomains and allow similar to caveolin-1 a concerted interaction of signaling molecules (Src family kinases and the CAP-associated signaling complex in cooperation with the small GTPase TC10). Beyond their involvement in membrane raft formation and signaling, flotillins bind to actin and interact in this way with the cytoskeleton [20]. Flotillin is anchored in the lipid bilayer via N-terminal myristoyl and palmitoyl groups and associates with the membrane by binding two hydrophobic subdomains. On co-expression in caveolar rafts flotillins can interact with caveolin-1, and may serve as a functional substitute in caveolin-1-deficient cells, such as MCF-7 breast cancer cells. These cells are negative for caveolin-1 and lipid raft-associated endocytosis is mediated by flotillin- and CDC42-dependent pathways. Summarized, reggie/flotillins show a distant relationship to other scaffolding proteins, in particular to stomatin, prohibitin, podocin and erlin.

2.1.6.2 Glycoprotein trafficking *via* multivesicular bodies (MVBs) to exosomes

The clustering of lipid rafts through oligomerization of raft components plays a role in the sorting of proteins and their trafficking to different cellular locations. Besides functioning in polarized sorting, raft formation might be involved in re-endocytosis and trafficking of membrane-bound glycoproteins to early endosomes, from where they can be transported to lysosomes or recycle back to the plasma membrane *via* the secretory pathway and undergo follow-up glycosylation (Fig. 8 Attm. p.71). A further possibility is that re-endocytosed membrane glycoproteins are sorted into exosomes for cellular export. An essential role of exosomes could be the homeostasis and adaptation of plasma membranous glycoprotein patterns. Hence, the exchange by *de novo* synthesized plasma membrane proteins and the

removal of immaturely glycosylated (undersialylated or unprocessed) species *via* lysosomal degradation or *via* exosomal export might be a way how cells regulate the exposure of a specifically glycosylated protein in apical membranes. One such protein, which is known to follow recycling and exosomal export pathways, is the type 1 transmembrane glycoprotein MUC1. This heavily O-glycosylated mucin was demonstrated to recycle several times through the trans-Golgi network and to gain in this way a maturation of sialylation. The re-endocytosis and vesicular transport of the protein were shown to follow a clathrin-mediated pathway and later confirmed to be dependent on specific Tyr residues (Tyr20, Tyr60) in the highly conserved cytosolic domain of MUC1, which are necessary for binding to adaptor-related protein complex 2 (AP2).

The re-entry into the secretory pathway of MUC1 was revealed to be dependent on S-palmitoylation of a CQC motif at the intersection of the cytosolic and transmembrane domains. The mucin can also be shed from the plasma membrane by action of specific sheddases or by dissociation of the heterodimeric complex formed by the extracellular tandem repeat domain and the membrane-bound component. Accordingly, exosome-depleted supernatant of cells transfected with a recombinant MUC1 probe was shown to contain a soluble form of the fusion protein that lacks the transmembrane and cytosolic domains (Razawi, H. and Hanisch, F.-G. unpublished results).

2.1.7 The Tamm-Horsfall glycoprotein (THP)

Tamm-Horsfall glycoprotein (THP, also called uromodulin) is highly (exclusively) N-glycosylated, exposed at the epithelial surface, and can be shed after cleavage of the GPI anchor. Urothelial cells are the origin of the most abundant glycoprotein in human urine. THP is integrated into the plasma membrane *via* a GPI-anchor and hence represents an integral membrane protein [21]. However, it is shed in large quantities into urine, where its concentration can reach 0.5mg/dl. Both urinary constituents, exosomal membranes and THP, may generally serve as a suitable non-invasive starting material for bio (glyco) marker discovery. The THP is found at the cell membrane of the proximal tubulus of the nephron.

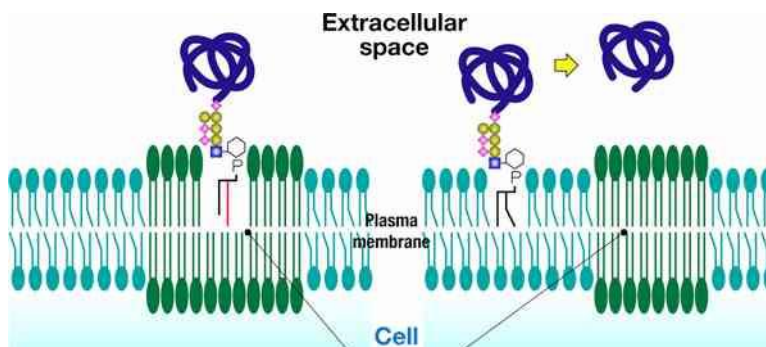


Fig. 9: Tamm-Horsfall protein, membrane integrated and cleaved.

http://www.aist.go.jp/aist_e/latest_research/2006/20061110/20061110.html

THP is a major contaminant that adheres to the surface of the exosomes as long filamentous protein polymers (Fig. 13 p.37 below). This oligomerisation is caused by disulfide linkage of cysteines inside the *zona pellicuda* domain of THP. THP polymers have been claimed to be removable under strong denaturing conditions [22], which was however not confirmed in our hands.

2.1.8 N-glycan processing

N-linked chains can be found in three different forms: The high-mannose-type, the hybrid-type, and the complex-type. High-mannose-type glycoproteins are presented at the cell surface if N-glycoproteins pass the Golgi-network only once as in case of secretory proteins. In contrast, the complex-type glycans, as the name already implies, represent a structurally more diverse family of related structures, which differ with respect to the number of antennae, the lengths of antennary polylactosamines and the terminal epitopes. The hybrid-type represents an intermediate form, which is generated during processing of high-mannose-type glycans to the complex-type, a process involving the trimming by mannosidases and the addition of GlcNAc and Gal (Fig. 10 see next p.). If the synthesis of glycoproteins is interrupted because of an enzyme deficiency a lot of CDGs (congenital disorder of glycosylation) develop. The assembly of high-mannose-type glycans is restricted to the ER and CDG I defects are either restricted to this compartment. The oligosyltransferase (OST) divides the CDG I and CDG II diseases. Enzymatically disglycosylation that happens behind the oligosaccharide transfer of the OST were described as CDG II. The most part of secondary CDGs (CDG II) were allocated to the Golgi compartment where the modification of glycoproteins to complex-type occurs.

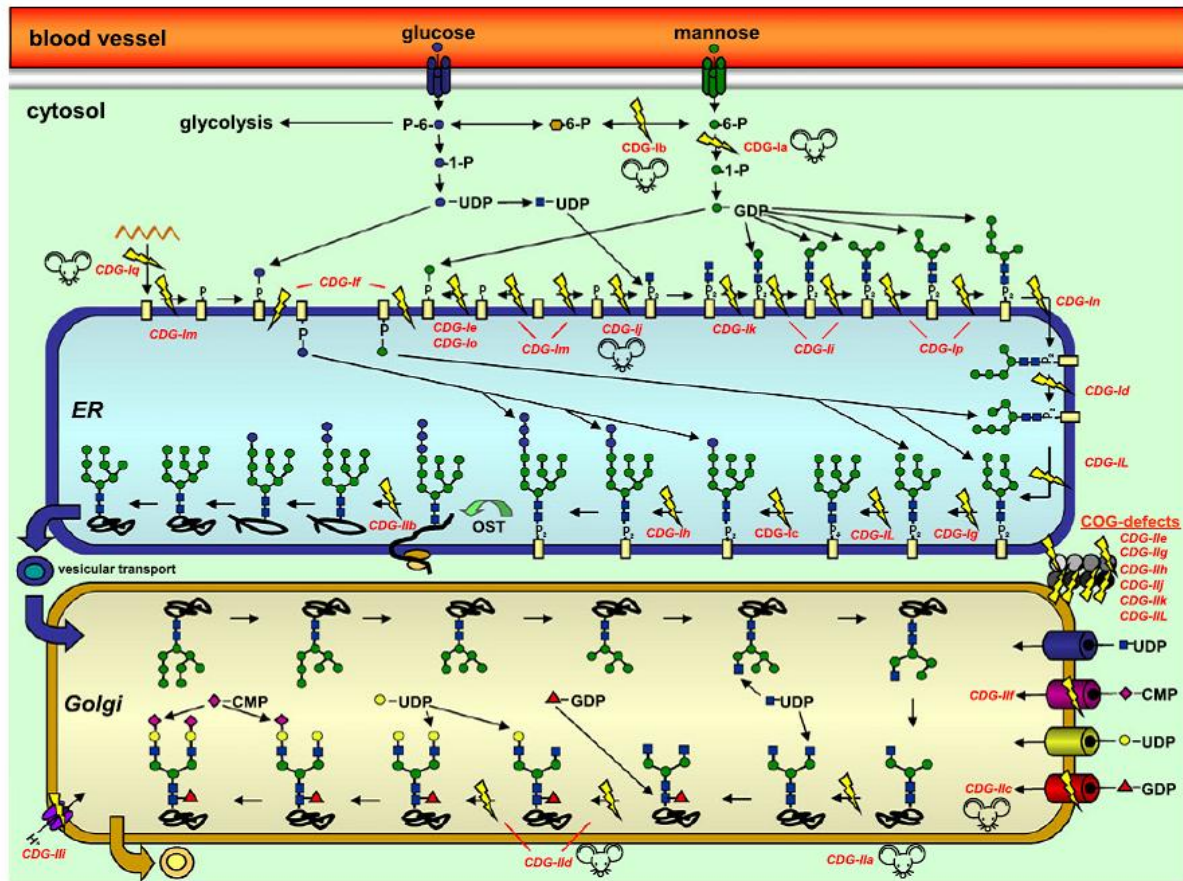


Fig. 10: The high-mannose-type glycoproteins are synthesized in the ER. The trimming to complex-type proceeds inside the Golgi. Involved in the restructuring process are mannosidases, GlcNAc-transferases, Gal-transferase and Sialyltransferase. (C. Thiel & C. Körner 2011/Springer V.)

2.1.9 Reabsorption of proteins in the kidney

2.1.9.1 Megalin cubilin receptor complex

“The kidney proximal tubule has a high capacity for the uptake of filtered proteins. Small proteins are mainly allowed to pass the glomerulus filtration barrier larger are filtered except in glomerulus dysfunction. The cut-off molecular weight for filtration of plasma proteins during normal conditions has generally been assumed to lie in the range of 60kD, which corresponds to the approximate molecular weight of serum albumin. However, the diversity of proteins filtered is large and includes also larger proteins such as transferrin (81kD). Thus,

the molecular apparatus for handling the reabsorption of these proteins must include the ability to recognize a large number of different proteins and at the same time provide for an efficient (re)uptake. The initial step in the reuptake of proteins involves receptor mediated endocytosis initiated by the binding of filtered ligands to receptors at the luminal surface, followed by the clustering of these receptors into clathrin coated pits at the base of the microvilli” [23].

“Furthermore, the accelerated tubular reabsorption of specific proteins is implicated in the progression of chronic renal disease characterized by proteinuria. The two large membrane-associated proteins megalin and cubilin serve as endocytic receptors mediating the luminal uptake of a large number of proteins, including albumin, which are filtered both in the normal glomeruli and as a result of glomerular dysfunction” [23]. The accelerated tubular reabsorption probably is a consequence of a higher expression rate of both complex proteins.

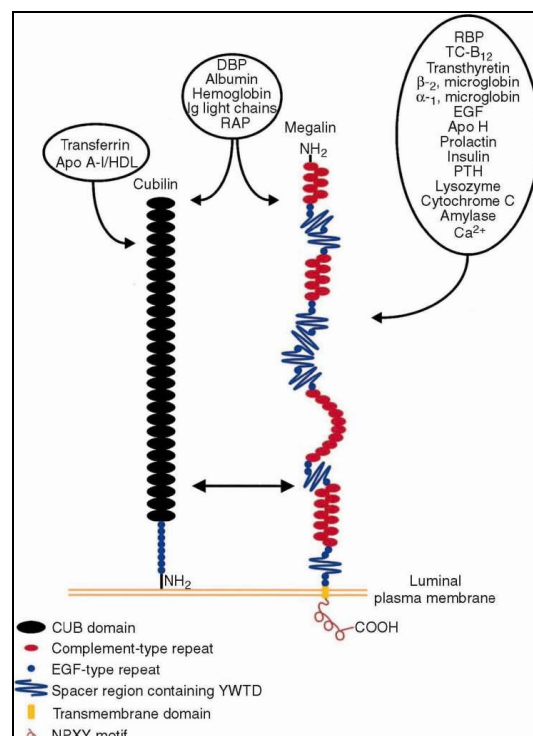


Fig. 11: Megalin cubilin reabsorption complex

Megalyn and cubilin was previously detected by a proteomic profiling study of exosomes by Pisitkun et al. but he could not link it to any disease dependent regulation [15]. Marzalo et al. [24] predicted the exosomal megalin involvement in renal diseases. Marzalo further describes the involvement of megalin in the central and peripheral nervous system and several of its ligands play a role in neuronal survival and regeneration [24].

2.2 The aims of the study

This work refers to the first comprehensive study of a cellular N-glycoprotein dysglycosylation associated with classical galactosemia. The results demonstrate that findings from analyses of secretory glycoproteins cannot be regarded as representative for changes in the glycosylation of cellular membrane-bound proteins. Strikingly, the GALT-deficiency does not result in an under-galactosylation of complex-type N-linked chains, but instead in a dramatic shift from preponderant high-mannose-type N-glycosylation in control samples to (galactosylated) complex-type chains in GALT-deficient patients.

The second part of this study recognizes renal failure in galactosemia and an increased amount of the megalin-cubilin complex that is strongly associated to proteinuria. The examination of urinary exosomal lipid rafts provides a new diagnostic method. Instead of kidney biopsy N-glycan analytic or the increased amount of some elected protein marker may serve for diagnoses of renal failure.

3. Materials & Methods

3.1 Materials

3.1.1 Samples from GALT deficient patients

Urine samples (approx. 500ml, collected in the morning) were obtained from healthy volunteers (adult individuals, n = 5) and from patients with classical galactosemia (12 adult individuals six female, six male; approved by the Ethical Commission of the University Clinic of Cologne on November 23rd, 2010) and kept frozen (-20°C) until use. The galactosemic patients carried the c.A1466G (p.Q188R) mutation homozygous and exhibited a very low residual GALT activity characteristic for classical galactosemia. All galactosemic patients were on a severely galactose-restricted diet.

3.1.2 SDS-Polyacrylamide-gel electrophoresis buffers

10 % SDS:	5g Na-dodecylsulfate in 50ml ddH ₂ O
Laemmli buffer (2x):	2 % SDS, 45 % glycerol, 0.01 % bromphenolblue, 100mM Tris-HCl (pH 6.8), 10 % β-mercaptoethanol
Electrophoresis buffer (10x):	0.25M Tris, 1.92M glycine, 1 % SDS, (pH 8.3)
TGP (4x):	90.93g Tris / 0.5l / pH 8.8 adjustment with HCl (conc.)
SGP (4x):	30.31g Tris / 0.5l / pH 6.8 adjustment with HCl (conc.)

3.1.3 Transfer buffer for Wet blot

Transfer buffer:	500ml 2x Towbin buffer (see below) 200ml methanol 5ml 10 % SDS solution fill up to 1000 ml
------------------	---

3.1.4 Other buffers

TBS(T):	50mM Tris-HCl pH 7.4, 0.15M NaCl, (0.05 % Tween 20)
Towbin buffer (2x):	0.39M glycine, 0.048M Tris, 20 % methanol
PBS:	PAA (Cölbe)

3.1.5 SDS-polyacrylamide gels

Resolving gels	5 %	20 %
Water	5.7	2.5
4 x TGP	2.5	2.5
AA-solution	1.7	5.0
SDS (10 %)	0.1	0.1
APS (10 %)	0.05	0.05
TEMED	0.005	0.005

Stacking gel	4 %
Water	6.1
4 x SGP	2.5
AA-solution	1.3
SDS (10 %)	0.1
APS (10 %)	0.05
TEMED	0.01

Charts: Components (percent per volume) of SDS-polyacrylamide gels

Protein samples were heated in sample buffer 5min. at 95°C. Afterwards these samples were subjected to SDS-PAGE. While the proteins pass through the stacking gel the amperage was set at 15mA. After entry into the resolving gel the amperage was increased to 20mA.

3.1.6 Inhibitors

Protease Inhibitor

Protease Inhibitor Cocktail (Sigma-Aldrich, Steinheim)

P8340 without EDTA (Sigma-Aldrich, Steinheim)

P2714 with EDTA (Sigma-Aldrich, Steinheim)

cOmplete Protease

Inhibitor Cocktail Tablets:

Roche Diagnostics (Mannheim)

3.1.7 Staining solutions and dye

10 % Ponceau-S-dye:

0.2 % Ponceau S (Merck, Darmstadt) in

3 % TCA / H₂O (Fluka, Seelze)

Coomassie Brilliant Blue

Stain (G250-solution):

50 % methanol (Sigma-Aldrich, Steinheim),

	12 % acetic acid (Sigma-Aldrich, Steinheim),
	0.04 % Servablue G-250 (SERVA, Heidelberg)
Destain-solution for	
Coomassie:	40 % methanol
	5 % acetic acid

3.1.8 N-glycan detachment / methylation

PNGase F:	New England Biolabs (NEB), Frankfurt
Bicarbonate buffer (99.5 %, puriss.):	KMF Laborchemie Handels GmbH (50mM)
Iodomethane:	Sigma-Aldrich, Steinheim
Acetic acid:	Sigma-Aldrich, Steinheim
Chloroform (>99 %; anhydrous):	Sigma-Aldrich, Steinheim
Methanol (spec. grade):	Sigma-Aldrich, Steinheim

3.2 Methods

3.2.1 BioRad DC protein assay for high concentration

A stock solution of 10mg/ml BSA was prepared to generate a standard curve (steps 0.2µg/µl; with eight dilutions 0-1.4µg/µl). The microplate “High-concentration assay” was chosen for protein determination. In brief, 5µl standards and samples, 25µl reagent A and 200µl reagent B were added to the microplate and incubated for 10-30min. The absorption (at 620nm) was measured by an ELISA Reader (TECAN).

3.2.2 Preparation of urinary exovesicles

Exosomes (and a minor proportion of other plasma membrane-derived vesicular material) were separated from 200ml urine by differential centrifugation at 4°C. The urine samples were initially filtered through Whatman filters and then centrifuged at 10.000 x g for 30min. This step was repeated to remove pelleted material, which was accidentally transferred during removal of the supernatant. In the next step the supernatant was ultracentrifuged at 114.000 x

g for 90min. The pelleted exovesicles were suspended in 200µl PBS and transferred into 1.5ml tubes for a final ultracentrifugation at 135.000 x g for 60min. The exovesicles obtained by this centrifugation step were stored frozen at -20°C.

3.2.3 Electron microscopy of exovesicular preparations

A Formvar[®] coated copper grid was placed on the exosome containing suspension for 30 minutes to allow adhesion of exosomes. Then the grid was shifted to a drop of fixative for 15 min. followed by washing 5 times for 1min in 0.1M PBS (after each washing step excessive liquid was removed with filter paper). Afterwards, the grid was applied to a solution containing 2 % uranylacetate for approximately 90s, washed 3 times on aqua bidest. for 1min. Finally, the excessive liquid was removed using filter paper. Thereafter, the grid dried at room temperature.

3.2.4 Isolation of Tamm-Horsfall protein

Exovesicle-depleted and neutralized urine was further processed for the isolation of Tamm-Horsfall protein (THP) by filtration over a layer of 20g diatomaceous earth as described by Serafini-Cessi et al. [25]. Loading excessive protein in SDS gel electrophoresis the presence of only small amounts of contaminating proteins was revealed, which were however identified as unglycosylated (protein identification by LC-MS/MS (Fig. 32 Attm. p.86) of tryptic peptides as described in [26]. For analysis of N-linked glycans on THP, the protein was digested in-gel after gel electrophoresis and the eluted glycopeptides were treated with PNGaseF (see below). In-gel digestion with trypsin was performed under standard conditions as applied in proteomics workflows [26]. The (glyco-) peptides were eluted into two aliquots of 0.5ml acetonitril in water (50 %) with rotation for 2 x 2h at RT. The eluate was heated to 90°C for 10min. to compensate residual protease activity and dried by vacuum rotation prior to addition of PNGaseF.

3.2.5 Release and purification of N-linked glycans

N-linked glycans were released from the protein cores by digestion with PNGaseF. In detail, the samples (exovesicles or THP, each corresponding to 10-100µg protein, or tryptic glycopeptides from in-gel digestion) were taken up in 50µl 50mM ammonium bicarbonate buffer, pH 8.5, and briefly sonicated. PNGaseF (NEB, 250 U) was added and the reaction mixture was kept at 37°C for 16h. After drying by vacuum rotation the glycans were solubilized in 0.1 % aqueous trifluoroacetic acid (100µl) and separated from residual protein/peptides by passage over BondElutC18 (Variant/Agilent, 100mg, column) and washing off with 0.9 ml 0.1 % TCA. The procedure was followed by derivatisation and mass spectrometry (see below). The whole flow chart is schematically represented in Fig. 12 N-glycosylation of exosomes (Attm. p.72)

3.2.6 Derivatization of N-linked glycans

The methylation procedure started after extensive drying of the sample by vacuum centrifugation followed by vacuum drying in a desiccator over P₂O₅/KOH for one hour. All procedures were performed in argon atmosphere. To the dry sample 100µl of alkaline (2.5 %, w/v, finely dispersed NaOH in dry DMSO) was added. The sample was briefly sonicated for 1 – 2min. and incubated for 3 min. at RT with occasional shaking. Finally, an aliquot of 50µl methyl-iodide was pipetted to the frozen reaction mixture followed by incubation for further 30-60min. at RT. Prior to the extraction step the reaction mixture can optionally be neutralized with 40µl of 1 M acetic acid. Extraction of methylated glycans was performed by stepwise addition of 0.3ml chloroform and 0.2ml bidest. water. After vigorous mixing and phase separation, the water layer was removed and repeatedly replaced by at least four further aliquots of 0.2ml. The chloroform phase was dried under nitrogen and the glycans were solubilized in methanol prior to application onto the MALDI target.

3.2.7 MALDI-TOF-TOF mass spectrometry of methylated glycans

Matrix-assisted laser desorption ionization (MALDI) mass spectrometry was performed on an UltrafleXtreme instrument (Bruker Daltonics, Bremen, Germany). The permethylated glycans

(approx. 500ng) resuspended in 20µl methanol were applied to the stainless steel target by mixing a 0.5µl aliquot of sample with 1.0µl of matrix (saturated solution of 2,5-dihydroxy benzoic acid in ACN / 0.1 % TFA, 1:2). Analyses were performed by positive ion detection in the reflectron mode. Ionization of crystallized analytes was induced with a pulsed Smart-beam laser (accumulation of about 5.000 shots) and the ions were accelerated in a field of 20kV and reflected at 23kV.

3.3 Differential proteomics by application of the i-TRAQ-technology

3.3.1 Preparation of lipid rafts out of urinary exovesicles

Exosomal lipid rafts were separated from 200ml urine by differential centrifugation and incubation with Triton X-100 at 4°C. The urine samples were initially filtered through Whatman filters and then centrifuged at 10.000 x g for 30min. The centrifugation step was repeated once. Eight centrifugation bottles (V = 26ml, Beckmann Ti 60 rotor) were layered with 2.6ml of 10 % Triton X-100 and filled up to a volume of 26ml to a final concentration of 1 % Triton X-100. The samples were incubated for 30 min. on a rotator at 4°C. The next step was an ultracentrifugation at 114.000 x g for 90min. The pelleted exosomal vesicles were suspended in 200µl cold PBS (4°C) combined and transferred into 1.5ml tubes for a final ultracentrifugation at 135.000 x g for 60min. (4°C). The pelleted exosomal lipid rafts obtained by this centrifugation step were stored frozen at -20°C after removal of nearly all aqueous supernatant with a pipette.

3.3.2 Protein quantitation in the context of i-TRAQ experiments

To the stored pelleted samples 100µl cold PBS was added the samples were sonicated on ice with three strokes at lowest energy level. The amount of protein was quantified using the standard Lowry DC assay. An aliquot equivalent to 50µg protein was chloroform/methanol precipitated, the pellet air dried for 10 minutes and further processed by filter-aided sample preparation (FASP).

3.3.3 Chloroform / methanol-precipitation

Proteins were precipitated by methanol/chloroform precipitation as follows:

One volume of sample was mixed with four volumes methanol, one volume of chloroform and 3 volumes of ddH₂O. After centrifugation at 16.100 g for 10 min. the aqueous phase was removed without disturbing the protein-containing interphase. Four volumes of methanol were added, the sample was mixed thoroughly and again centrifuged at 16.100 g for 10 min.

The supernatant was removed and the pellet air dried for 10min.

3.3.4 Filter assisted sample preparation (FASP)

A volume of 20µl 125 mM Tris HCl pH 6.8, 4 % SDS, 20 % glycerol was added to the air dried sample. To lyse proteins, 2µl 1M dithiothreitol were added, the samples were heated to 96°C for 10min, cooled down to ambient temperature and sonicated 3 x 10sec. After centrifugation at 14.000rcf for 5min. at 20°C the supernatants were transferred to Amicon Ultra™ centrifugal filter units (0.5ml, 10K). Filter assisted sample preparation (FASP) with sequential Lys C (40ng/µl) and trypsin (10ng/µl) digestion was performed according to Wisniewski et al. [27] with minor modifications: Briefly, apart from the initial lysis buffer, 0.1M TrisHCl was replaced by 0.1M triethylammonium bicarbonate (TEABC) pH 8.5 in all buffers used. After digestion the samples were centrifuged and filtrates were collected. 60µl 10 % acetonitril in water were added to the filter, mixed with the residual sample and the units were centrifuged once more. Combined filtrates were applied to C18 Pepclean™ spin columns (Thermo) activated with 80 % acetonitril and equilibrated to 0.1M TEABC. The absorbed sample was washed two times with 100µl 0.1M TEABC and desalted peptides were eluted with 20µl 80 % acetonitril in 0.1M TEABC.

3.3.5 iTRAQ labeling

Sample volumes were reduced to approximately 10µl in a centrifugal evaporator, 15µl of 1M TEABC were added and volumes were adjusted to 30µl with bidest. water. iTRAQ reagents (AB Sciex) were dissolved in 70µl ethanol and mixed with the corresponding samples immediately. After 2h incubation at ambient temperature in the dark, labeled samples were combined and desalted using a PepClean™ spin column as described above. However, 0.1M TEABC was replaced by 0.1 % formic acid in all steps. After salt removal, samples were dried in a centrifugal evaporator and resuspended in 50µl of 40 % acetonitril in 0.1 % formic acid. SCX tips were prepared with 1mg BioBasic 5µm SCX resin (Thermo) packed into a 200µl C8 StageTip. Samples were loaded onto a SCX tip equilibrated in 40 % acetonitril in 0.1 % formic acid. After washing with 2 x 20µl equilibration buffer, peptides were eluted with 20µl 0.5M sodium chloride, 40 % acetonitril in 0.1 % formic acid. Acetonitril was removed by brief vacuum centrifugation and samples volumes were adjusted to 20µl with 0.1 % TFA.

3.3.6 MALDI Spotting

Peptides were separated by reversed phase HPLC on an Eksigent nanoLC 1D plus system (Axel Semrau GmbH, Sprockhövel, Germany) using a vented column setup comprising a 0.1-mm-by-20-mm trapping column and a 0.075-by-200-mm analytical column, both packed with ReproSil-Pur C18-AQ, 5µm (Dr. Maisch, Ammerbuch, Germany) and operated at 40°C. 18µl sample were aspirated into the sample loop and a total of 30µl was loaded onto the trap column using a flow rate of 6µl/min. Loading pump buffer was 0.1 % TFA. Peptides were eluted with a gradient of 5 % to 35 % acetonitril in 0.1 % TFA over 70min. and a column flow rate of 300nl/min. 0.7mg/ml alpha-Cyano-4-hydroxycinnamic acid (HCCA) in 95 % acetonitril in 0.1 % TFA, 1mM ammonium phosphate were fed in using a syringe pump operated at 150µl/h and a post column T-union. 384 fractions (10 seconds) were deposited onto a MTB AnchorChip 384-800™ MALDI target (Bruker Daltonics, Bremen, Germany) using a Probot™ (Dionex, Idstein, Germany) fraction collector.

3.3.7 LC-MALDI MS/MS analysis

MALDI MS and MS/MS analysis were carried out on an Ultraflextreme™ MALDI-TOF/TOF mass spectrometer (Bruker Daltonics) operated with a laser repetition rate of 1 GHz. The process of data acquisition was controlled by Flexcontrol 3.0 and WarpLC. MALDI MS spectra were acquired over a mass range from 700Da – 4.000Da. Spectra were calibrated externally using the Peptide Calibration Standard II (all Bruker Daltonics) on the designated target calibration spots. The laser was used with a fixed energy setting and 3.000 shots / spectrum were collected from random raster points. Precursor ions with a signal to noise ratio equal or better than 10, were chosen for MS/MS analysis. Identical peaks in adjacent spots were measured only once, generally from the spot with maximum peak intensity. The software was programmed possibly not to take more than 20 MS/MS spectra from one spot. However, this is a “soft” value that was exceeded if no alternative positions were available. Polymer signals and peaks appearing in more than 40 % of all spots were filtered out. MS/MS spectra (3.500 shots) were acquired with the instrument calibration and iTRAQ reporter ions as well as peptide immonium ions were used for internal recalibration.

3.3.8 Database Searches

MASCOT 2.2 (Matrix Science Ltd, London, UK) was used to search a composite decoy database which was built from the UniProt database (August 10th 2010, 519348 sequences; 183273162 residues). The composite database was generated with the Perl script makeDecoyDB (Bruker Daltonics, Bremen, Germany) which added a shuffled sequence and a tagged accession number for each entry. The tagged accessions were used for the calculation of false positive rates in Proteinscape 2.1. Searches were submitted via Proteinscape (Bruker Daltonics, Bremen, Germany) and the following parameter settings: enzyme “trypsin” with 1 missed cleavage; species “human”; fixed modifications “carbamidomethyl”, “iTRAQ4plex (K)”, “iTRAQ4plex (N-term)”; optional modifications “Methionine oxidation”, “iTRAQ4plex (Y)”. The mass tolerance was set to 20ppm Da for MS and 0.8Da for MS/MS spectra. Protein lists were compiled in Proteinscape. Peptide hits were accepted when the ion score exceeded a value of 20. Protein hits required at least one peptide hit exceeding a peptide score of 30. In addition, the hits to decoy entries were used to calculate a minimal protein score which is required to keep the false positive rate below 2 % on the protein level [28].

3.4 Identification of exosomal vesicles by detection of marker proteins in density gradient fractions

3.4.1 Preparative gradient centrifugation of urinary vesicles

Exosomes (and a minor proportion of other plasma membrane-derived vesicular material) were separated from 200ml urine by differential centrifugation at 4°C. The urine samples were initially filtered through Whatman filters and then centrifuged at 10.000 x g for 30min. This step was repeated to remove pelleted material, which could be accidentally transferred during removal of the supernatant. In the next step the supernatant was ultracentrifuged at 114.000 x g for 90min. The pelleted exovesicles were suspended in a total volume of 400µl in PBS and layered on top of a sucrose gradient. The gradient 5-45 % sucrose was generated using a gradient mixer. The gradient was prepared in 8.5ml tubes (SW41) for a final ultracentrifugation at 114.000 x g for 4h. The exovesicles were collected in six fractions (1.4ml) by the use of an electric pump. The fractions were diluted with PBS and finally centrifuged in 8.5ml tubes (SW41) 200.0000 x g for 1.5h. The pellet was suspended in Laemmli buffer and applied on SDS-PAGE.

3.4.2 Detection of exosomal marker proteins by Western blot

Exosomal lipid rafts were prepared as described above by gradient centrifugation at 114.000 g and a final washing step. SDS-buffer was added to dissolve the proteins from rafts and the sample was heated to 70°C for 15min. The samples were centrifuged at 13.000rpm at 4°C for 5min. Supernatant was stored at -20°C or subsequently loaded onto SDS-PAGE (4 % stacking gel, 5–20 % gradient running gel) in a Mini Protean 3 cell (BioRad, Munich, Germany). The gel was equilibrated in transfer buffer (20M glycine, 24mM Trizma-base, 20 % methanol) before it was wet-blotted (BioRad) onto a nitrocellulose membrane (Schleicher and Schuell, Einbeck, Germany) at 90mA overnight. Thereafter, the membrane was blocked in TBS containing 5 % non-fat dried milk and 0.1 % Tween 20 for 1h at room temperature (RT) before incubation with the primary antibody (overnight at 4°C). Immunocomplexes were labeled with HRP-conjugated secondary antibody and detected using a Lumilight Kit (Roche). Between each incubation step, the membrane was washed three times with TBS (20mM Tris-HCl, 137mM NaCl, pH 7.6). Exosomes were isolated as described in section 3.2.2

(Preparation of urinary exosomes). For Western blotting, exosomes were heated for 15min. at 70°C in SDS-buffer, following the same procedure described above.

3.4.3 Antibodies

Primary antibodies: anti-MUC1, C595 IgG (mouse monoclonal IgG), 1.1mg/mL, kindly provided by Dr. M. Price, Cancer Research Laboratory, University of Nottingham, Nottinghamshire, UK; anti-flotillin-2, sc-28320, Santa Cruz Biotechnology (mouse monoclonal IgG); anti-Hsp70, 3C5 hybridoma, (mouse monoclonal IgG), kindly provided by workgroup Prof. Höning, Cologne; anti- β -actin, A5316, Sigma (mouse monoclonal IgG); anti- α -tubulin, T5168, Sigma (mouse monoclonal); anti-G α subunit, sc-262, Santa Cruz Biotechnology (rabbit polyclonal IgG); anti-glyceraldehyde-3-phosphate dehydrogenase (GAPDH), MAB374, Chemicon (mouse monoclonal IgG); anti-alix, sc-166952, Santa Cruz Biotechnology (mouse monoclonal IgG), anti-hsp27, sc-13132, Santa Cruz Biotechnology (mouse monoclonal IgG); anti-CD81, sc-7637 Santa Cruz Biotechnology (mouse monoclonal IgG); anti-cav-1, sc-894, Santa Cruz Biotechnology (rabbit polyclonal IgG); anti-EGFR, sc-1005, Santa Cruz Biotechnology (rabbit polyclonal IgG). Secondary antibodies: Rabbit anti-mouse IgG, HRP (P0260/Dako, Hamburg, Germany); swine anti-rabbit IgG, HRP (P0399/Dako).

4. Results

4.1. Vesicle classification by electron microscopy and exosomal marker proteins

Besides exosomes the exovesicle fraction of human urine possibly contains other types of vesicular material derived from epithelial plasma membranes of the urothelium, apoptotic blebs (AB), microparticles (MPs) or microvesicles (MVs)[12]. Exosomes comprise vesicles with a size of 40-100nm while microvesicles are generally larger, ranging between 100 and >1000nm. Differing from exosomes the microvesicles bud directly from the plasma membrane. MVs were described as vesicles secreted as response to biological stimuli which could partially overlap in size with exosomes and MPs [12]. Furthermore MPs with a size of 100-1000nm are larger than exosomes.

In this study electron microscopy of crude exovesicle fractions from human urine revealed exosome-like, cup-shaped vesicles in the expected size range (Fig. 13).

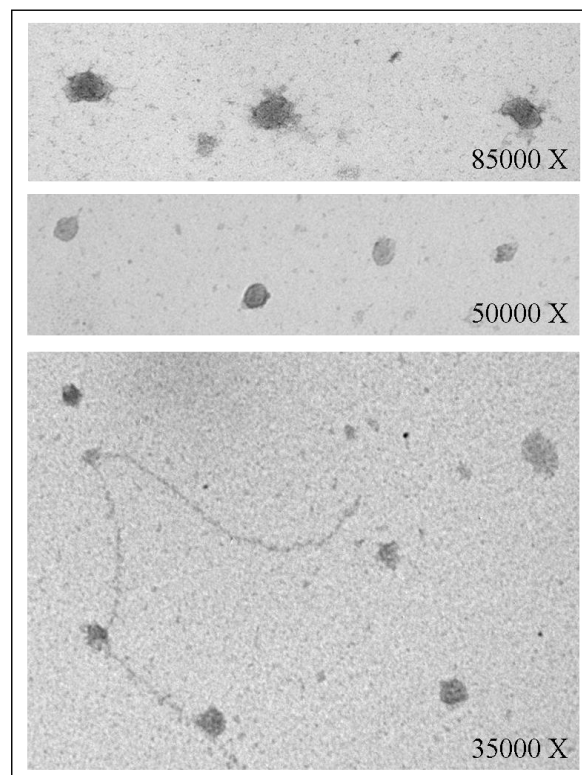


Fig. 13: Electron micrograph of exovesicular preparations from human urine demonstrating the preponderant presence of exosomes (upper and middle panel) and the binding of exosomes to polymerized THP (lower panel).

Western blot analyses of marker proteins, like alix, exclusively belong to the endocytic pathway *via* MVBs (Fig. 14 Attm. p.73) and confirmed the presence of exosomes.

At this point reference to the differential proteomics experiments is made (see Tab. 4a Attm. p.90) which revealed a series of further marker proteins exclusively found in the exosomal pathway. The detection of genuine raft proteins, MVB proteins (e.g. Tsg101, or vacuolar sorting proteins), lysosomal proteins and many exosome associated proteins, leads to the conclusion that in fact mostly exosomal vesicles were enriched from the urine samples.

In previous studies exosomes were often found to adhere to filamentous structures [22], which arise from THP polymerization via disulfide linkage from inside the *zona pellucida* domains. This phenomenon likely explains the contamination of exovesicular proteins by THP (see Fig. 13 p.37 and Fig. 15 Attm. p.74). Filtered exovesicular fractions (cut-off at 100nm), which were depleted of MPs, revealed similarly high THP contaminations, but drastically reduced yields and a membrane fragmentation was observed (Fig. 16 Attm. S.75). Western blots of fractions from a density gradient centrifugation demonstrated that the exovesicles from human urine preferentially co-migrate with high-density fractions characterizing the buoyant density of exosomes and were positive for a variety of exosome characteristic marker proteins (Fig. 14 Attm. p. 73). Irrespective of these findings, this report refers only to urinary exovesicles (without further specification) as an easily accessible source of material from patient-derived epithelial membranes.

4.2 N-glycosylation of exosomes

4.2.1 Differential N-glycomics of the urinary exovesicles from galactosemia patients and healthy controls

Exovesicles prepared from 100ml of human urine were measured to contain an average of about 200 μ g protein (with individual fluctuations between 60 and 600 μ g). Enzymatically cleaved N-linked glycans were estimated by reference to an internal standard (lacto-N-fucopentaose I) to make up 0.5-5 μ g per 100 μ g of protein. The permethylated glycans were analysed by MALDI-TOF and TOF/TOF mass spectrometry to permit insight into the patterns of N-linked chains based on molecular masses and the calculated monosaccharide compositions in terms of Fuc (F), Hex (H), HexNAc (N), or NeuAc (S) and based on fragment masses (sequence information from protonated B-type ions according to the nomenclature of Domon and Costello [29]). In figure 17 and 18 two representative survey

spectra of methylated N-glycans from a galactosemic patient and from a healthy control individual are shown:

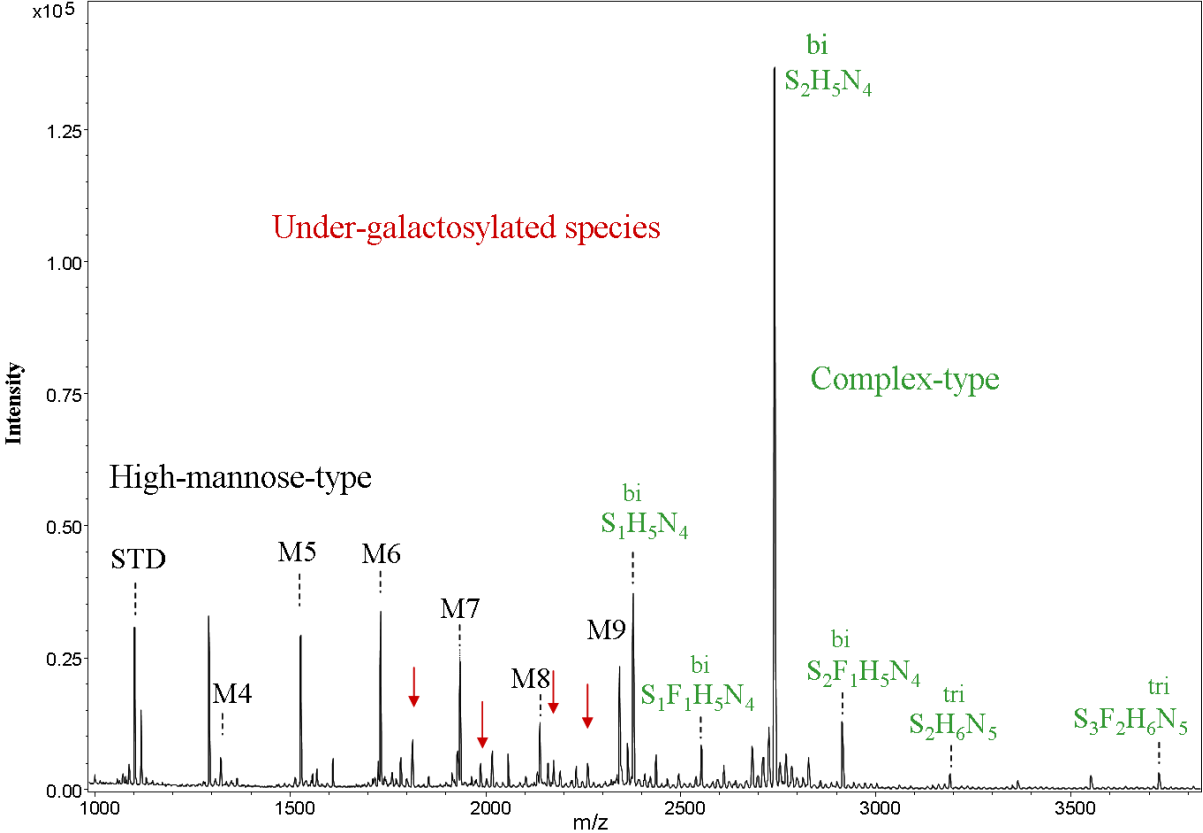


Fig. 17: MALDI mass spectrum exosome derived N-glycans of a galactosemic patient

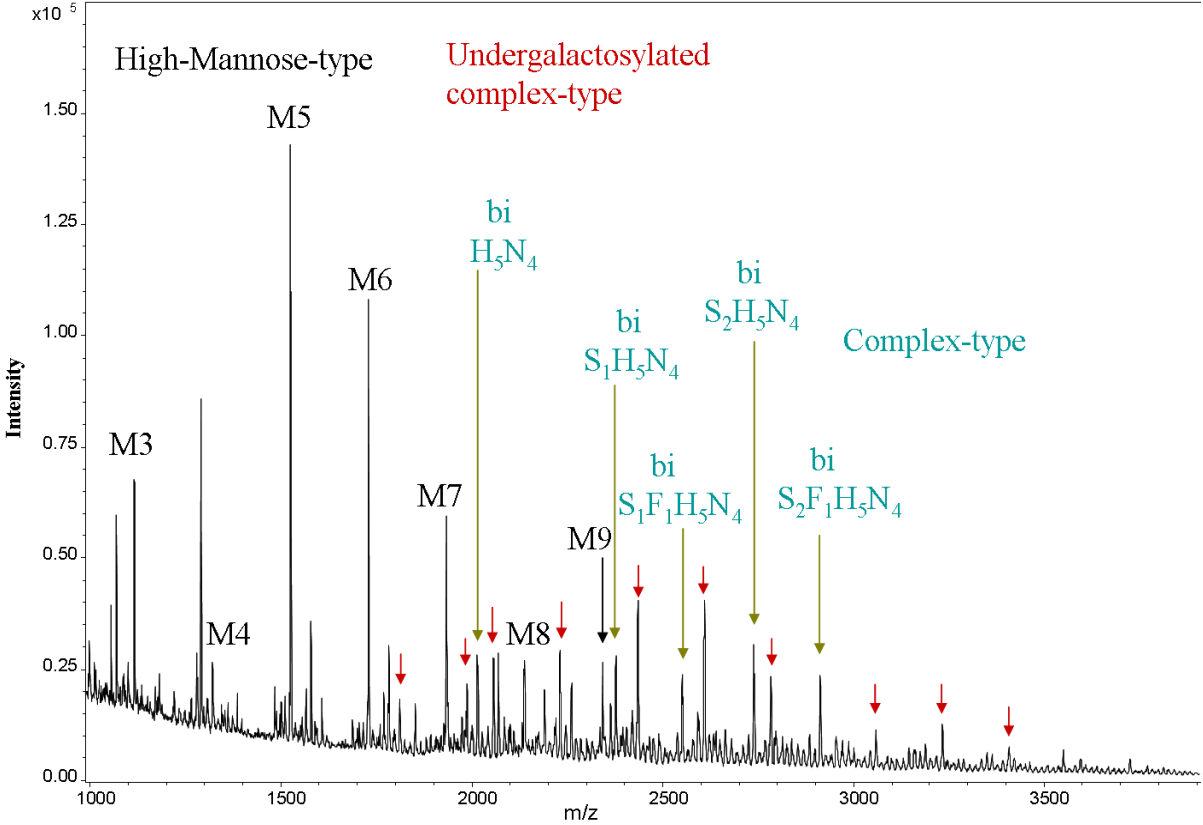


Fig. 18: MALDI mass spectrum; exosome derived N-glycans of a healthy persons

Fig. 17/18: Representative MALDI mass spectra of permethylated N-glycans from urinary exovesicles of GALT-deficient patients and healthy control subjects

Mass signals corresponding to a calculated composition of $H_{3+n}N_2$, with $n = 0-6$ represent high-mannose-type glycans M3 to M9; mass signals corresponding to a calculated composition of H_nN_n (with $n>3$) represent undergalactosylated complex-type species, and mass signals corresponding to a composition of $H_{3+n}N_{2+m}$, with $n = 1-4$, $m = 2-4$ represent complex-type N-glycans. Major signals correspond to the sodium adducts $M+Na$ that have lost $NaOCH_3$. STD refers to the internal standard LNFPI.

4.2.2 High-mannose and complex-type N-glycans

The mass spectrometry patterns of N-linked glycans on urinary exovesicles were characterized by the presence of two classes of chains, the high-mannose-type glycans comprising mostly M4 to M9, and the complex-type glycans, which were predominantly of the bi-antennary subtype A2 without core-fucosylation (Fig. 19 Attm. p.76). Other subtypes were undergalactosylated complex-type species with GlcNAc terminating antennae and glycans of higher antennarity. Qualitatively, the patterns revealed for GALT-deficient patients and the respective healthy controls overlapped to a large extent. On quantitative evaluation of the data, which were based on the summarized signal intensities for high-mannose-type glycans ($H_{3+n}N_2$, with $n = 0-6$) and complex-type glycans ($H_{3+n}N_{2+m}$, with $n = 1-4$, $m = 2-4$) exovesicles from healthy controls showed patterns of N-glycans that were dominated by high-mannose-type *vs.* complex-type glycans (ratio about 3:1) (Table 1 see below).

Table 1

Relative amounts of High-mannose- and Complex-type N-glycans in exovesicular membranes from galactosemic patients and healthy control subjects

Galactosemic patient		1	2	3	4	5	6	
N-linked Glycans		m/z	%	%	%	%	%	
High mannose		1322	4,43	2,73	9,52	6,64	6,99	4,78
		1526	16,93	9,77	19,58	12,50	16,41	12,97
		1730	16,13	27,73	20,37	10,55	29,18	11,60
		1934	10,08	7,81	7,14	4,69	6,08	5,46
		2138	4,03	1,17	3,17	2,34	2,13	4,44
		Σ	51,6	49,21	59,78	36,72	60,79	39,25
Complex type		2378	8,06	17,19	12,17	12,50	13,98	14,33
		2552	4,44	3,52	3,44	3,13	1,82	11,60
		2739	29,4	17,58	18,52	39,84	17,93	22,53
		2913	5,64	3,52	2,65	5,08	1,82	8,53
		3188	0,4	6,64	2,65	1,56	3,34	2,39
		3724	0,4	2,34	0,79	1,17	0,30	1,37
		Σ	48,34	50,79	40,22	63,28	39,19	60,75

Galactosemic patient		7	8	9	10	11	12	
N-linked Glycans		m/z	%	%	%	%	%	
High mannose		1322	7,73	10	9,04	8,30	10,26	8,06
		1526	14,49	8,75	18,81	12,91	34,38	22,82
		1730	12,08	17,5	9,76	8,75	8,92	18,79
		1934	4,83	7,5	2,53	2,50	2,09	6,71
		2138	3,38	2,5	2,71	2,92	3,80	2,68
		Σ	42,51	46,25	42,85	35,38	59,45	59,06
Complex type		2378	13,53	15	11,21	13,33	6,93	12,08
		2552	10,63	10	3,98	2,91	2,85	4,03
		2739	13,53	16,25	36,89	42,08	24,98	24,83
		2913	12,56	6,25	3,62	5,00	2,94	0,00
		3188	4,35	3,75	0,54	0,41	1,71	0,00
		3724	2,90	2,5	0,90	0,83	1,34	0,00
		Σ	57,50	53,75	57,14	64,56	40,75	40,94

Healthy control		1	2	3	4	5	
N-linked Glycans		m/z	%	%	%	%	
High mannose		1322	3,59	6,51	5,04	1,83	4,73
		1526	34,08	29,99	30,56	7,93	23,67
		1730	22,87	23,20	22,85	62,80	23,27
		1934	10,31	11,32	12,46	7,93	14,60
		2138	4,93	4,81	5,34	0,61	7,30
		Σ	75,78	75,83	76,25	81,10	73,57
Complex type		2378	6,28	3,96	5,64	3,05	7,10
		2552	2,69	6,51	4,75	4,88	4,34
		2739	11,21	5,37	6,23	1,83	6,70
		2913	1,79	6,51	4,75	3,66	5,52
		3188	1,79	0,71	1,48	3,05	1,58
		3724	0,45	1,13	0,89	2,44	1,18
		Σ	24,21	24,19	23,74	18,91	26,42

% = ratio of single peak intensities to total listed peak intensities. m/z-values correspond to the molecular ions M+ Na (-54). Only major signals were considered in the quantitative evaluation.

Contrary to this, GALT-deficient patients expressed dramatically increased proportions of complex-type chains on exovesicular glycoproteins with a ratio of about 1:1 (Fig. 20).

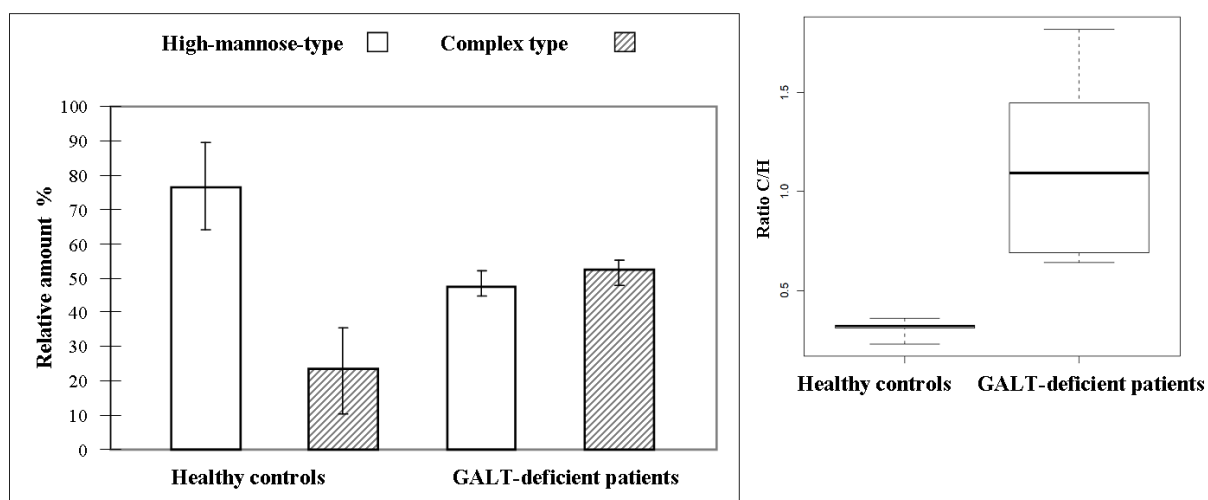


Fig. 20: Column diagram showing relative amounts of high-mannose-type vs. complex-type.

N-glycans on urinary exovesicular membranes from GALT-deficient patients and healthy controls.

Left panel: column diagram of relative amounts of high-mannose-type and complex-type N-glycans with indicated standard deviations; right panel: box-and-whisker plot of the ratio of relative amounts of complex-type vs. high-mannose-type N-glycans. The box indicates the lower and upper quartiles and the central lines are the medians. The points at the ends of the whiskers show the 2.5% and 97.5% values (centiles). Healthy controls, n = 5; GALT-deficient patients, n = 12.

The shift of relative amounts of complex-type vs. high-mannose-type glycans from 0.32 to 1.08 (factor: 3.4) can be regarded as even underestimated due to the presence of THP in exovesicular fractions, which is shown in this study to be glycosylated preponderantly with high-mannose-type glycans in patients and healthy controls. The presence of THP in exovesicular preparations however did not strongly influence the ratios of complex- vs. high-mannose-type glycans in samples with high or low THP content (Suppl. Tab. 1 p.88). The variations of ratios (complex-type vs. high-mannose-type glycans) measured for independent urine samples from individual healthy control subjects were only small (Suppl. Tab. 2 p.89).

4.2.3 Bi-antennary complex-type glycan, the most abundant structure

The most dominant complex-type glycans from exovesicular membranes of GALT-deficient patients were of bi-antennary structure and lacked core fucosylation (Fig. 17 p.39). Only trace amounts of structures with higher antennary branching were found. There was a considerable fraction of N-glycans with complex-type structure that had a monosaccharide composition of

H_nN_n (with $n = 4$ or 5) and fluctuated from 15 % to 30 % between individual samples in that fraction. These compositions indicate the presence of under-galactosylated species, which were however found in both sample series from GALT-deficient patients and healthy controls without obvious quantitative correlation with one of the sample groups. The structures of the major components in the fractions of N-linked glycans were corroborated by MALDI-TOF-TOF MS2 analysis (representative examples shown in Fig. 21/22 (see below)). The $M+Na$ (-54) species (loss of sodium methylate) fragment under laser-induced dissociation conditions similar to the protonated MH species, which yield preferentially B-type proton adduct ions from the non-reducing terminal of the glycans in all MS2 spectra. Fragmentation by post-source decay is preferred at C1-O bonds of HexNAc moieties explaining the restricted set of B ions.

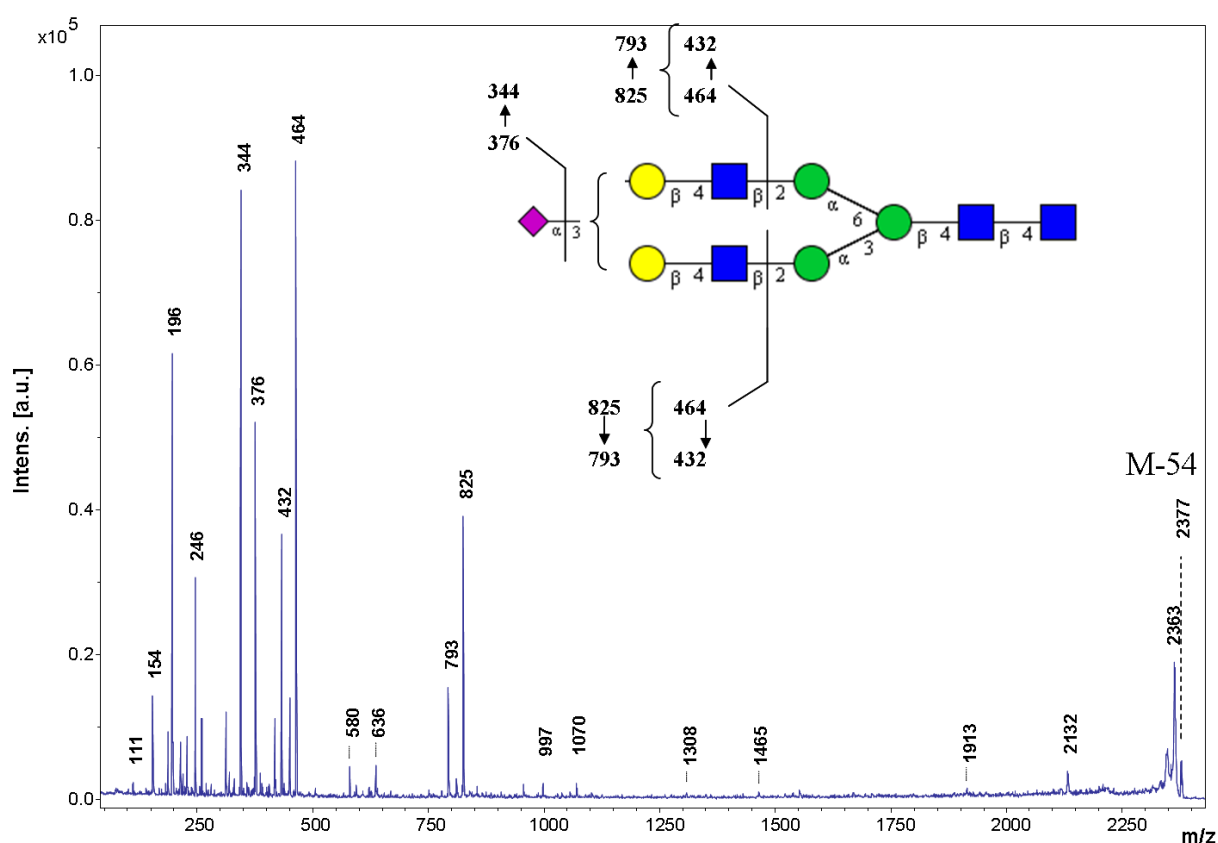


Fig. 21: MS2 spectrum of the monosialylated bi-antennary complex-type N-glycan registered at the precursor ion mass ($M+Na$) at m/z 2377

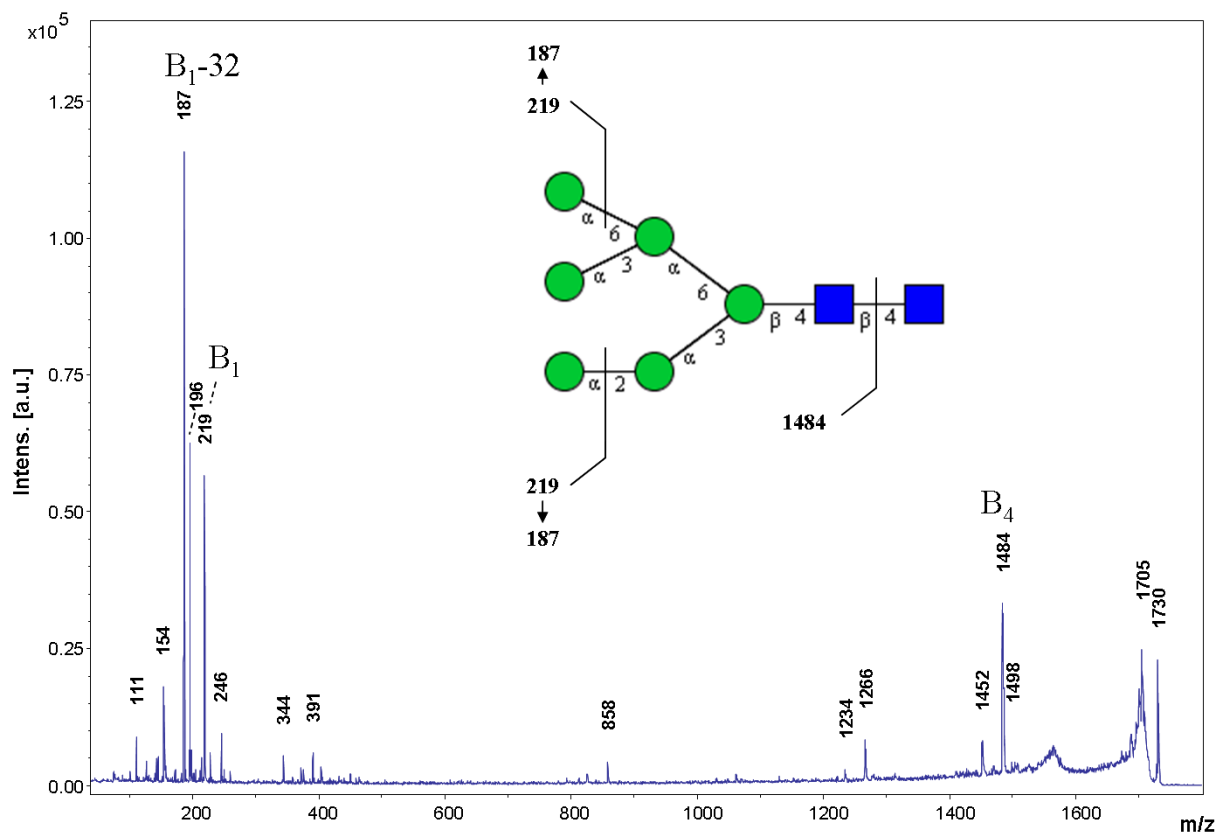


Fig. 22: MS2 spectrum of the high-mannose-type N-glycan M6 registered at m/z 1730

4.3 The GPI-anchored transmembrane Tamm-Horsfall Protein

4.3.1 N-Glycosylation of urinary Tamm-Horsfall Protein (THP)

The analysis of urinary THP, the major N-glycoprotein shed exclusively by epithelial cells of the thick ascending limb of Henle's loop (TALH) and of the distal convoluted tubule lumen (UniProt), offers the chance to get independent evidence on disease-related alterations in cellular N-glycosylation of proteins. However, there is also a necessity to characterize the N-glycoprofiles of this protein, since it generally forms a major protein component of exovesicular preparations from urine due to its adherence to the outer surface of exovesicles as a long filamentous protein polymer (Fig. 13 p.37). These THP polymers have been claimed to be removable under strong denaturing conditions [22], which was however not confirmed in our hands. We used DTT, 200mg/ml at 37°C, 10min. to remove THP from complete exosomes and exosomal lipid rafts (Fig. 23 Attm. p.77). We compared fresh isolated exosomal samples of a healthy person with stored samples (-20°C) of a galactosemia patient. Both samples exhibit high amounts of THP in the untreated samples (shown in line 1 and 4). The DTT treated samples (lines 2 and 5) show a decrease of THP, which was however not

removed completely. Also after addition of TritonX-100, a detergent often used in the preparation of exosomal lipid rafts (lines 3 and 6), the samples still exhibit strong THP contamination after DTT treatment. The results suggest DTT does not completely remove THP, it merely reduces the amount slightly. The THP contamination is also independent of the preparation route starting from fresh or thawed urine. Both samples, either from healthy controls or from galactosemia patients, contained THP and it adhered strongly to the exosomes.

4.3.2 Validation of predominant high-mannose-type N-glycosylation of exosomal lipid raft associated THP

Coomassie-stained SDS-gels of exovesicular proteins display THP as a major contaminant, which could have impact on the measured glycoprofiles. For this reason we analyzed the N-glycans on THP separated from whole exosomal lipid raft samples, of patients as well as controls, by in-gel trypsin digestion of the electrophoretically separated protein, followed by elution of the glycopeptides and PNGaseF catalyzed liberation of the N-linked glycans. In contrast to the total exovesicular membranes, THP was characterized by the predominant expression of high-mannose-type N-glycans (Fig. 24/25 Attm. p.78/79). Throughout the M6 isoform was most dominant, which is in agreement with earlier studies on THP glycosylation [30]. The N-glycosylation pattern of THP showed no major individual fluctuations and was unchanged in samples from patient urine (Table 2 see below). These data strikingly support the validity of the above described N-glycosylation shifts on exovesicular membranes, since the contaminating THP can only contribute to the pool of high-mannose-type chains in samples, but cannot be responsible for the dramatic increases of complex-type chains (Table 1 p. 41).

Table 2

Relative Amounts of High-Mannose- and Complex-Type N-Glycans on Urinary THP from Galactosemic Patients and Healthy Control Subjects

Galactosemic patient		1	2	3	4	5
N-linked Glycans	m/z	%	%	%	%	%
High mannose type	1322	8,6	6,0	15,9	7,5	7,7
	1526	20,3	16,8	32,7	22,6	27,3
	1730	57,5	68,8	34,1	54,9	56,9
	1934	7,4	6,4	12,0	6,0	7,7
	2138	6,2	0,0	5,3	0,9	0,0
	Σ	100,0	98,0	100,0	91,9	99,6
Complex type	2378	0,0	2,0	0,0	3,1	0,4
	2552	0,0	0,0	0,0	5,0	0,0
	2739	0,0	0,0	0,0	0,0	0,0
	2913	0,0	0,0	0,0	0,0	0,0
	3188	0,0	0,0	0,0	0,0	0,0
	3724	0,0	0,0	0,0	0,0	0,0
Σ	0,0	2,0	0,0	8,1	0,4	

Healthy control		1	2
N-linked Glycans	m/z	%	%
High mannose	1322	5,78	7,47
	1526	14,05	16,95
	1730	60,33	62,64
	1934	7,44	11,49
	2138	0,00	0,86
	Σ	87,60	99,41
Complex type	2378	2,73	0,57
	2552	0,00	0
	2739	0,91	0
	2913	0,00	0
	3188	0,00	0
	3724	0,00	0
Σ	3,64	0,57	

% refers to the ratio of single peak intensities to sum of annotated peak intensities. m/z-values correspond to the molecular ions measured as M-54 (loss of sodium methylate). Only major signals were considered in the quantitative evaluation.

4.4 Differential proteomics of exosomal membranes

4.4.1. Isobaric tags for relative and absolute quantitation

Two samples of exosomal lipid rafts from galactosemic patients and two corresponding controls were analyzed by an in vitro technique (iTRAQ). The four samples were previously

applied on SDS-PAGE (Fig. 26 Attm. p.80). Remarkable was that the protein pattern of the two galactosemia samples were similar among each other. In the same way the samples of the healthy persons, but between healthy and galactosemia they were markedly different.

iTRAQ is based on the differential labeling of proteome-derived peptides isobaric mass tags. These mass tags generate reporter ion fragments in MS2, which are used for the quantification of the protein-derived peptides. We used an offline nano-LC-MALDI-TOF-TOF setting without intermediate prefractionation, since the proteome under analysis was of low to medium complexity. Statistical evaluation of the four data sets revealed high validity for both the protein identification (Mascot scores) as well as the regulation factors (coefficient of variation). More than 200 proteins were identified, among which only a minor fraction was assigned to be genuine exosomal proteins. A major portion of the proteins was either of serum origin (serum glycoproteins) or had a functional relationship with the extracellular matrix. Many identified genuine exosome (Tab. 4a p.90) as well as exosome associated (Tab. 4b p.91) proteins were detected in accordance with published data of urinary exosomes proteomics [15-16,31-32]. The proteins listed under MVB and lysosomal proteins (Tab. 4f p.95) are characteristically found in exosomes, even though these proteins were divided into subgroups to give a better overview.

Genuine exosomal lipid raft proteins, MVB and lysosome-associated proteins are slightly less than two-fold increased and are only rarely N-glycosylated. But alix, for example, was found in slightly reduced amount (Tab. 4e p.93) and we were able to validate this by Western blot (Fig. 27 Attm. p.81). Adversely, CD81 seems to be slightly more abundant in galactosemia (Fig. 27 Attm. p.81) and MUC1 expression was shown to be constant in several Western blots (Fig. 31 Attm. p.85). In contrast to the not markedly varying amounts of genuine exosomal proteins, there are many N-glycosylated proteins found in strongly increased amounts in patient-derived exosomes. All markedly increased proteins that are listed in Tab. 4b p.91 under the topic “Exosome-(assoc.)” carry N-glycans and most of them exhibit a function as membrane-integrated cell surface located protein (UniProt).

4.4.2 Proteins found increased

4.4.2.1 Serum proteins

As shown in Tab. 4c p.92, under subcategory “disease associated proteins”, the most abundant proteins are amylase, LRG1 (leucine-rich alpha-2-glycoprotein), fetuin,

prostaglandin, perlecan, alpha-1-microglobulin protein (AMBP) and serum albumin. All these proteins were connected in UniProt to TBMN/IgAN, proteinuria and renal damage. Even in healthy persons amylase could be measured in the blood serum and in low amounts in urine, yet it is only found more abundant in urine of renal failure. Only little information was found about LRG1 in UniProt. Li *et al.* detected the glycoprotein in urine as well [33] and suggests the protein as a biomarker candidate for detecting NSCLC (non-small cell lung cancer). At this research stage this assumption is not justified, because any cancer-associated changes are likely to be superimposed by renal failure-associated changes. Heo *et al.* noticed elevated glycoprotein levels in blood sera [34] (in human lung adenocarcinoma). Despite the devious marker function for cancer it seems to be a typical serum protein that could be found in high levels in renal failure. More abundant fetuin (alpha-2-HS-glycoprotein) is proposed to be a biomarker in urinary exosomes for detection of acute kidney injury (AKI), which has a high mortality and morbidity rate [35-37]. Proteinuria reveals significant reduced fetuin in the blood sera and increased in urine [37]. Prostaglandin is proposed to be a sensitive indicator of renal damage (UniProt), if found in large amounts in urine and serum. Its formation depends on renin secretion, renal regulation of sodium chloride balance and the control of blood pressure [38-40]. Perlecan (basement membrane-specific heparan sulfate proteoglycan core protein HSPG2) has been found in urine of patients with end-stage renal disease and in the amniotic fluid of pregnant women with premature rupture of fetal membranes (UniProt). Alpha-1-microglobulin protein (AMBP) is found to be one of six proteins which were able to discriminate endemic nephropathy (EN) with low and high proteinuria (<150mg/l) and high significance [36]. Serum albumin is a typical blood system protein and increased amount is a strong sign for kidney failure [36,41].

4.4.2.2 ECM-related proteins

We found a number of ECM-associated proteins: perlecan, agrin, collagen IV, biglycan, hemicentin and fibronectin. These proteins are all involved in ECM-assembly and thus in basement membrane assembly. Except collagen IV, all of them are N-glycosylated [42]. Glomerulus endothelial cells contribute importantly to the assembly of the glomerulus basement membrane (GBM) [43]

If N-glycosylation is changed, we probably have an influence on the basement membrane assembly of the glomerulus, thus we can expect disturbed cell adhesion and a heightened permeability of the filtration network, the clinical picture of renal failure.

4.4.3 Identification of exosomal raft proteins by LC-ESI of SDS-gel fractions

Exosomal lipid rafts were separated by gel-electrophoreses and four selected coomassie-stained gel fractions were excised (Fig. 33 Attm. p.87). Only gel fractions were excised that showed differences between galactosemic patients and controls. The LC-ESI-MS analysis revealed a large overlap with the iTRAQ data, but also identified a couple of proteins that had not been found in the differential approach (Fig. 29 Attm. p.83 yellow): The renin receptor, acid ceramidase, ladinin (an IgA binding protein), robo4, VP37B (a vacuolar sorting protein), CHM2A (a charged multivesicular body protein), RhoA (validated by WB as well), ARF1, tetranectin, RAC1, RAP1A, arylsulfatase, matrix-remodelling-associated protein 8, transgelin-2 and kallikrein to name some.

Obviously, the LS-ESI-MS analysis offers a higher sensitivity compared to the offline LC-MALDI approach, which however is the only applicable one in the context of iTRAQ-labelled peptides based on the equipment of the CMMC facility.

The aim of using the complementary LC-ESI technique was to recognize qualitative differences between galactosemia and healthy persons by comparing the protein pattern, to excise them from Coomassie-stained gel and identify them by LC-ESI after extraction out of the gel slices.

The top scores found by Mascot Search are perlecan (basement membrane-specific heparan sulfate proteoglycan core protein (PGBM)), serum albumin, tetranectin and inter-alpha-trypsin inhibitor heavy chain H4 (Fig. 29 Attm p.83). Supporting these results, perlecan was found to be more abundant *via* the iTRAQ experiment (6.4 fold, Tab. 4c p.92). It emphasizes again the essential and disturbed function of basement membrane assembly in galactosemia. The loss of perlecan at the glomerulus is probably associated with a decreased retention capacity and renal failure that is supposed to occur prematurely.

Serum albumin, the proteinuria marker, was found to have a high Mascot Score as well. The iTRAQ experiment offered a 4.8 fold abundance of the protein. Serum albumin is described for both a marker for insufficient glomerulus filtration and an overloaded protein dependent on reabsorption process (megalin-cubilin-complex) [23].

5. Discussion

5.1 A multitude of N-glycosylated proteins

The reason for finding such a great number of N-glycosylated proteins is probably that the origin of exosomes are membranous cellular lipid rafts and that membrane proteins often carry carbohydrate branches exposed to the extracellular space. A closer look at the exosomal membrane (EM Fig. 13 p.37 / zoom 85000 X) reveals that the exosomal surface is comparable to epithelial surface that exhibits the characteristic glycocalyx surface surrounding the membrane. Conclusively many glycoproteins were exposed at the exosomal surface.

Surface exposition and secretion of glycoproteins is a defence mechanism of epithelial cells that prevents bacterial contamination of the urinary system or the bloodstream in *E.coli*-sepsis [44]. Obviously disglycosylation could lead to failure of the defence mechanism against bacterial infiltration.

We determined a probable interdependence between N-glycosylation and increased protein amount. On the one hand, most of the detected N-glycosylated proteins are found in more than twofold amounts and, on the other hand, most of these proteins carry N-glycans. Surprisingly, high amounts of immunoglobulins were detected. Their respective amounts are increased more than twofold in galactosemia, and they mostly bear N-glycosylation. This elevation gravely hints at the clinical picture of renal failure, because serum proteins are not typical urinary proteins. Four most relevant diseases out of a multitude of renal failure diseases are related to this clinical picture: thin basement membrane nephropathy, IgA-nephropathy (IgAN) [45], acute kidney injury (AKI) [35] and proteinuria [41]. The UniProt database presents exemplary clinical symptoms as followed: kidney injury, renal damage, inflammation, dementia, amyloidosis, loss of myelin, GM1-gangliosidosis. All these symptoms are closely connected to galactosemia.

The normal size of filtrated molecules by the glomerulus is 6-15kDa. The intact glomerulus is impermeable for proteins greater than 80kDa, even for immunoglobulins, especially those that build di- and pentamers. The increased amount of immunoglobulins (Igs) that are found in Tab. 4c p.92 (disease associated proteins), lead to the assumption of an existing renal damage in galactosemic patients. An inflammatory response is possibly the cause of this damage. In IgAN, the IgA is embedded in the mesangial cells of the glomerulus that leads to inflammation [45]. Because of a defect in O-glycosylation (reduced glycosylation) the Igs adhere at the cell surface, they are not retained as usual due to their bulky carbohydrate

branches. Moreover, the disglycosylation leads to host recognition of the autoimmune system, and proinflammatory cytokine response.

Albumin (66-69kDa) exhibits a filtration coefficient of 0,001 and 96% of the protein, which passes the filter, is reabsorbed at the proximal tubulus. More abundant amounts of albumin in urine are related to an enlarged glomerulus pore coinciding with an overloaded reabsorption process.

The reabsorption process is ATP dependent and initiated by a megalin-cubilin-complex [23]. Both complex proteins were detected with top scores in the list of exosome associated proteins (Tab. 4b p.91). Cubilin, a membrane anchored protein, is able to interact with transferrin, apolipoprotein, albumin, Ig light chains and megalin. The transmembrane receptor protein megalin interacts even more strongly with lysozyme, amylase, epidermal growth factor, α -1-microglobulin (AMBP) and retinol binding protein for instance; those all were listed proteins in Table 4. Megalin (LRP2) is a LDL receptor, the C-terminus is believed to mediate endocytosis and apical sorting [23]. The endocytic pathway initiated by the megalin-cubilin-complex is proposed to be clathrin dependent.

5.2 Disglycosylation and targeting of glycoproteins

Evidence that the sorting for targeted trafficking of membrane glycoproteins to the apical plasma membrane is under partial control of N- and/or O-glycosylation has recently been provided [7]. Accordingly, it can be postulated that the expression of glycosylated receptors, like the epithelial growth factor receptor, EGFR, in membrane rafts requires specific glycan signals for (galectin-mediated [46]) entrapment in specific rafts [47]. A disglycosylation should have impact on these sorting and trafficking events and could result in a mislocalization of prominent membrane receptors with concomitant perturbations in the cellular signaling [48]. In a cellular model of GALT deficiency it has been shown that EGFR is actually lacking in lipid rafts, when the cells are grown under galactose stress (Fig. 30 Attm. p.84) [49].

Disglycosylation possibly affects basement membrane assembly. The nephridial glomerulus for example, needs correct basement membrane assembly to develop its full filtration capacity. For the correct assembly many glycoproteins interact stepwise to build up a network: perlecan, agrin, nidogen, fibronectin to name some (Fig. 34 see next p.) [42].

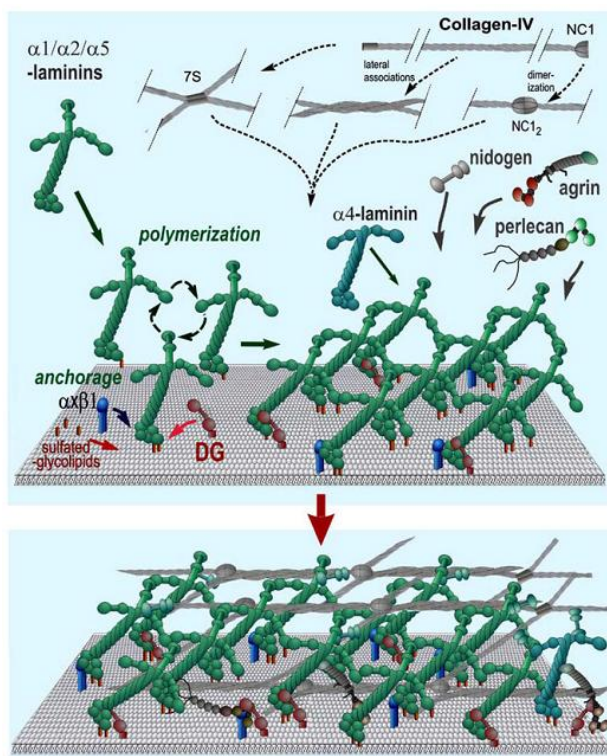


Fig. (34). Basement Membrane Assembly

In this simplified model, laminins become anchored to the cell surface through their LG domains. Anchorage is further enhanced through binding of the α -LN domain to sulfated glycolipids. If the laminin has three LN domains it polymerizes, creating a “nascent” scaffolding. Nidogens, type IV collagens, perlecan, and agrin, are incorporated into this initial matrix by binding to laminin (or by binding through a nidogen bridge). The type IV collagen self-assembles into a covalently-crosslinked network. The non-laminin components provide crucial stability and increase ligand complexity. The basement membrane ligands interact with integrins and dystroglycan and the heparan sulfates of agrin and perlecan enable the tethering of tissue-specific growth factors.

Yurchenco and Patton, 2009

If the network is disturbed, possibly by disglycosylation, renal failure could be the consequence. In principal all epithelial cells that are layered on basement membranes could be affected. It is imaginable that the assembly of the blood-brain barrier is disturbed, resulting in neurological degeneration. In galactosemia however, these disassembly processes, probably occur prenatally. The clinical picture of treated galactosemia does not exhibit deterioration of the patient’s state of health.

It cannot be ruled out that other causes for the observed glycosylation shift are possible, i.e. disease-associated kidney insufficiencies that lead to secretion of complex-type serum glycoproteins [50] into urine and the partial association of these glycoproteins with exosomes as shown for fetuin and ceruloplasmin [35,45].

5.3 Secreted high-mannose-type glycoproteins probably do not recycle through the Golgi compartment

Why does THP N-glycosylation not fluctuate in GALT deficiency as found on other membrane-integral N-glycoproteins in the urothelial membrane? It is known that THP is produced and shed from cellular membranes at high rates, which could imply that it passes the Golgi apparatus only once. We and others have demonstrated for single-passage

glycoproteins, like secreted isoforms of human MUC1, that these proteins preferentially carry high-mannose-type N-glycans compared to their membrane-tethered isoforms expressing more complex-type chains [51]. The latter often recycle after re-endocytosis through the Golgi compartments or the trans-Golgi network back to the plasma membrane [52], a process which could be accompanied by further processing of initially formed high-mannose-type to complex-type glycans.

5.4 Criteria for Tamm-Horsfall Protein being membrane integrated or associated

Because of the fact that THP is a cell surface protein, it is possible that the protein is not only secreted into the extracellular space, rather more it might be integrated into the membrane of the exosomes. The glycoprotein is integrated in lipid rafts at the plasma membrane of the cell surface and a part of it is perhaps endocytosed and sorted into vesicles for secretion, following the characteristic exosomal pathway. In comparison, Mucin-1 (MUC1) is a glycoprotein that either belongs to the exosomal secretion pathway (confirmed by WB, by the use of a MUC1-C-terminal cytosolic domain-specific antibody H295). A part of the membrane located protein is cleaved and shed extracellularly. After cleavage the cytosolic domain that travels by HSP interaction to the nucleus or mitochondria remains intracellular [53]. The fact that after PNGaseF digestion THP was still abundant is a reason for being integrated into the exosomal membrane. An antibody raised against the cytosolic domain of THP could eventually answer the question of the exact location of THP, whether it is membrane integrated or only adherent as a filamentous polymer.

5.5 Galactosemia - a secondary dual congenital disorder of glycosylation (CDG)

According to detected disglycosylation of exosomes disglycosylation of serum proteins could be expected. For example the FSH could be assumed to be dysglycosylated and that would give a reason for female infertility caused by galactosemia. But Gubbels *et al.* published that FSH isoform patterns do not favor FSH dysfunction due to hypoglycosylation as a mechanism in the pathophysiology of ovarian failure in classic galactosemia [5]. Referring to this normal

FSH bioactivity was measured in women with classic galactosemia [54] pointing to an ovarian insufficiency in galactosemia. Many publications found abnormal isoforms corresponding to reduced sialylation of carbohydrate branches but these are found in untreated galactosemic patients that are not on strict diet. In this special case transferrin, FSH, and lysosomal enzymes α -fucosidase and β -hexoaminidase are more neutral charged because of a lower degree of sialylation [6,55-57], transferrin is undergalactosylated, fucosylated to a higher extent and branched in N-glycosylation, but these abnormalities found in galactosemic patients normalized upon dietary treatment [11]. Summarized the glycosylation affects characterize galactosemia as a secondary dual CDG with an assembly defect and a processing defect (secondary CDG-I/II) [11].

The glycans from normal transferrin consisted predominantly (86%) of the disialylated biantennary complex type [6] and serotransferrin is 2.7 fold more abundant, as found *via* the iTRAQ experiment (Tab. 4b p.91). The analysed complex-type shift could therefore be influenced by exosome adherent protein.

6. Conclusion

6.1 N-Glycan remodelling of high-mannose to complex-type

It was demonstrated that a dysglycosylation of cellular membrane-bound proteins occurs in galactosemic subjects adhering to a galactose-restricted diet. Thus, it seems that aberrant glycosylation is a consequence of the relatively high amounts of endogenously synthesized galactose. The shift in expression from preferentially high-mannose-type to complex-type glycans reflects an increased processing rate in early Golgi compartments comprising three steps, the trimming by α -mannosidases I and II, the GlcNAc transfer by β -GlcNAc-transferases GlcNAc-T I and -T II and the galactosylation by the β -4Gal-T. The complexity of the entire trimming and reglycosylation process lets it seem unlikely that only co-substrate levels of UDP-Gal, which may be altered in galactosemic patients, are the primary and direct cause of these dramatic changes. Other specific or global alterations on the proteomic level will have to be identified by differential proteomics. Severe cellular pathomechanistic effects can be expected to result from the described N-glycoprofile changes. As N-linked glycans form signals in the sorting for targeted traffic of membranous glycoproteins, profound effects on the (apical) membrane localization and function of glycosylated receptors in lipid rafts can be expected.

6.2 Clinical pictures of renal failure

The differential proteomics of exosomal lipid rafts in galactosemia revealed protein changes corresponding to the clinical picture of renal kidney failure or damage. Because we selected samples that showed strong N-glycosylation shifts from high-mannose to complex-type N-glycosylation, the results of differential glycomics could be affected strongly by N-glycoproteins associated with kidney failure. At this state of research we can only hypothesize that renal failure is caused by premature protein dysglycosylation leading to disturbed basement assembly. We were not able to conclude whether the actually detected shift was a result of serum proteins passed through the filtration apparatus, or if we identified a chronic intracellular dysglycosylation process.

We found four clinical pictures with strong overlap concerning the more abundant proteins:

1. IgAN 2. TBMN 3. Proteinuria 4. AKI

Almost all marker proteins that distinguish between IgAN and TBMN [45] are found to be more abundant in our study, thus we were not able to differentiate between both clinical pictures applied to galactosemia. There appears to be a closer relationship to IgAN, because the more abundant markers are those characterizing IgAN. In comparison, especially the slightly decreased amounts of MVB proteins and the markedly down-regulated galectin-3-binding-protein were found in both studies. Markers identified by Moon for TBMN were: aminopeptidase N, vasorin, α -1-antitrypsin and ceruplasmin. The marker proteins chosen by Moon were all found in our study to be markedly increased.

At this stage we were not able to distinguish whether the N-glycosylation shift is caused by an intracellular change in the glycosylation machinery or by serum proteins passing the disturbed filtration apparatus of the glomerulus.

6.3 Reasons for detecting serum proteins in urine

There are two main reasons for detecting high levels of serum protein in urine.

Firstly, galactosemia induces renal failure, a condition during which the glomerulus will not efficiently filter proteins out of urine. Secondly, the reabsorption efficiency of proteins passing through the proximal tubulus is thought to be diminished. It is known from previous studies that glycoproteins of the blood serum, e.g. transferrin, bear complex-type N-glycosylation. It is possible that these glycoproteins stick together with glycoproteins at the

surface of the exosomal lipid rafts and that the elevation of these sticky glycoproteins in exosomal membranes results in the observed N-glycosylation shift from high mannose to complex-type. The kind of detergent (Triton X-100) and the amount implemented was probably not sufficient to prevent “stickiness” between N-glycans of glycoproteins in urine and of exosomal lipid rafts.

The exosomes were purified in high quality using modified published methods and the shift may belong to the glycoproteins that are integrated and strongly associated with the membrane. If so we detect the actual glycosylation shift of the exosomal glycoproteom. In Western blot was shown that MUC1 for example exhibits a glycosylation shift in galactosemia, it runs slower in galactosemia than in control person (Fig. 31 Attm. p.85). MUC1 carries high-mannose-glycosylation under healthy conditions and not complex type. In Western blot and in the iTRAQ experiment (Tab. 4a p.90) we found that the amount of MUC1 in exosomal protein seems to be very constant.

6.4 Hypergalactosylation in samples from galactosemia patients

O-glycosylation of the exosomal glycome was examined twice and compared with each other. Mass spectrometry could not reveal any differences in o-glycosylation pattern. We expected to detect undergalactosylation of the glycoproteins [11], but undergalactosylation was not detectable. Classic galactosemia patients have a low UDP-galactose/UDP-glucose ratio [58], in addition a UDP-hexose deficit was found [59]. *Via* mass spectrometry we found the phenomenon of less undergalactosylated species in galactosemia. This contradicts previous observations [60]. If serum proteins are only responsible for the complex-type shift, theoretically they should cause a shift to hypogalactosylation. But the opposite was detected: hypergalactosylation of N-glycans in samples from galactosemic patients in comparison to those of healthy persons.

6.5 Hypertension in combination with renal failure is dangerous in galactosemia

We cannot corroborate which theory is applicable at this state. Either the glycosylation shift is caused by adherent serum glycoproteins or integrated exosomal proteins. In future experiments we can check the N-glycosylation of the supernatant glycome in comparison to the exosomal and can then distinguish if the shift is caused by protein not correctly filtered or by protein only found on and in exosomes.

However the results may be, we were able to detect a direct relation to the N-glycosylation shift found in galactosemia, correspondent to renal failure. Furthermore we identified an expanded list of abundant typical marker proteins detectable in proteinuria and renal failure. Summarized, the N-glycosylation shift is a strong predictor for galactosemia patients to get or with higher probability to have got renal failure. For that reason it is not necessary to make a biopsy of the kidney anymore to clarify the state of the kidney filter function.

Galactosemia patients on diet are able to live in normal fashion, but hypertension in combination to this clinical picture of kidney dysfunction is dangerous. The findings strongly suggest regular check-ups of hypertension in galactosemia. Hypertension could lead to enlargement of the filtration cut-off causing excess loss of serum proteins and non-reversible damage of the glomerulus.

We can not conclude at this moment if the dysglycosylation chronically affects the thin basement membrane of the glomerulus, and in concordance we found exosomal dysglycosylation. Maybe because of renal failure we found increased amounts of serum proteins (e.g.: Immunoglobulins / Igs) in the urine that caused the glycosylation shift.

To validate the results, a second iTRAQ analysis is necessary, again divided in at least two galactosemia patient samples and two controls. If the results were in accordance and exhibit the same clinical picture, and the results were validated by Western blot a second time we assume with high certainty that the found exosomal N-glycosylation shift is related to chronic renal failure.

Methodologically iTRAQ is a valuable form to compare quantitative content and regulation of exosomes. To detect all proteins without regarding to the regulation the sample analyzation using LC-ESI after gel electrophoreses, Coomassie staining, cutting gel slices and protein digestion is able to raise the amount of detecting proteins. Thus it seems to present a reasonable additive extension for whole proteome detection.

7. Future experiments: Glycolipid analysis of urinary exosomes

In future experiments it will be most interesting to analyse glycolipids of urinary exosomes. Using classical lipid extraction methods they could be isolated in high purity and potentially sticking serum proteins could be detached easily to reveal significant alteration in lipids and glycosylation.

These lipids as well as their glycan part could be qualitatively and quantitatively analysed [61]. A preceding impressive study of lipid alteration in galactosemia brain ascertained: “Galactosylceramide appeared to be reduced about 3-fold in the galactosemic brain when compared to the two controls. Furthermore, there was a 3- to 4-fold increase in the amount of glucosylceramide in the galactosemic sample. This is to be expected since glucosylceramide is next substituted by galactose from the UDP-Gal donor to form lactosylceramide and, with UDP-Gal being limiting, the precursor, glucosylceramide, will accumulate. Finally, the alteration observed for each lipid leads to a 10-fold reduction in the ratio of galactosylceramide/glucosylceramide in the galactosemic brain” [62]. Differences in vesicle lipid composition and glycosylation probably will give indirect hints to brain lipid alteration. Additionally it is easier to retrieve samples from living persons for the generation of urinary exosomes instead of being dependent on organ donation.

In accordance with the reported findings above and their hypothetical implications we are currently performing a differential proteomic study based on the GALT-deficient fibroblast cell model (grown under galactose-free and under galactose stress conditions) to reveal insight into changes of the lipid raft (glyco) proteomes. These analyses will hopefully give insight into cellular changes and pathomechanisms induced by endogenous galactose-stress *via* protein disglycosylation.

Acknowledgements

This study was supported by the Galactosemie Initiative Germany. We acknowledge the kind support of Fabian Staubach for box plot visualization, Christian Hoffmann, who provided high-quality electron microscopic pictures of exovesicle preparations.

8. References

1. Thoden JB, Ruzicka FJ, Frey PA, Rayment I, Holden HM. Structural analysis of the H166G site-directed mutant of galactose-1-phosphate uridylyltransferase complexed with either UDP-glucose or UDP-galactose: detailed description of the nucleotide sugar binding site. *Biochemistry*, 36(6), 1212-1222 (1997).
2. Marabotti A, Facchiano AM. Homology modeling studies on human galactose-1-phosphate uridylyltransferase and on its galactosemia-related mutant Q188R provide an explanation of molecular effects of the mutation on homo- and heterodimers. *J Med Chem*, 48(3), 773-779 (2005).
3. Lai K, Willis AC, Elsas LJ. The biochemical role of glutamine 188 in human galactose-1-phosphate uridylyltransferase. *J Biol Chem*, 274(10), 6559-6566 (1999).
4. Fridovich-Keil JL, Gubbels CS, Spencer JB, Sanders RD, Land JA, Rubio-Gozalbo E. Ovarian function in girls and women with GALT-deficiency galactosemia. *J Inherit Metab Dis*, 34(2), 357-366 (2011).
5. Gubbels CS, Thomas CM, Wodzig WK *et al.* FSH isoform pattern in classic galactosemia. *J Inherit Metab Dis*, 34(2), 387-390 (2011).
6. Charlwood J, Clayton P, Keir G, Mian N, Winchester B. Defective galactosylation of serum transferrin in galactosemia. *Glycobiology*, 8(4), 351-357 (1998).
7. Potter BA, Hughey RP, Weisz OA. Role of N- and O-glycans in polarized biosynthetic sorting. *Am J Physiol Cell Physiol*, 290(1), C1-C10 (2006).
8. Stoffel W, Bosio A. Myelin glycolipids and their functions. *Curr Opin Neurobiol*, 7(5), 654-661 (1997).
9. Bosch A. Classical galactosaemia revisited. *Journal of Inherited Metabolic Disease*, 29(4), 516-525 (2006).
10. Berry GT, Elsas LJ. Introduction to the Maastricht workshop: lessons from the past and new directions in galactosemia. *J Inherit Metab Dis*, 34(2), 249-255 (2011).
11. Sturiale L, Barone R, Fiumara A *et al.* Hypoglycosylation with increased fucosylation and branching of serum transferrin N-glycans in untreated galactosemia. *Glycobiology*, 15(12), 1268-1276 (2005).
12. Simpson RJ, Jensen SS, Lim JW. Proteomic profiling of exosomes: current perspectives. *Proteomics*, 8(19), 4083-4099 (2008).
13. Rabesandratana H, Toutant JP, Reggio H, Vidal M. Decay-accelerating factor (CD55) and membrane inhibitor of reactive lysis (CD59) are released within exosomes during In vitro maturation of reticulocytes. *Blood*, 91(7), 2573-2580 (1998).
14. Koppen T, Weckmann A, Muller S *et al.* Proteomics analyses of microvesicles released by *Drosophila* Kc167 and S2 cells. *Proteomics*, 11(22), 4397-4410 (2011).
15. Pisitkun T, Shen RF, Knepper MA. Identification and proteomic profiling of exosomes in human urine. *Proc Natl Acad Sci U S A*, 101(36), 13368-13373 (2004).
16. Moon PG, You S, Lee JE, Hwang D, Baek MC. Urinary exosomes and proteomics. *Mass Spectrom Rev*, (2011).
17. Simpson RJ, Lim JW, Moritz RL, Mathivanan S. Exosomes: proteomic insights and diagnostic potential. *Expert Rev Proteomics*, 6(3), 267-283 (2009).
18. Staubach S, Razawi H, Hanisch FG. Proteomics of MUC1-containing lipid rafts from plasma membranes and exosomes of human breast carcinoma cells MCF-7. *Proteomics*, 9(10), 2820-2835 (2009).
19. Browman DT, Hoegg MB, Robbins SM. The SPFH domain-containing proteins: more than lipid raft markers. *Trends Cell Biol*, 17(8), 394-402 (2007).
20. Otto GP, Nichols BJ. The roles of flotillin microdomains - endocytosis and beyond. *J Cell Sci.*, 124(23), 3933-3940 (2011).

21. Rindler MJ, Naik SS, Li N, Hoops TC, Peraldi MN. Uromodulin (Tamm-Horsfall glycoprotein/uromucoid) is a phosphatidylinositol-linked membrane protein. *J Biol Chem*, 265(34), 20784-20789 (1990).
22. Fernandez-Llama P, Khositseth S, Gonzales PA, Star RA, Pisitkun T, Knepper MA. Tamm-Horsfall protein and urinary exosome isolation. *Kidney Int*, 77(8), 736-742 (2010).
23. Verroust PJ, Birn H, Nielsen R, Kozyraki R, Christensen EI. The tandem endocytic receptors megalin and cubilin are important proteins in renal pathology. *Kidney Int*, 62(3), 745-756 (2002).
24. Marzolo MP, Farfan P. New insights into the roles of megalin/LRP2 and the regulation of its functional expression. *Biol Res*, 44(1), 89-105 (2011).
25. Serafini-Cessi F, Bellabarba G, Malagolini N, Dall'Olio F. Rapid isolation of Tamm-Horsfall glycoprotein (uromodulin) from human urine. *J Immunol Methods*, 120(2), 185-189 (1989).
26. Albert TK, Laubinger W, Muller S *et al.* Human intestinal TFF3 forms disulfide-linked heteromers with the mucus-associated FCGBP protein and is released by hydrogen sulfide. *J Proteome Res*, 9(6), 3108-3117 (2010).
27. Wisniewski JR, Zougman A, Mann M. Combination of FASP and StageTip-based fractionation allows in-depth analysis of the hippocampal membrane proteome. *J Proteome Res*, 8(12), 5674-5678 (2009).
28. Thiele H, Glandorf J, Hufnagel P, Korting G, Bluggel M. Managing Proteomics Data: From Generation and Data Warehousing to Central Data Repository. *Journal of Proteomics & Bioinformatics*, Vol. 1(9), 485-507 (2008).
29. Domon B, Costello CE. A systematic nomenclature for carbohydrate fragmentations in FAB-MS/MS spectra of glycoconjugates. *Glycoconjugate Journal*, 5(4), 397-409 (1988).
30. van Rooijen JJ, Voskamp AF, Kamerling JP, Vliegthart JF. Glycosylation sites and site-specific glycosylation in human Tamm-Horsfall glycoprotein. *Glycobiology*, 9(1), 21-30 (1999).
31. Gonzales PA, Pisitkun T, Hoffert JD *et al.* Large-scale proteomics and phosphoproteomics of urinary exosomes. *J Am Soc Nephrol*, 20(2), 363-379 (2009).
32. Smalley DM, Sheman NE, Nelson K, Theodorescu D. Isolation and identification of potential urinary microparticle biomarkers of bladder cancer. *J Proteome Res*, 7(5), 2088-2096 (2008).
33. Li Y, Zhang Y, Qiu F, Qiu Z. Proteomic identification of exosomal LRG1: A potential urinary biomarker for detecting NSCLC. *Electrophoresis*, (2011).
34. Heo S-H, Lee S-J, Ryoo H-M, Park J-Y, Cho J-Y. Identification of putative serum glycoprotein biomarkers for human lung adenocarcinoma by multilectin affinity chromatography and LC-MS/MS. *Proteomics*, 7(23), 4292-4302 (2007).
35. Zhou H, Pisitkun T, Aponte A *et al.* Exosomal Fetuin-A identified by proteomics: a novel urinary biomarker for detecting acute kidney injury. *Kidney Int*, 70(10), 1847-1857 (2006).
36. Pešić I, Stefanović V, Müller GA *et al.* Identification and validation of six proteins as marker for endemic nephropathy. *Journal of Proteomics*, 74(10), 1994-2007 (2011).
37. Kishore BK, Gejyo F, Arakawa M. Alpha 2HS-glycoprotein in the serum and urine of patients with renal diseases. *Postgrad Med J*, 59(691), 304-307 (1983).
38. Weber PC. Renal prostaglandins, kidney function and essential hypertension. *Contrib Nephrol*, 23, 83-92 (1980).
39. Natchin YV, Bogolepova AE, Kuznetsova AA, Shakhmatova EI. Study of the role of prostaglandin E2 in urine flow regulation in chronic renal failure. *Scand J Urol Nephrol*, 34(5), 327-330 (2000).

40. Wu T, Fu Y, Brekken D *et al.* Urine proteome scans uncover total urinary protease, prostaglandin D synthase, serum amyloid P, and superoxide dismutase as potential markers of lupus nephritis. *J Immunol*, 184(4), 2183-2193 (2010).
41. Hemmelgarn BR, Manns BJ, Lloyd A *et al.* Relation Between Kidney Function, Proteinuria, and Adverse Outcomes. *JAMA: The Journal of the American Medical Association*, 303(5), 423-429 (2010).
42. Yurchenco PD, Patton BL. Developmental and pathogenic mechanisms of basement membrane assembly. *Curr Pharm Des*, 15(12), 1277-1294 (2009).
43. Abrahamson DR. Development of kidney glomerular endothelial cells and their role in basement membrane assembly. *Organogenesis*, 5(1), 275-287 (2009).
44. Barr PH. Association of Escherichia coli sepsis and galactosemia in neonates. *J Am Board Fam Pract*, 5(1), 89-91 (1992).
45. Moon PG, Lee JE, You S *et al.* Proteomic analysis of urinary exosomes from patients of early IgA nephropathy and thin basement membrane nephropathy. *Proteomics*, 11(12), 2459-2475 (2011).
46. Braccia A, Villani M, Immerdal L *et al.* Microvillar membrane microdomains exist at physiological temperature. Role of galectin-4 as lipid raft stabilizer revealed by "superrafts". *J Biol Chem*, 278(18), 15679-15684 (2003).
47. Merlin J, Stechly L, de Beauce S *et al.* Galectin-3 regulates MUC1 and EGFR cellular distribution and EGFR downstream pathways in pancreatic cancer cells. *Oncogene*, 30(22), 2514-2525 (2011).
48. Staubach S, Hanisch FG. Lipid rafts: signaling and sorting platforms of cells and their roles in cancer. *Expert Rev Proteomic*, 8(2), 263-277 (2011).
49. Slepak TI, Tang M, Slepak VZ, Lai K. Involvement of endoplasmic reticulum stress in a novel Classic Galactosemia model. *Mol Genet Metab*, 92(1-2), 78-87 (2007).
50. Mattu TS, Pleass RJ, Willis AC *et al.* The glycosylation and structure of human serum IgA1, Fab, and Fc regions and the role of N-glycosylation on Fc alpha receptor interactions. *J Biol Chem*, 273(4), 2260-2272 (1998).
51. Parry S, Hanisch FG, Leir SH *et al.* N-Glycosylation of the MUC1 mucin in epithelial cells and secretions. *Glycobiology*, 16(7), 623-634 (2006).
52. Litvinov SV, Hilkens J. The epithelial sialomucin, episialin, is sialylated during recycling. *J Biol Chem*, 268(28), 21364-21371 (1993).
53. Ren J, Bharti A, Raina D, Chen W, Ahmad R, Kufe D. MUC1 oncoprotein is targeted to mitochondria by heregulin-induced activation of c-Src and the molecular chaperone HSP90. *Oncogene*, 25(1), 20-31 (2006).
54. Sanders RD, Spencer JB, Epstein MP *et al.* Biomarkers of ovarian function in girls and women with classic galactosemia. *Fertil Steril*, 92(1), 344-351 (2009).
55. Jaeken J, Kint J, Spaapen L. Serum lysosomal enzyme abnormalities in galactosaemia. *Lancet*, 340(8833), 1472-1473 (1992).
56. Prestoz LL, Couto AS, Shin YS, Petry KG. Altered follicle stimulating hormone isoforms in female galactosaemia patients. *Eur J Pediatr*, 156(2), 116-120 (1997).
57. Stibler H, von Dobeln U, Kristiansson B, Guthenberg C. Carbohydrate-deficient transferrin in galactosaemia. *Acta Paediatr*, 86(12), 1377-1378 (1997).
58. Ng WG, Xu YK, Kaufman FR, Donnell GN. Deficit of uridine diphosphate galactose in galactosaemia. *J Inherit Metab Dis*, 12(3), 257-266 (1989).
59. Lai K, Langley SD, Khwaja FW, Schmitt EW, Elsas LJ. GALT deficiency causes UDP-hexose deficit in human galactosemic cells. *Glycobiology*, 13(4), 285-294 (2003).
60. Ornstein KS, McGuire EJ, Berry GT, Roth S, Segal S. Abnormal galactosylation of complex carbohydrates in cultured fibroblasts from patients with galactose-1-phosphate uridylyltransferase deficiency. *Pediatr Res*, 31(5), 508-511 (1992).

61. Frank S, Geyer H, Geyer R. Microscale Analysis of Glycosphingolipids from *Schistosoma mansoni* Cercariae. *Journal of Carbohydrate Chemistry*, 30(4-6), 233-248 (2011).
62. Petry K, Greinix HT, Nudelman E *et al.* Characterization of a novel biochemical abnormality in galactosemia: deficiency of glycolipids containing galactose or N-acetylgalactosamine and accumulation of precursors in brain and lymphocytes. *Biochem Med Metab Biol*, 46(1), 93-104 (1991).

9. Legends to attached figures

Fig. 2 (p.68)

Mislinkage of arginine 188

Mislinkage of the hydrogen bond from the upper phosphoryl groups (O2A/O1B) to the lower situated hydrogen bond types (O5'/O2B) dependent on the amino acid exchange Q188R. The mislinkage drastically reduces the enzymatic turnover rate.

Fig. 3 (p.69)

Bulky residue of arginine disturbs dimeric close up of subunits and active sites

The bulky arginine residue exhibits a longer side chain in comparison to glutamine and therefore causes a destabilization effect. It negatively influences the substrate fitting to the surrounding hydrophobic pocket of the active site.

Fig. 4 (p.70)

Ping-Pong double displacement reaction of GALT

The first substrate UDP-glucose in composition with GALT binds to the active site that forms the intermediate complex GALT-UDP-glucose. It is subsequently cleaved to GALT-UMP. It remains attached to the enzyme in complex. Glucose-1-phosphate the first product that is released (“ping-reaction”). The second (co-)substrate added is galactose-1-phosphate that forms the second intermediate complex GALT-UDP-galactose with GALT-UMP. During the final step the second product UDP-Galactose is released by the enzyme (“pong-reaction”) and the GALT is ready to take part in another turnover cycle.

Fig. 8 (p.71)

Glycoprotein travelling *via* lipid rafts

Lipid raft endocytosis takes place in two different ways: (1) *via* the caveolin and dynamin dependent manner or (2) *via* flotillin (a scaffold protein); in this case dynamin independent. MUC1 is a membrane-bound glycoprotein which travels inside these lipid raft originated vesicles to the early endosomes (E). It then recycles through the trans-Golgi network (TGN) and a recycling endosome (RE) back to the cell surface.

A further possibility is that re-endocytosed membrane glycoproteins are sorted into exosomes for cellular export (4). If the glycoprotein is not targeted to the lysosome (Lys) the endosome converts to a MVB that proceeds to fuse with the membrane and secretes the exosomes into the extracellular space.

Fig. 12 (p.72)

N-glycosylation exosomes

Glycoproteins located at the exosomal surface were digested by PNGaseF subsequently the N-glycans were purified over C18 column, methylated and analyzed by mass spectrometry.

Fig. 14 (p.73)

Western blot of exosomal marker proteins separated by continuous gradient centrifugation

Western blot of fractions from density gradient centrifugation of urinary exovesicles, demonstrating the presence of exosomal markers preferentially in the high-density fraction 5 (MUC1, mucin-1; Alix, apoptosis-linked gene-2 interacting protein X; hsp70, heat-shock protein 70; Flot-2, flotillin-2; Gi α , G protein subunit α ; hsp27, heat-shock protein 27).

Fig. 15 (p.74)

Tamm-Horsfall protein contamination of urinary exosomal vesicles (Coomassie stain)

Representative Coomassie-stained SDS-polyacrylamide gels of exovesicular preparations from a galactosemia patient (lane 1) and two controls c1 and c2 (lanes 2 and 3) showing the presence of THP as a major protein.

Fig. 16 (p.75)

Filtration of exosomes (0.1µm filter)

The Electron microscopy (85000 X) picture of 100nm filtered exosomes exhibits fragmented exosomal structures. The mechanical shearing force by filtration leads to lysis and fragmentation of exosomes.

Fig. 19 (p.76)

High-mannose (left) versus complex-type (right) species detected by mass spectrometry.

Five high-mannose- and six complex-type structures were mainly detectable. The high-mannose-type N-glycans varied between four and eight terminal mannoses (Fig. 19/left side). The complex-type mainly varied between six different structures: four species exemplary for the biantennary species with GlcNAc-Gal added to the core structure that could be single- or double sialylated, with both structures fucosylated or non-fucosylated, respectively. The tetra-antennary structure was identified as double sialylated and tetra sialylated species (Fig. 19/right side). Many undergalactosylated species were detected for the bi- and tetra-antennary carbohydrate branches, but they were not considered for the calculation of the shift (example: Fig.19/right side below). If they were added, the result would be more intense than already detected.

Fig. 23 (p.77)

DTT to remove THP from exosomes

Coomassie stained exosomal proteins separated in 1DE. Membranous samples were incubated with DTT collected by ultracentrifugation and prepared with Laemmli-SDS-buffer for 1DE. DTT 200mg/ml at 37°C, 10min, was used to remove THP from whole exosomes and exosomal lipid rafts. Three lanes at the left side: fresh isolated exosomal samples of a healthy control, three lanes at the right side: samples of a galactosemia patient after storage of a period of some weeks (-20°C).

High amounts of THP were visible in both untreated samples (lane 1 and 4). The DTT treated samples (lines 2 and 5) show a loss, but a lot of THP remains. The exosomal lipid rafts (lines 3 and 6) still exhibit a lot of THP after DTT incubation and an additional TritonX-100 incubation step for the generation of rafts. DTT could not be used to completely remove THP, rather reduces the amount slightly. The THP amount does not markedly depend on preparing the sample fresh or using a thawed one. Both samples, whether from healthy person or from

galactosemia patients, contained THP and it adhered strongly to the exosomes. Unfortunately the total intensity of the protein pattern weakens either after DTT treatment.

Fig. 24, 25 (p.78/79)

Representative MALDI mass spectra of permethylated N-glycans from urinary THP of GALT-deficient patients and healthy control subjects

A, Representative MALDI mass spectrum of permethylated N-glycans liberated from electrophoretically purified THP contaminating the exovesicular preparation of a galactosemic patient; B, the respective sample from a healthy control subject. STD refers to the internal standard LNFPI.

Fig. 26 (p.80)

Coomassie stained 1D gel-electrophoreses

An aliquot of the exosomal lipid raft extracted proteins (15µg) was applied on a gradient 1D-gel (5-15 %). The gel-electrophoreses was done for visually examination of the protein pattern after precipitation (chloroform/methanol) of the samples previous to the iTRAQ application.

The first two lanes represent two different samples of galactosemia patients and the last two lanes two control persons. The protein pattern of both galactosemia patients is comparable just as well as the pattern of both control persons. The protein pattern of galactosemia patients and control persons in contrast is strikingly distinct.

Fig. 27 (p.81)

Validation of up and down regulated proteins by Western blot

Three elected proteins one of them was found to be increased one decreased (see results of the iTRAQ experiment) and one constant were compared by Western blot. In concordance to the detected regulation of proteins by iTRAQ, the CD81 tetraspanin a characteristically exosomal marker protein was upregulated in galactosemia (lane 1 and 2). In contrast the exosomal marker Alix was markedly down regulated in galactosemia (lane 3 and 4). MUC1 was recognized in several Western blots to be expressed in nearly constant quantities regardless which sample was applied (galactosemia patient or healthy person).

Fig. 28 (p.82)

THP identification

Four different samples of coomassie stained 1D gel-electrophoretically separated proteins (15µg/lane) of exosomal lipid rafts. The THP mass is equal in galactosemia- and control-samples and is typically found between 75 and 100kDa after 1DE. One band of the control 1 was excised, protein digested, analyzed by LC-ESI and identified by the mascot search database. The most dominant found protein was as expected uromodelin (Fig. 32 p.86) mascot search result).

Fig. 29 (p.83)

Mascot Search results after LC-ESI analyzation

The identified proteins were sorted into equal subclasses according to the iTRAQ tables. The identified proteins exhibit semantic overlaps (see iTRAQ) but additional proteins were found that expand the list of proteins detected by the iTRAQ method. Additional detected proteins were highlighted in yellow.

Fig. 30 (p.84)

EGFR expression in healthy and diseased fibroblasts

Westernblot EGFR with house keeping protein under different sugar addition to the cell culture supernatant (30µg protein / lane)

Left side: Healthy fibroblasts (FibH) were incubated for 48h with 0.1 % galactose (five lanes left) or 0.1 % glucose (five lanes right). α -Tubulin was used as house keeping protein. Independent of the added sugar, a relative high amount of EGFR expression was found.

Right side: Healthy fibroblasts (FibH) and GALT deficient fibroblasts (FibQ) were grown under high glucose level. Caveolin-1 was used as house keeping protein.

Independent of the constant sugar amount, but dependent on cell type, the EGFR was detected in healthy fibroblasts but was nearly absent in GALT deficient fibroblasts (FibQ).

Fig. 31 (p.85)

Glycosylation shift of MUC1 detected by Western blot

Exosomal MUC1 of galactosemia patients runs higher in 1DE than MUC1 of healthy controls. Different causes could explain this phenomenon. Shorter carbohydrate branches, a glycosylation shift from high-mannose to complex-type or charge alterations caused by sialylation or SDS binding.

Fig. 32 (p.86)

Mascot search result

THP (uromodelin) was identified by the top score of 1180, followed by galectin-3-binding protein 402 and three further proteins under the off cut of 100. THP was validated to be the high abundant protein that was found in exosomal samples.

Fig. 33 (p.87)

1DE of exosomal lipid rafts (Coomassie stained) for LC-ESI-MS-MS analyzation

An aliquot of the exosomal lipid raft extracted proteins was applied on a gradient 1D-gel (5-20%). The first two lanes represent the glycosylation pattern of two different galactosemia patients and the last two lanes two controls. Visually detected different protein bands of the second galactosemia patient were excised and analyzed after extraction by LC-ESI. One diverging protein was found to be most dominant in galactosemia: Perlecan (PGBM_Human / Basement membrane-specific heparin sulphate proteoglycan core protein).

10. Legends to supplements

Suppl. Tab.1 (p.88)

THP variation of samples were previously visualized by 1DE Coomassie stain and afterwards used for N-glycan analytic. Ratio of complex- to high-mannose-type glycans in exosome samples with high or low THP content. The presence of THP in exovesicular preparations however did not strongly influence the ratios of complex- vs. high-mannose-type glycans in samples with high or low THP content.

Suppl. Tab.2 (p.89)

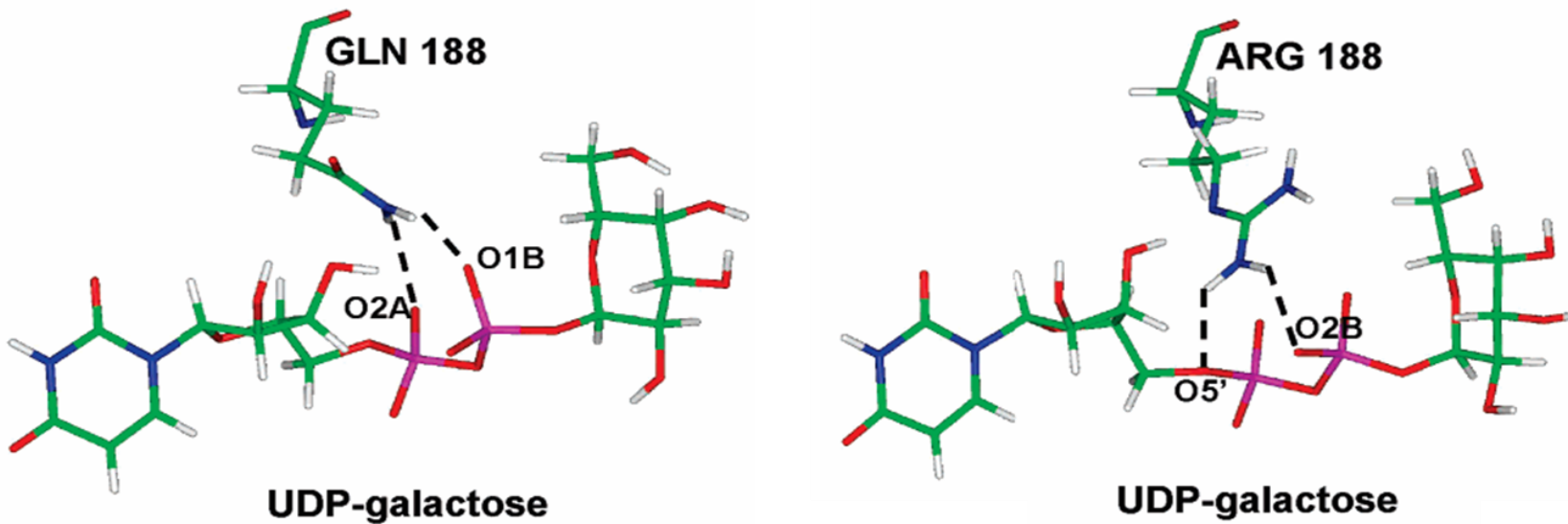
Variation between independent urine samples from one healthy control.

The variations of ratios (complex-type vs. high-mannose-type glycans) measured for independent urine samples from individual healthy control subjects were only small.

11. Attachment

11. Attachment

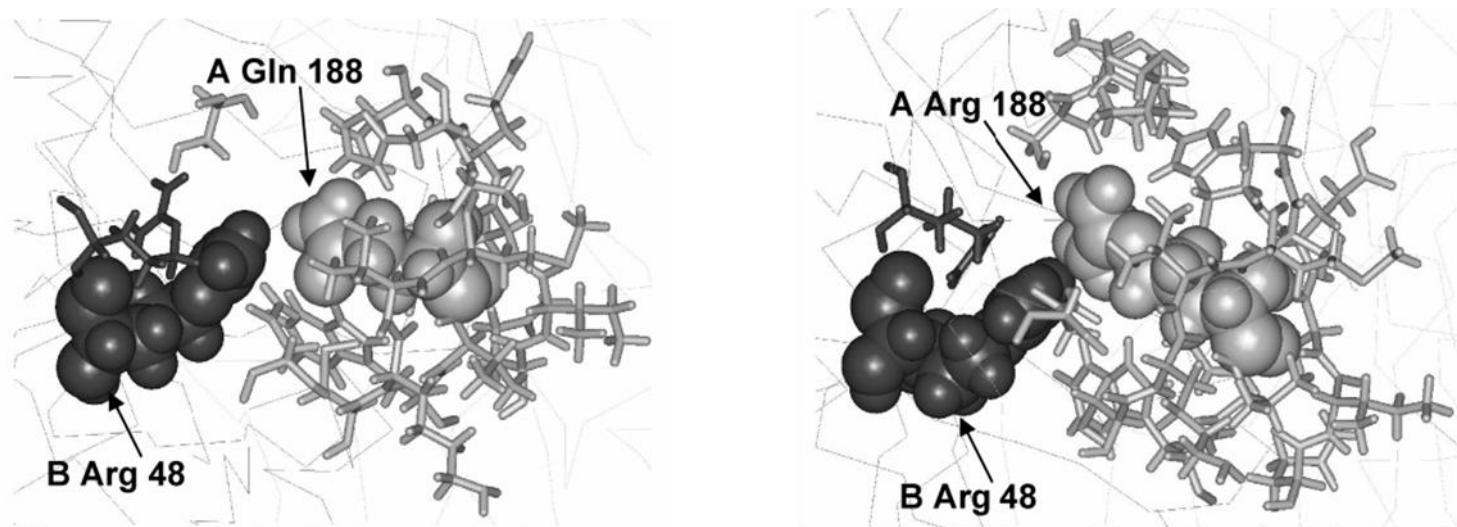
Fig. 2: Misl linkage of Arginin 188



From left: uridine, ribose, phosphoryl groups, galactose. Left healthy GALT, right mutated GALT

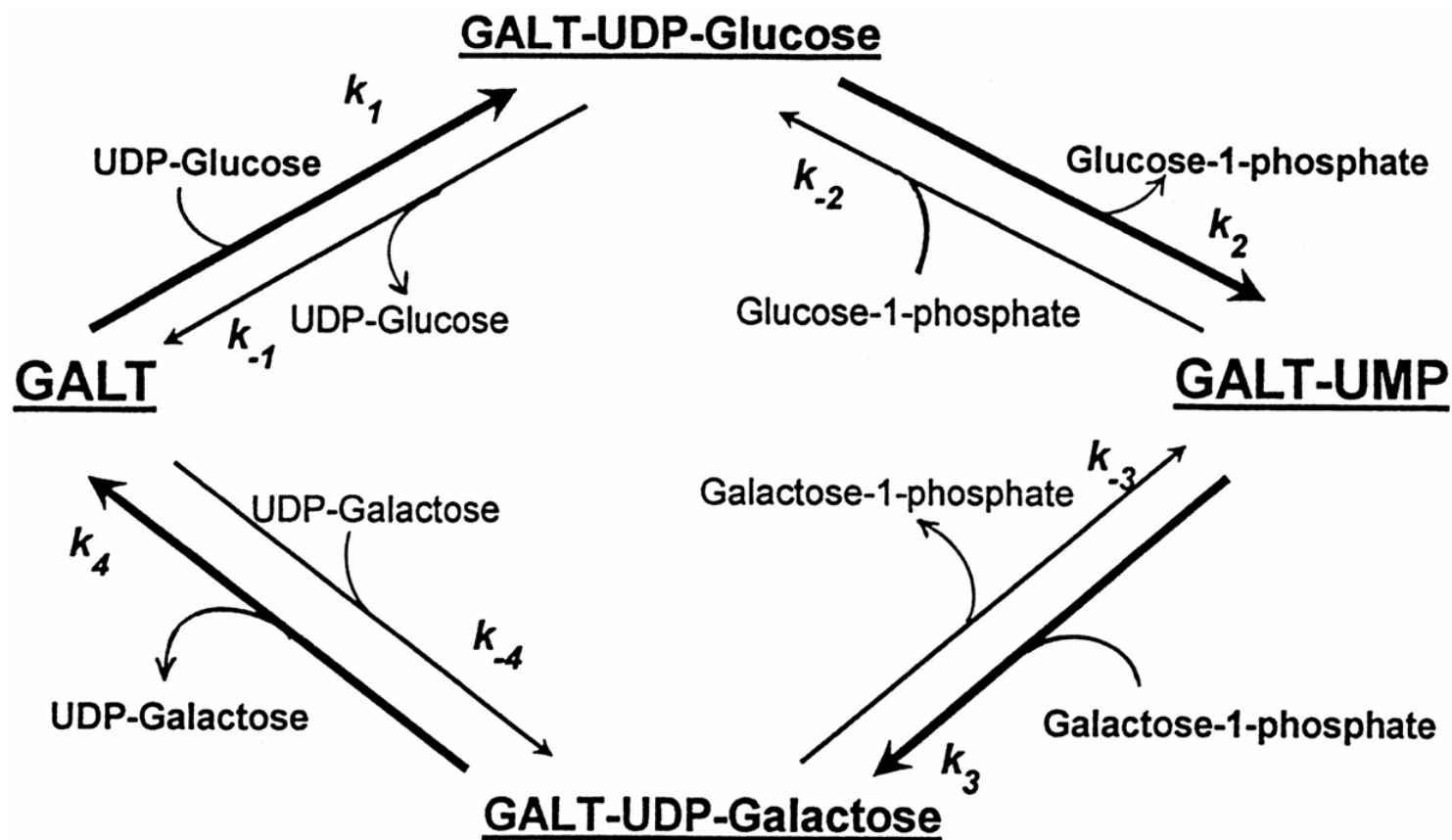
A. Marabotti, J. Med. Chem. 2005, 48, 773-779

Fig. 3: Bulky residue of arginine disturbs dimeric close up of subunits and active sites



A. Marabotti, *J. Med. Chem.* 2005, 48, 773-779

Fig. 4: Ping-Pong double displacement reaction of GALT



Lai, K. et al. J. Biol. Chem. 1999;274:6559-6566

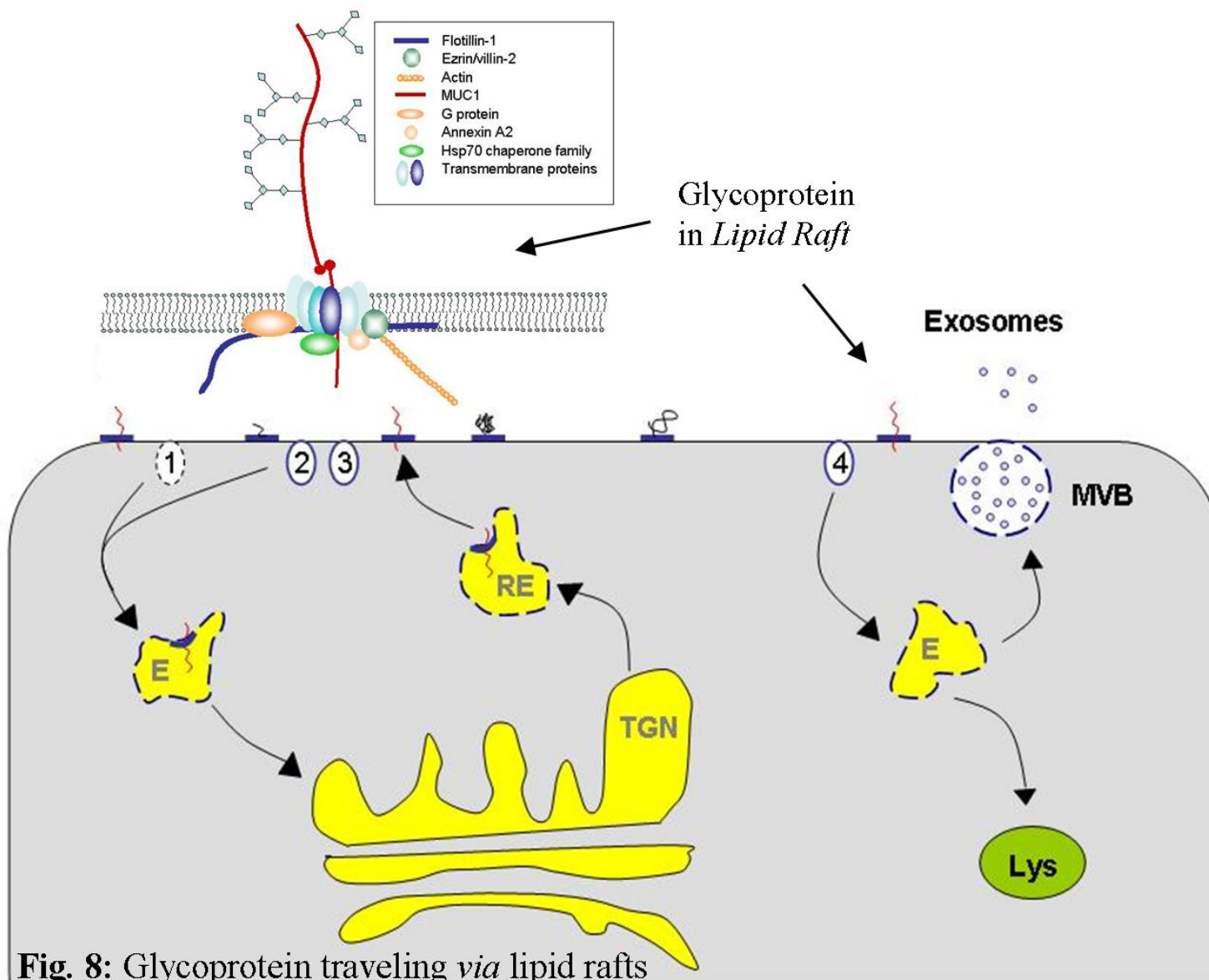


Fig. 12

N-glycosylation exosomes

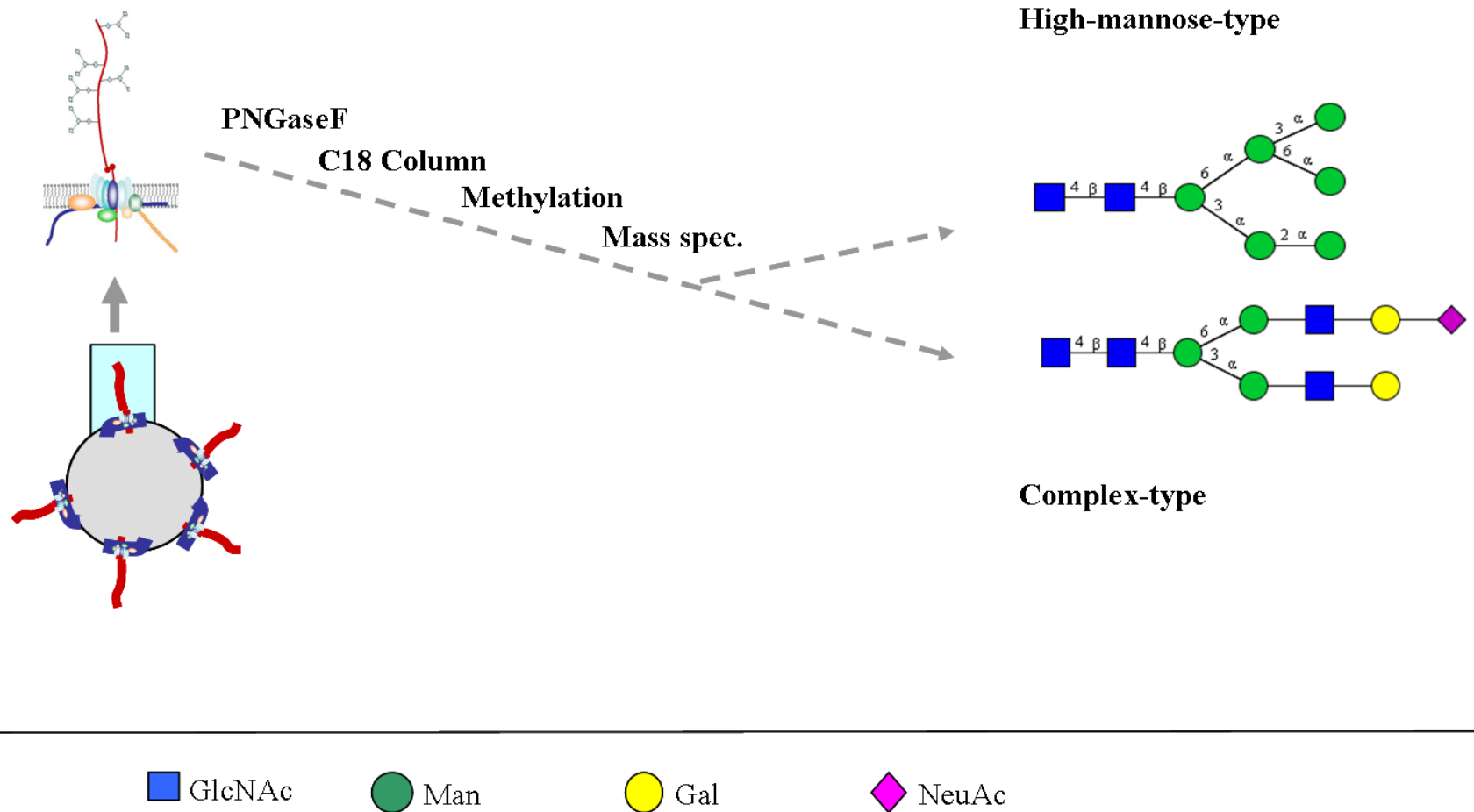


Fig. 14

Western blot of exosomal marker proteins separated by continuous gradient centrifugation

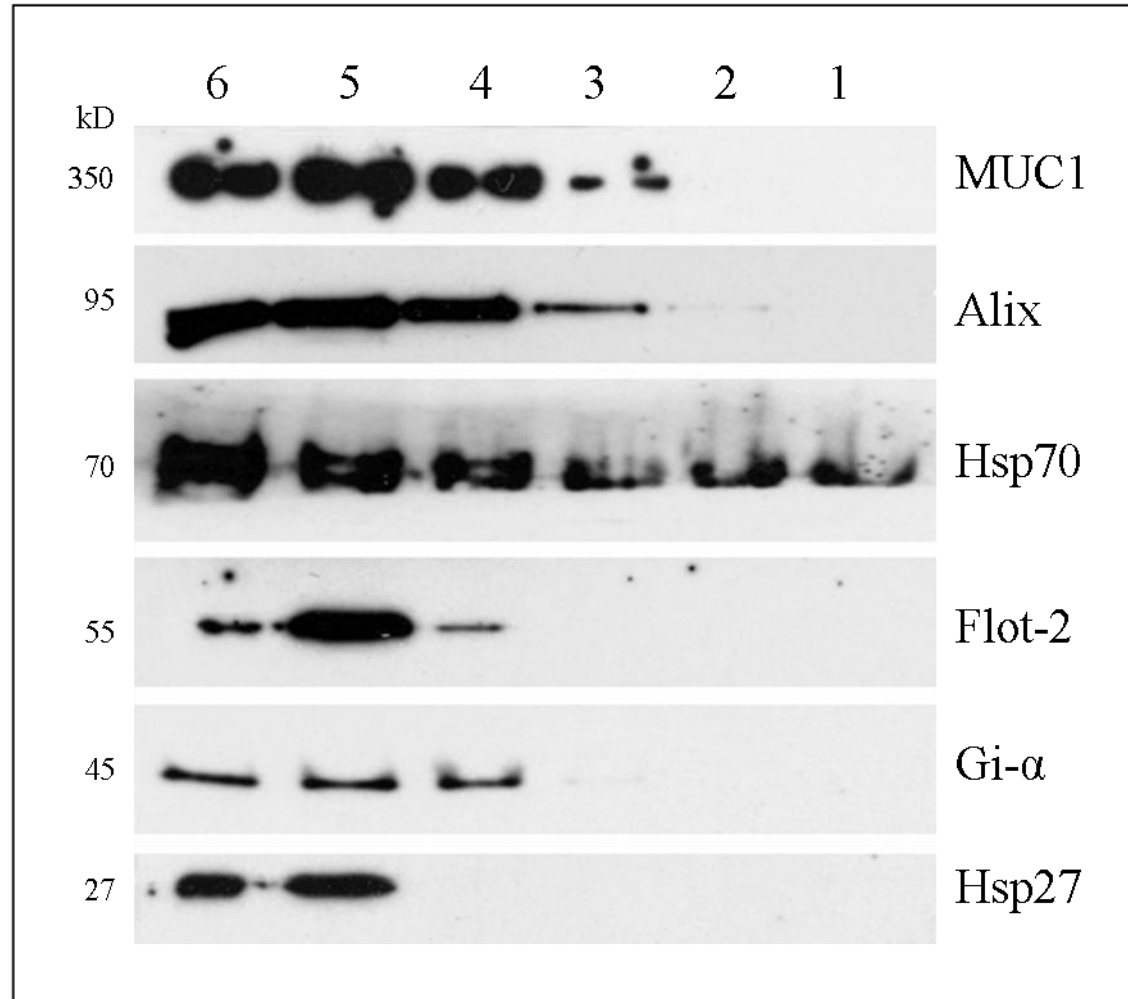


Fig. 15

Tamm-Horsfall protein contamination of urinary exosomal vesicles (Coomassie stain)

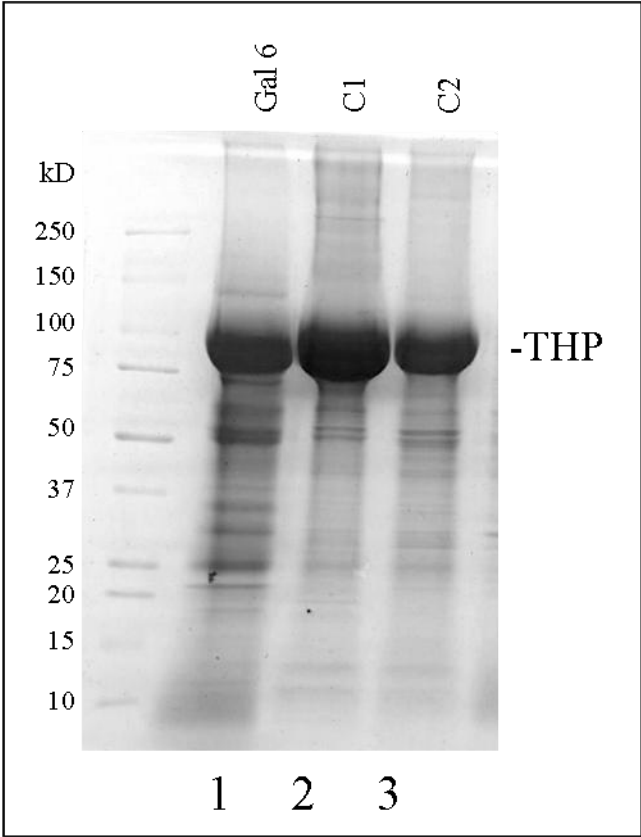
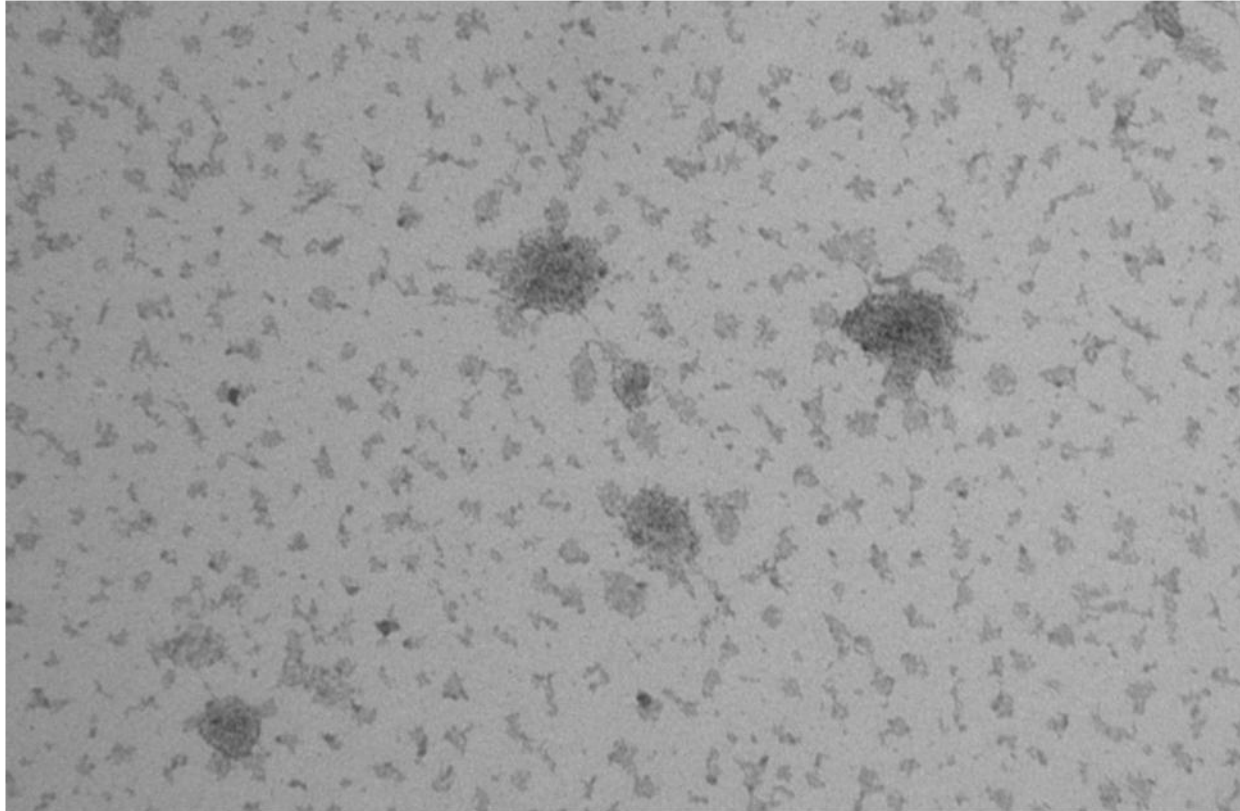


Fig. 16

Electron microscopy of 0,1 μ m filtered exosomes



Filtration of exosomes (0,1 μ m) leads to fragmentation

Fig. 19: High-mannose (left) *versus* complex-type (right) species detected by mass spectrometry.
 One example of an undergalactosylated species

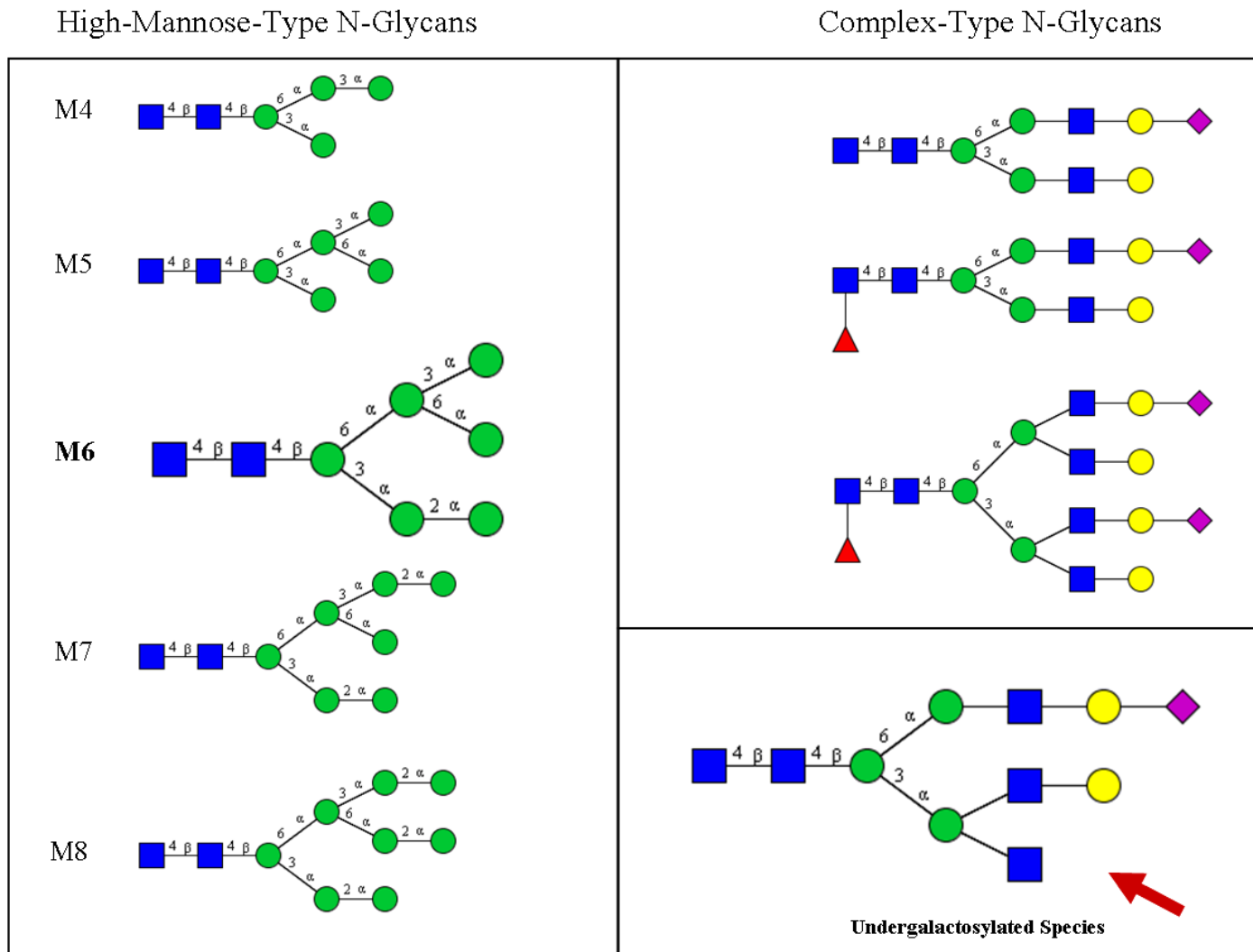
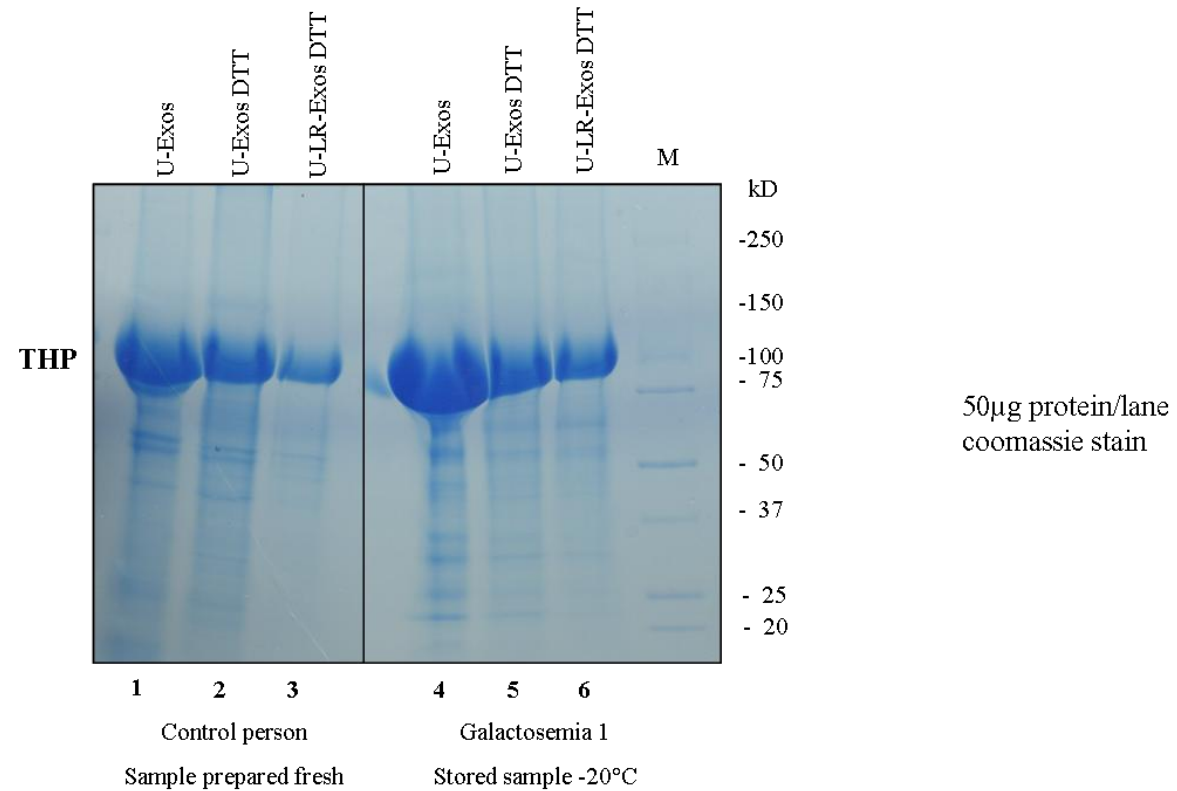


Fig. 23

THP removal from urinary-exosomes using DTT



DTT incubation of exosomes/exosomal lipid rafts 200mg/ml, 37°C 10 min

Result: DTT treatment could not completely remove THP

Fig. 24 N-glycans electrophoretically purified THP exovesicular origin galactosemic patient

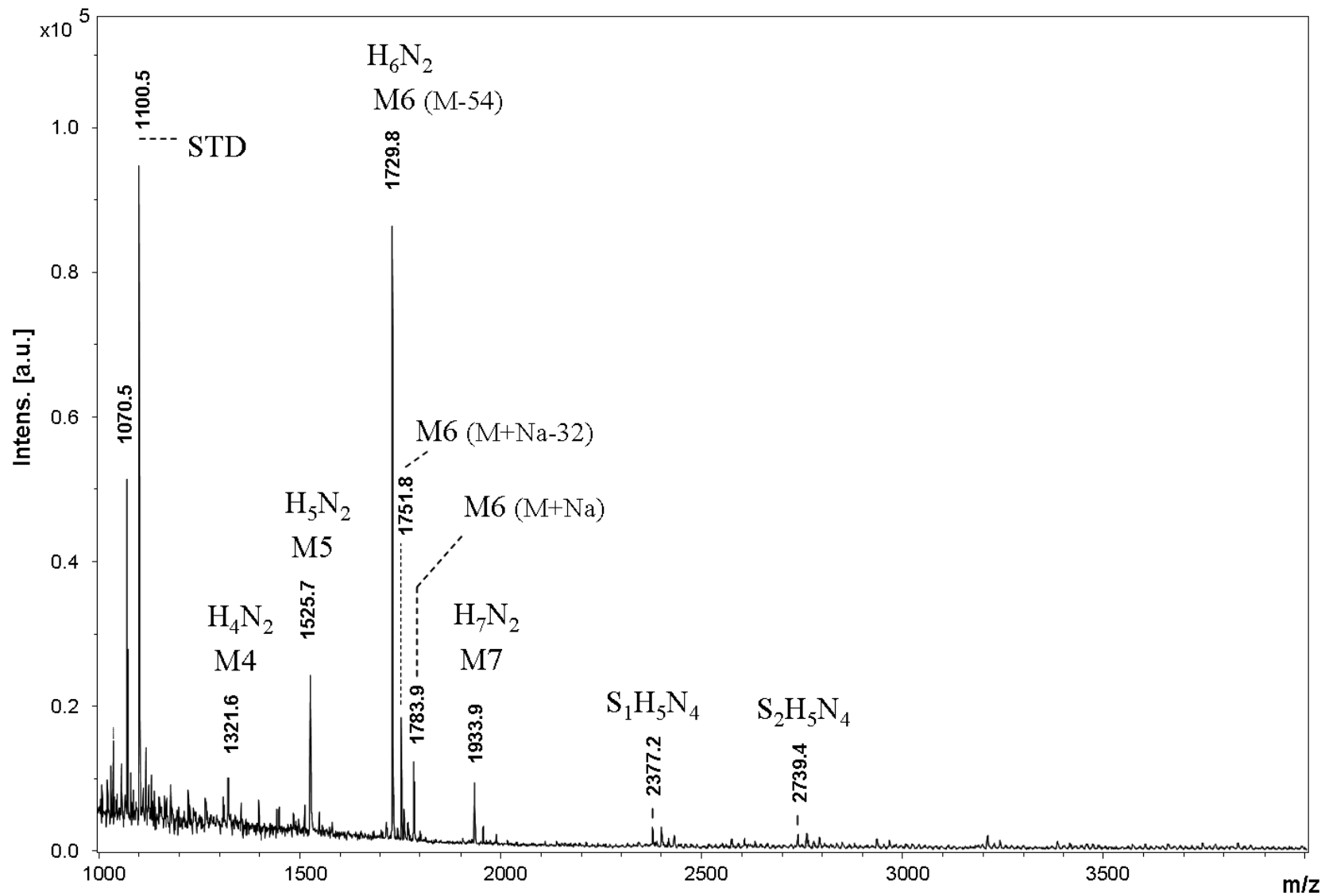


Fig. 25 N-glycans electrophoretically purified THP exovesicular origin healthy person

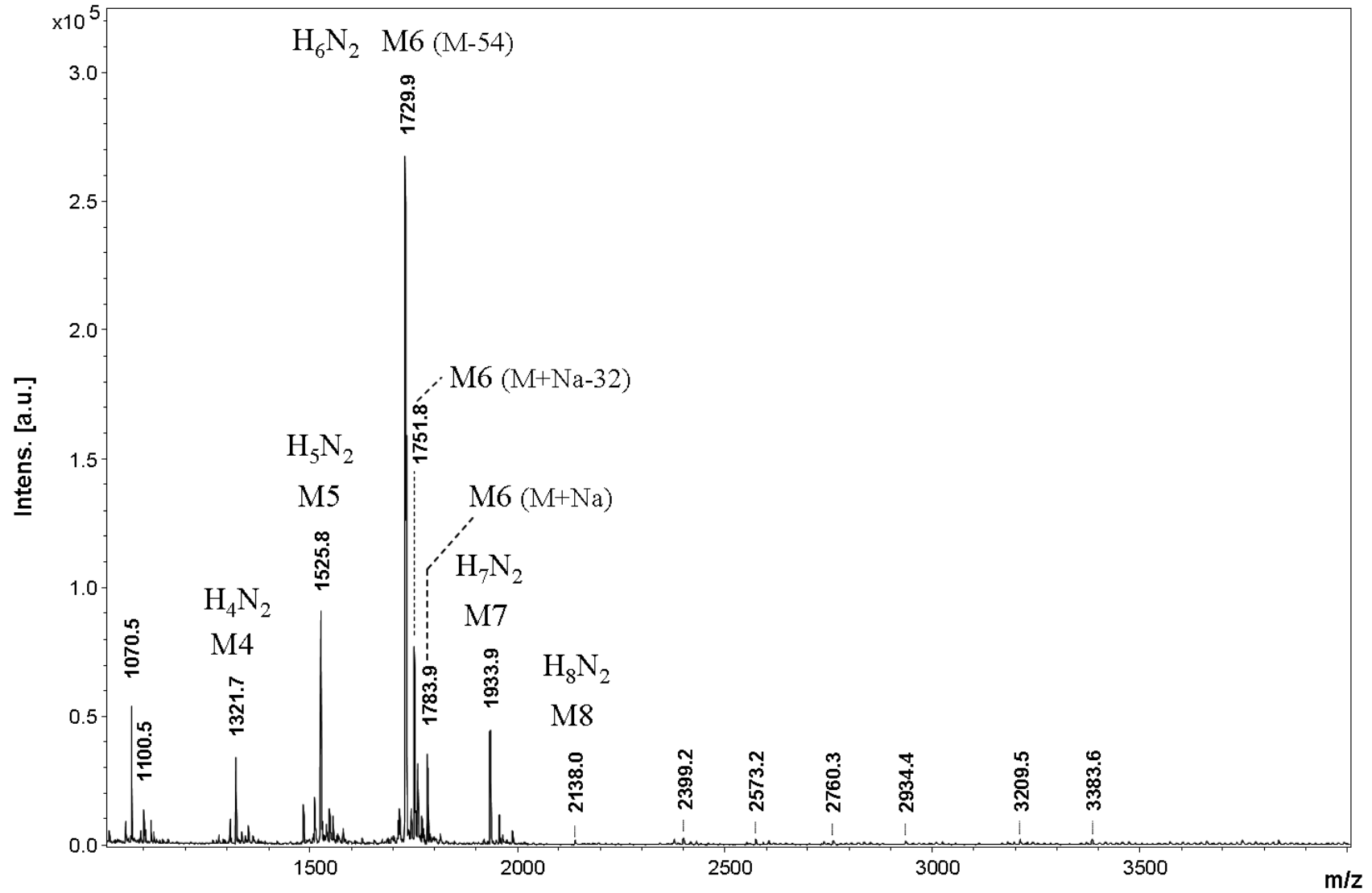


Fig. 26

1DE of exosomal lipid rafts (Coomassie stained)
prior to iTRAQ experiment

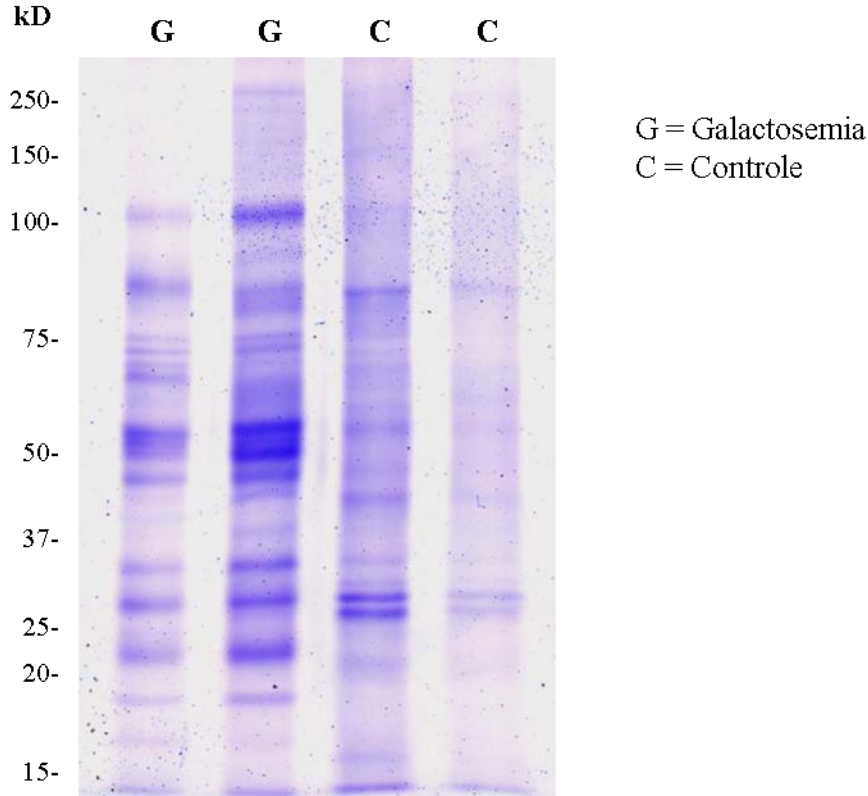
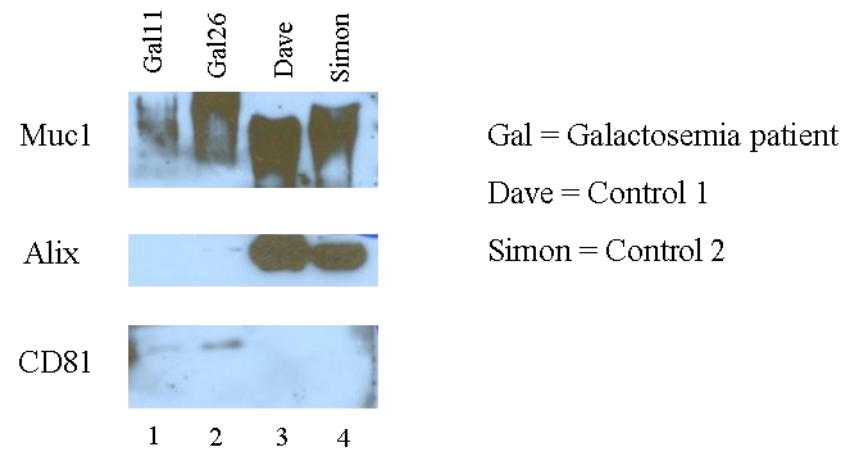


Fig. 27

Validation of regulated proteins (iTRAQ) by Western blot

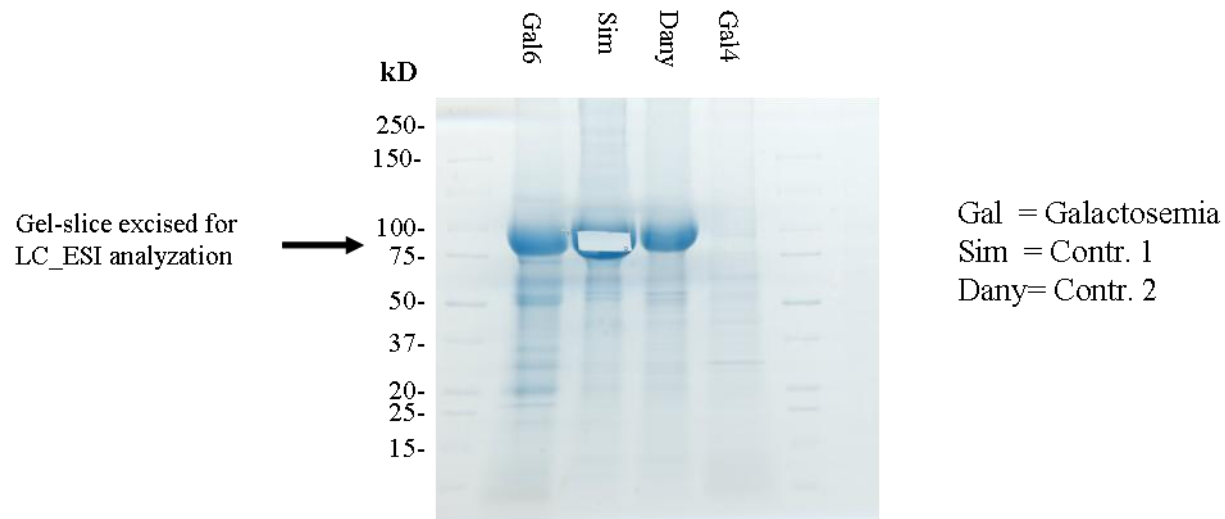


CD81 was increased in galactosemia
Alix was decreased in galactosemia
MUC1 was nearly constant
iTRAQ results were validated

Fig. 28

THP-identification

Coomassie stained protein pattern of exosomal lipid rafts inclusively adherent THP



Mascot Search Result:

[UROM_HUMAN](#) Mass: 72451 Score: 1180 Queries matched: 65 emPAI: 3.20

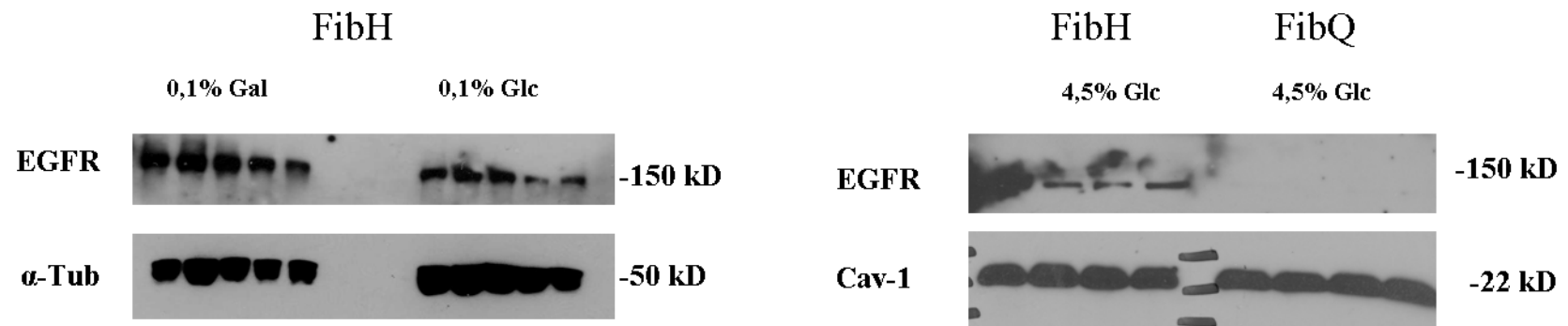
Fig. 29

Mascot Search results (LC-ESI) of four gel slices

Ergebnisse LC-ESI/4 Gelstücke aus Coomassie / GAD6 / Dateien 81-84 (v. Stefan) zusammengefügt			
Exosome			ECM
MUC1 HUMAN	Mucin-1 MUC1	NID1 HUMAN	Nidogen-1 NID1
RHOA HUMAN	Transforming protein RhoA	HMCN1 HUMAN	Hemicentin-1 HMCN1
BROX HUMAN	BR01 domain-containing protein BROX	COL1A1 HUMAN	Collagen alpha-1(XVIII) chain COL18A1
ZA2G HUMAN	Zinc-alpha-2-glycoprotein MHC1	COLFA1 HUMAN	Collagen alpha-1(XVI) chain COL15A1
CATD HUMAN	Cathepsin D	COL6A3 HUMAN	Collagen alpha-3(VI) chain COL6A3
IST1 HUMAN	IST1 homolog KIAA0174	CILP2 HUMAN	Cartilage intermediate layer protein 2 CILP2
AF2 HUMAN	AF2 cell surface antigen heavy chain SLC3A2	MYRAS HUMAN	Multicatalase associated protein 8 MYRAS
GELS HUMAN	Gelsolin GSN / Brevin	AGRIN HUMAN	Agrin AGRN
VASN HUMAN	Vasorin	PGBM HUMAN	Basement membrane-specific heparan sulfate proteoglycan core protein
CLUS HUMAN	Clusterin		
CD14 HUMAN	Monocyte differentiation antigen CD14		
CSPG4 HUMAN	Chondroitin sulfate proteoglycan 4	Secreted	
RAC1 HUMAN	Ras-related C3 botulinum toxin substrate 1 RAC1	UROD HUMAN	Uromodulin
RAP1A HUMAN	Ras-related protein Rap-1A RAP1A	ALBU HUMAN	Serum albumin ALB
SDCB1 HUMAN	Syntenin-1 Expressed in fetal kidney	KNG1 HUMAN	Kinogen-1 KNG1
ARF1 HUMAN	ADP-ribosylation factor 1 ARF1	IPSP HUMAN	Plasma serine protease inhibitor
		AMY1 HUMAN	Alpha-amylase 1 AMY1A
MYB		A1AT HUMAN	Alpha-1-antitrypsin SERPINA1
CHM4B HUMAN	Charged multivesicular body protein 4b CHMP4B	AACT HUMAN	Alpha-1-antichymotrypsin SERPINA3
CHM1B HUMAN	Charged multivesicular body protein 1b CHMP1B	DNASE1 HUMAN	Deoxyribonuclease-1 DNASE1
CHM2A HUMAN	Charged multivesicular body protein 2a CHMP2A	TETN HUMAN	Tetranectin CLECSB
LMAN2 HUMAN	Vesicular integral-membrane protein VIP36 LMAN2	APOD HUMAN	Apolipoprotein D APOD
VP37B HUMAN	Vacuolar protein sorting-associated protein 37B VPS37B	AMYP HUMAN	Pancreatic alpha-amylase AMY2A
		A2GL HUMAN	Leucine-rich alpha-2-glycoprotein LRG1
Ig		FETUA HUMAN	Alpha-2HS-glycoprotein AHS3
IGLL5 HUMAN	Immunoglobulin lambda-like polypeptide 5	RET4 HUMAN	Retinol-binding protein 4 RBP4
IGJ HUMAN	Immunoglobulin J chain	KLK1 HUMAN	Kallikrein-1 KLK1
IKV02 HUMAN	Ig kappa chain V.II region SIE	TAGLN2 HUMAN	Tranexelin-2 TAGLN2
IKV012 HUMAN	Ig kappa chain V.II region HAH	CRYAB HUMAN	Alpha-crystallin B chain CRYAB
IKV108 HUMAN	Ig kappa chain V.I region WEA	LCA1 HUMAN	Phosphatidylcholine-sterol acyltransferase
IGHA1 HUMAN	Ig alpha-1 chain C region IGHA1	C9ORF8 HUMAN	Uncharacterized protein C9orf8 C9orf8
IGHG1 HUMAN	Ig gamma-1 chain C region IGHG1	PTGDS HUMAN	Prostaglandin-H2 D-isomerase PTGDS
IGHA2 HUMAN	Ig alpha-2 chain C region IGHA2	EGF HUMAN	Pro-epidermal growth factor EGF
IGHG3 HUMAN	Ig gamma-3 chain C region IGHG3	THRB HUMAN	Thyroxine-binding globulin SERPINA7
IGHG4 HUMAN	Ig gamma-4 chain C region IGHG4	CD4A HUMAN	Complement C4A C4A
IGHG2 HUMAN	Ig gamma-2 chain C region IGHG2	PRDX1 HUMAN	Peroxiredoxin-1 PRDX1
IGKC HUMAN	Ig kappa chain C region IGKC	DDAH2 HUMAN	N(G),N(G)-dimethylarginine dimethylaminohydrolase 2
LY02 HUMAN	Ig lambda chain V.III region LOI	PGRP1 HUMAN	Peptidoglycan recognition protein 1 PGLYRP1
LAC2 HUMAN	Ig lambda-2 chain C regions IGLC2	A1BG HUMAN	Alpha-1B-glycoprotein A1BG
LVD01 HUMAN	Ig lambda chain V region 4A	NAPSA HUMAN	Napsin-A NAPSA
KV106 HUMAN	Ig kappa chain V.I region EU	ITIH4 HUMAN	Inter-alpha-trypsin inhibitor heavy chain H4ITIH4
KV120 HUMAN	Ig kappa chain V.I region Mew	ANGL2 HUMAN	Angiotensin-related protein 2 ANGPL2
KV201 HUMAN	Ig kappa chain V.II region Cum	PEPA HUMAN	Pepsin A PEA3
KV204 HUMAN	Ig kappa chain V.II region TEW	IBP7 HUMAN	Insulin-like growth factor-binding protein 7 IGFBP7
KV303 HUMAN	Ig kappa chain V.III region N99 (Fragment)	NADC HUMAN	Nicotinate nucleotide pyrophosphorylase [carboxylating]
KV308 HUMAN	Ig kappa chain V.III region V9 (Fragment)	IBP2 HUMAN	Insulin-like growth factor-binding protein 2
KV401 HUMAN	Ig kappa chain V.IV region (Fragment) IGKV4.1	QPCT HUMAN	Glutamyl-peptide cyclotransferase QPCT
KV113 HUMAN	Ig kappa chain V.I region Lav	ANGT HUMAN	Angiotensinogen AGT
HV305 HUMAN	Ig heavy chain V.III region BRD	6PGL HUMAN	6-phosphogluconolactonase 6PGL
ROBO4 HUMAN	Roundabout homolog 4 ROBO4	THMT HUMAN	3-mercaptopyruvate sulfurtransferase MPST
LAD1 HUMAN	Ladinin-1 Linear IgA disease antigen	ABHEB HUMAN	Abhydrolase domain-containing protein 14B
		PIP HUMAN	Prolactin-inducible protein PIP
Lysosome		GSTA1 HUMAN	Glutathione S-transferase A1 GSTA1
LYAG HUMAN	Lysosomal alpha-glucosidase GAA	GPX3 HUMAN	Glutathione peroxidase 3 GPX3
PPAL HUMAN	Lysosomal acid phosphatase ACP2	AMBP HUMAN	Protein AMBP
ARSA HUMAN	Arylsulfatase A ARSA		
ASAH1 HUMAN	Acid ceramidase ASAH1 SVF5	Cytosol	
BGAL HUMAN	Beta-galactosidase GLB1	PEBP1 HUMAN	Phosphatidylethanolamine-binding protein 1 PEBP1
SPLM HUMAN	N-sulphoglucosamine sulphohydrolase SUSH	LDHB HUMAN	L-lactate dehydrogenase B chain LDHB
TP1 HUMAN	Tripeptidyl peptidase 1 TP1	GSTP1 HUMAN	Glutathione S-transferase P GSTP1
RENH HUMAN	Renin receptor ATP6AF2		

yellow: additionally identified proteins

Fig. 30 EGFR expression in healthy and diseased fibroblasts (whole cell lysate)

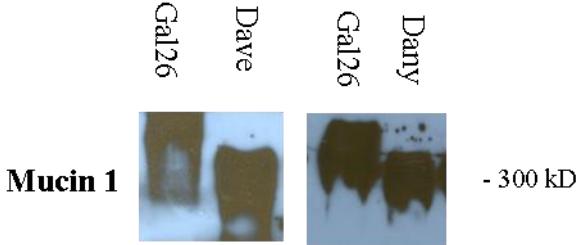


FibH: healthy fibroblasts
FibQ: GALT deficient fibroblasts
EGFR: EGF- Receptor
 α -Tub: α -Tubulin
Cav-1: Caveolin-1
Gal: Galactose
Glc: Glucose

Fig. 31

Glycosylation shift of Muc1

Westernblot MUC1 (C595)



Result: detectable MUC1 shift in galactosemia

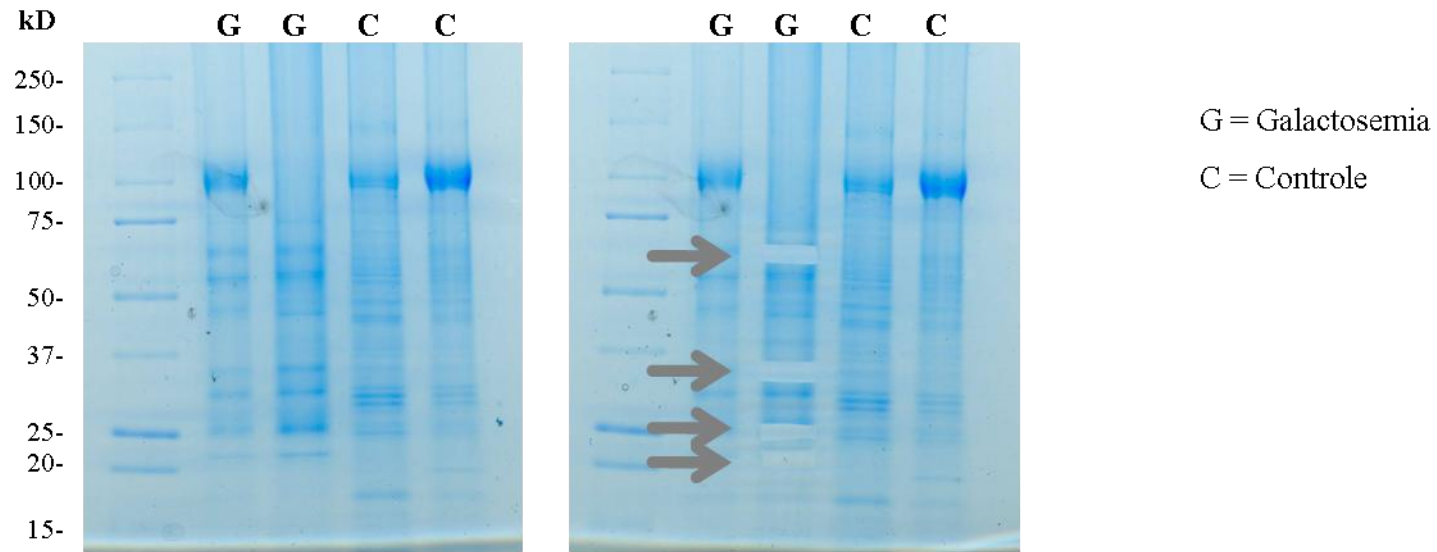
Fig. 32

THP (Uromodelin) identified by top Score (LC-ESI/Mascot Search)

1. UROM HUMAN Mass: 72461 Score: 1180 Queries matched: 86 emPAI: 3.20									
Uromodulin O5=Homo sapiens GN=UMOD PE=1 SV=1									
Query	Observed	M(r)exp(t)	M(r)calc(d)	Delta	Miss	Score	Expect	Rank	Peptide
68	396.2000	790.3855	790.4086	-0.0231	0	36	0.042	1	R.FVGGGGR.M
140	457.7000	913.3855	913.4480	-0.0625	0	42	0.0078	1	R.FSVQMF.R.F
165	465.7000	929.3855	929.4429	-0.0575	0	(34)	0.059	1	R.FSVQMF.R.F 167
189	477.7000	953.3855	953.4971	-0.1116	0	36	0.028	1	K.YFIQDR.C 190
205	491.7000	981.3855	981.4556	-0.0701	0	36	0.027	1	R.TLDEYWR.S
238	512.7000	1023.3855	1023.5172	-0.1317	0	80	1.1e-006	1	R.VGGTGMFTV.R.M
247	520.7000	1039.3855	1039.5121	-0.1266	0	(73)	5.4e-006	1	R.VGGTGMFTV.R.M 248 249 250 251 253 254
273	538.2000	1074.3855	1074.5128	-0.1273	0	57	0.00025	1	R.DGPGTALTR.N 274
292	558.2000	1116.3854	1116.5274	0.0680	0	(61)	9.1e-005	1	K.VEMYLSDSR.C
301	565.2000	1128.3854	1128.5929	-0.0073	0	88	0.00023	1	R.DMYSVAVTP.R.D
303	567.2000	1132.3855	1132.5223	-0.1368	0	63	6e-005	1	K.VEMYLSDSR.C
333	588.2000	1174.3855	1174.5838	-0.1984	0	75	3.5e-006	1	R.MPETCVPLR.C
344	596.2000	1190.3854	1190.5788	0.0067	0	(85)	1.9e-005	1	R.MPETCVPLR.C 342 343
446	707.4000	1412.3855	1412.7809	0.0046	0	98	1.9e-008	1	K.TALQPMVSLNIR.V 446
451	715.4000	1428.3855	1428.7759	0.0095	0	(86)	2.5e-007	1	K.TALQPMVSLNIR.V 450 452
468	729.8000	1467.3854	1467.6683	-0.0829	0	78	1.5e-006	1	K.INFACS.YPLDMK.V
480	737.8000	1473.3854	1473.6632	-0.0778	0	(84)	3.9e-005	1	K.INFACS.YPLDMK.V 479
504	757.9000	1513.3855	1513.7837	0.0217	1	43	0.0049	1	R.DNRDMVSVTPAR.D 503
512	769.2000	1536.3854	1536.7276	-0.1422	1	48	0.0013	1	R.LECGANQMKVSLGK.C 511
593	853.2000	1704.3854	1704.7915	-0.2060	0	113	2.8e-010	1	R.DSTIQAVENGESDGR.F 592 594 595 596 597 598 5
625	868.8000	1735.3854	1735.6995	-0.1141	0	84	2.1e-007	1	R.STEYGEYACDTDLR.G 624
635	882.9000	1763.3855	1763.8653	-0.0898	1	75	2.4e-006	1	K.SLGFQKFMVSLSDSR.C 636
644	890.9000	1779.3855	1779.8502	-0.0647	1	(74)	3.1e-006	1	K.SLGFQKFMVSLSDSR.C 640 645 646
888	757.9000	2270.6782	2270.9772	-0.2990	0	47	6.7e-005	1	K.ACAHWISGHCLMDASVQVKA
904	766.9000	2297.6782	2297.9648	-0.2865	1	41	0.00025	1	R.STEYGEYACDTDLRGMVYR.F
926	786.2000	2355.8781	2356.0826	-0.2045	1	46	0.001	1	R.CPHRTDSTIQAVENGESDGR.F
1045	957.4000	2899.1782	2899.2397	-0.0615	0	26	0.082	1	R.FAGNVDLVLHCEVLCOTMNEK.C
2. LG3BP HUMAN Mass: 66202 Score: 402 Queries matched: 9 emPAI: 0.45									
Galectin-3-binding protein O5=Homo sapiens GN=LGAL3BP PE=1 SV=1									
Query	Observed	M(r)exp(t)	M(r)calc(d)	Delta	Miss	Score	Expect	Rank	Peptide
50	368.2000	734.3855	734.3288	0.0467	0	20	1.4	1	R.YFYSR.R
404	663.8000	1325.3854	1325.6483	-0.0809	0	65	3.2e-005	1	R.A6HEEVEQLVEK.I 406
416	678.4000	1354.3855	1354.7708	0.0147	0	58	0.00018	1	R.SDLAVPSELALK.A
546	796.9000	1591.3855	1591.7842	0.0013	0	85	2.5e-007	1	R.EI.SEALGQIIEIDQR.G
550	799.8000	1597.3854	1597.6685	-0.0831	0	80	8e-007	1	K.YSDFYGFAPSDYR.Y
796	992.5000	1982.3854	1983.0942	-0.1087	0	50	0.00061	1	K.TLQALEFHTVFFQLLAR.Y 755
845	721.4000	2161.1782	2161.0116	0.1666	0	44	0.0022	1	R.IYTSPTWISAFVTDSSVSR.K
3. K1C10 HUMAN Mass: 59020 Score: 97 Queries matched: 1 emPAI: 0.05									
Keratin type Icytoskeletal 10 O5=Homo sapiens GN=KRT10 PE=1 SV=6									
Query	Observed	M(r)exp(t)	M(r)calc(d)	Delta	Miss	Score	Expect	Rank	Peptide
520	775.2000	1548.3854	1548.6700	-0.0846	0	97	1.8e-008	1	R.SGGGGGGGGCGGGGGVSLR.I
4. K2C1 HUMAN Mass: 66170 Score: 87 Queries matched: 1 emPAI: 0.05									
Keratin type Icytoskeletal 1 O5=Homo sapiens GN=KRT1 PE=1 SV=6									
Query	Observed	M(r)exp(t)	M(r)calc(d)	Delta	Miss	Score	Expect	Rank	Peptide
397	651.9000	1301.3855	1301.7078	0.0777	0	88	1.5e-007	1	R.SLDLDSIAEVKA

Fig. 33

1DE of exosomal lipid rafts (Coomassie stained)
for LC-ESI MS analysis



Four gel-slices exhibiting differences in the protein pattern
were excised for LC-ESI anlyzation

Suppl. Tab. 1 Ratio of complex- to high-mannose-type glycans in exosome samples with high or low THP content

	M-54	Composition	high THP	high THP	low THP	low THP	low THP
Galactosemic patient			8	12	9	10	11
N-linked Glycans	m/z		%	%	%	%	%
High mannose type	1322	H4N2	10.0	8.1	9.0	8.3	10.3
	1526	H5N2	8.8	22.8	18.8	12.9	34.4
	1730	H6N2	17.5	18.8	9.8	8.8	8.9
	1934	H7N2	7.5	6.7	2.5	2.5	2.1
	2138	H8N2	2.5	2.7	2.7	2.9	3.8
	Σ		46.3	59.1	42.9	35.4	59.5
Complex type	2377	S1H5N4	15.0	12.1	11.2	13.3	6.9
	2551	S1F1H5N4	10.0	4.0	4.0	2.9	2.9
	2738	S2H5N4	16.3	24.8	36.9	42.1	25.0
	2913	S2F1H5N4	6.3	0.0	3.6	5.0	2.9
	3188	S2H6N5	3.8	0.0	0.5	0.4	1.7
	3723	S3F2H6N5	2.5	0.0	0.9	0.8	1.3
	Σ		53.8	40.9	57.1	64.6	40.8

Suppl. Tab. 2 Variation between independent urine samples from one healthy control

	M-54	Composition				Median
Control samples			C1-1	C1-2	C1-3	
N-linked Glycans	m/z		%	%	%	
High mannose type	1321.7	H4N2	1.2	1.4	14.2	
	1525.8	H5N2	7.9	6.7	36.8	
	1729.8	H6N2	62.4	73.8	21.9	
	1934.0	H7N2	7.9	9.9	11.6	
	2138.1	H8N2	1.2	0.0	5.2	
	Σ		80.6	91.9	89.7	87.4
Complex type	2377.2	S1H5N4	3.0	3.6	6.5	
	2551.3	S1F1H5N4	4.9	1.4	0.0	
	2738.4	S2H5N4	1.8	1.4	3.9	
	2912.5	S2F1H5N4	3.6	0.7	0.0	
	3187.6	S2H6N5	3.0	1.1	0.0	
	3722.9	S3F2H6N5	2.4	0.0	0.0	
	Σ		18.8	8.2	10.3	12.4

Tab. 4a

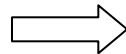
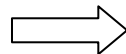
Genuine exosome proteins

Exosome (genuine)			Score	m
ANX11_HUMAN	Annexin A11 ANXA11		250,1	1,50
DPEP1_HUMAN	Dipeptidase 1 DPEP1 / apical cell membrane; Lipid-anchor > GPI-anchor	N	227	1,45
HSP71_HUMAN	Heat shock 70 kDa protein 1A/1B HSPA 1A		208,8	1,59
HS71L_HUMAN	Heat shock 70 kDa protein 1-like HSPA 1L		203,1	1,23
HSP7C_HUMAN	Heat shock cognate 71 kDa protein HSPA8		190,2	1,18
HSPB1_HUMAN	Heat shock protein beta-1 HSPB1		85,5	1,14
GPC5B_HUMAN	G-protein coupled receptor family C group 5 member B /membrane integrated		145,5	0,99
GPC5C_HUMAN	G-protein coupled receptor family C group 5 member C		675	0,67
GNAI3_HUMAN	Guanine nucleotide-binding protein G(k) subunit alpha		240,5	1,12
GNAI2_HUMAN	Guanine nucleotide-binding protein G(i) subunit alpha-2		236,7	1,46
GNAS2_HUMAN	Guanine nucleotide-binding protein G(s) subunit alpha isoforms short GNAS		116,8	1,01
GBB2_HUMAN	Guanine nucleotide-binding protein G(l)/G(S)/G(T) subunit beta-2		137,8	1,21
MUC1_HUMAN	Mucin-1	NO	198,9	1,00
BROX_HUMAN	BRO1 domain-containing protein BROX		323,3	0,97
TS101_HUMAN	Tumor susceptibility gene 101 protein TSG101		131,9	1,04
G3P_HUMAN	Glyceraldehyde-3-phosphate dehydrogenase GAPDH		363,3	0,94
ACTB_HUMAN	Actin, cytoplasmic 1 ACTB		970	1,04
TBA1A_HUMAN	Tubulin alpha-1A chain TUBA1A		233,4	1,14
TBB2C_HUMAN	Tubulin beta-2C chain TUBB2C		111,9	1,00

Tab. 4b

Exosome associated proteins

Exosome (as soc.)			Score	m
A2GL_HUMAN	Leucine-rich alpha-2-glycoprotein LRG1	N,O	1101,6	8,67
FETUA_HUMAN	Alpha-2-HS-glycoprotein AHSG	N	779,4	7,69
PGBM_HUMAN	Basement membrane-specific heparan sulfate proteoglycan core protein HSPG2	N	1615,6	6,39
VASN_HUMAN	Vasorin / membrane protein	N	561,1	4,29
ACE2_HUMAN	Angiotensin-converting enzyme 2 / secreted + single-pass type I membrane protein	N	124,5	3,18
UFO_HUMAN	Tyrosine-protein kinase receptor UFO AXL / Single-pass type I membrane protein	N	168,3	3,16
LRC15_HUMAN	Leucine-rich repeat-containing protein 15 / Single-pass type I membrane protein	N	180,7	2,72
TRFE_HUMAN	Serotransferrin TF	N	960,1	2,71
ZA2G_HUMAN	Zinc-alpha-2-glycoprotein / MHC I	N	260,7	2,53
PPAP_HUMAN	Prostatic acid phosphatase / integral membrane / interact Flot1	N	254	2,52
AMPN_HUMAN	Aminopeptidase N / single pass membrane bound	N,O	625,6	2,46
UROM_HUMAN	Uromodulin UMOD	N	1237,5	2,41
MXRA8_HUMAN	Matrix-remodeling-associated protein 8 / integral membrane protein	N	645	2,38
MGA_HUMAN	Maltase-glucoamylase, intestinal / apical cell membrane	N,O	334,4	2,28
CSPG4_HUMAN	Chondroitin sulfate proteoglycan 4 / Single-pass type I membrane protein	N	145,7	2,47
MEGF8_HUMAN	Multiple epidermal growth factor-like domains protein 8 / Single-pass type I membrane protein	N	110,5	2,47
CUBN_HUMAN	Cubilin CUBN	N	2831,2	1,80
CLUS_HUMAN	Clusterin CLU		376,8	1,55
LRP2_HUMAN	Low-density lipoprotein receptor-related protein 2 / cubilin interactor	N	1986,1	1,32
S12A3_HUMAN	Solute carrier family 12 member 3 SLC12A3 / Multi-pass membrane protein		223,8	1,47
S12A1_HUMAN	Solute carrier family 12 member 1 / integral membrane		298,8	0,82
EZRI_HUMAN	Ezrin EZR		614,4	1,14
UPK1A_HUMAN	Uroplakin-1a UPK1A / Multi-pass membrane protein / urothelial cells / tetraspanin 21		85,2	1,20
EHD1_HUMAN	EH domain-containing protein 1 EHD1 / endocytic membrane fusion and membrane trafficking		118,5	1,13
NHRF3_HUMAN	Na(+)/H(+) exchange regulatory cofactor / Membrane / kidney (brush border of proximal tubule)		95,5	0,83
SDCB1_HUMAN	Syntenin-1		365,8	0,64



Tab. 4c

Disease associated proteins

Disease Proteins					
IGHG4_HUMAN	Ig gamma-4 chain C region	N	797,8	8,81	kidney injury / inflammation
IGHG2_HUMAN	Ig gamma-2 chain C region	N	1381,4	6,35	kidney injury / inflammation
IGHG1_HUMAN	Ig gamma-1 chain C region	N	1702,7	5,24	kidney injury / inflammation
IGHG3_HUMAN	Ig gamma-3 chain C region	N	925,6	3,71	kidney injury / inflammation
LA C3_HUMAN	Ig lambda-3 chain C regions IGLC3	N	659	5,52	kidney injury / inflammation
IGHA1_HUMAN	Ig alpha-1 chain C region	N	935,2	3,27	kidney injury / inflammation
LV403_HUMAN	Ig lambda chain V-IV region HII	N	61,5	3,45	kidney injury / inflammation
LV106_HUMAN	Ig lambda chain V-I region WAH	N	115,2	2,07	kidney injury / inflammation
LV105_HUMAN	Ig lambda chain V-I region NBWM		108,2		kidney injury / inflammation
IGKC_HUMAN	Ig kappa chain C region IGKC	N	924,2	5,85	kidney injury / inflammation
KV204_HUMAN	Ig kappa chain V-II region TEW	N	165,2	3,44	kidney injury / inflammation
KV402_HUMAN	Ig kappa chain V-IV region Len	N	83,5	2,53	kidney injury / inflammation
KV305_HUMAN	Ig kappa chain V-III region WOL	N	90,2	2,51	kidney injury / inflammation
KV105_HUMAN	Ig kappa chain V-I region DEE	N	131,8	2,81	kidney injury / inflammation
IGHA2_HUMAN	Ig alpha-2 chain C region IGH2	N	728	2,07	kidney injury / inflammation
HV307_HUMAN	Ig heavy chain V-III region CAM		162,8	1,81	kidney injury / inflammation
HV320_HUMAN	Ig heavy chain V-III region GAL	N	123,5	4,80	kidney injury / inflammation
HV305_HUMAN	Ig heavy chain V-III region BRO	N	202,3	2,43	kidney injury / inflammation
HV304_HUMAN	Ig heavy chain V-III region TIL	N	129,9	2,48	kidney injury / inflammation
HV311_HUMAN	Ig heavy chain V-III region KOL		104,4		kidney injury / inflammation
AMYP_HUMAN	Pancreatic alpha-amylase AMY2A	N	1524,8	14,40	amyloidosis?
AMY2B_HUMAN	Alpha-amylase 2B		1483,5	6,16	amyloidosis?
AMY1_HUMAN	Alpha-amylase 1	N	1559,1	5,68	amyloidosis?
A2GL_HUMAN	Leucine-rich alpha-2-glycoprotein LRG1	N,O	1101,6	8,67	thin basement membrane nephropathy
FETUA_HUMAN	Alpha-2-HS-glycoprotein AHSG	N,O	779,4	7,69	kidney injury
PTGDS_HUMAN	Prostaglandin-H2 D-isomerase	N	744,8	6,99	indicator of renal damage !!!
PGBM_HUMAN	Perlecan / Basement membrane-specific heparan sulfate proteoglycan core protein HSPG2 /	N,O	1615,6	6,39	has been found in the urine of patients with en
AMBP_HUMAN	Protein AMBP / complexes with IgA and albumin	N,O	637,2	5,96	
ALBU_HUMAN	Serum albumin ALB		1795,7	4,79	
CD14_HUMAN	Monocyte differentiation antigen CD14 / GPI-anchor	N,O	992,4	4,43	inflammatory response
ARSA_HUMAN	Arylsulfatase A / Lysosome	N	759,8	3,51	diffuse loss of myelin in the central nervous s
FIBA_HUMAN	Fibrinogen alpha chain FGA	N	216	3,35	renal amyloidosis resulting in nephrotic synd
ANGT_HUMAN	Angiotensinogen AGT	N	181,2	3,23	Cause of renal tubular dysgenesis / persist
ROBO4_HUMAN	Roundabout homolog 4 / immunoglobulin superfamily / (membrane + secreted)	N	431	3,06	involved in angiogenesis

Tab. 4d

ECM / Basement membrane assembly

ECM Basement membrane assembly				
PGBM_HUMAN	Perlecan / Basement membrane-specific heparan sulfate proteoglycan core protein HSPG2 / membr	N,O	1615,6	6,39
NID1_HUMAN	Nidogen-1	N,O	250,8	3,73
CILP2_HUMAN	Cartilage intermediate layer protein 2	N	824,1	3,51
QPCT_HUMAN	Glutaminy-peptide cyclotransferase	N	788,2	3,49
AGRIN_HUMAN	Agrin AGRN / laminin binding	N	171	3,23
CSPG4_HUMAN	Chondroitin sulfate proteoglycan 4 / Single-pass type I membrane protein / ECM binding	N	145,7	2,47
HMCN1_HUMAN	Hemicentin-1 HMCN1	N	327,6	2,43
COFA1_HUMAN	Collagen alpha-1(XV) chain COL15A1	N	356,7	2,20
CO6A1_HUMAN	Collagen alpha-1(VI) chain COL6A1	N	650,5	2,28
CO4A2_HUMAN	Collagen alpha-2(IV) chain COL4A2		157,8	1,89
CO6A3_HUMAN	Collagen alpha-3(VI) chain COL6A3		134,8	1,97
PGS1_HUMAN	Biglycan BGN / bone cartilage	N	84,7	2,04
COMP_HUMAN	Cartilage oligomeric matrix protein COMP		90,3	1,94
FBLN3_HUMAN	EGF-containing fibulin-like extracellular matrix protein 1 EFEMP1		260,4	1,57
FBLN4_HUMAN	EGF-containing fibulin-like extracellular matrix protein 2 EFEMP2		85,7	1,44
PGK1_HUMAN	Phosphoglycerate kinase 1 PGK1		250,8	1,48
FINC_HUMAN	Fibronectin FN1 / interacts with COMP	N,O	135,2	1,39
PVRL4_HUMAN	Poliovirus receptor-related protein 4 PVRL4	(N)	99,6	1,33
TSP1_HUMAN	Thrombospondin-1 / binds laminin, collagen and integrins	N,O	99,7	1,21
B4GT1_HUMAN	Beta-1,4-galactosyltransferase 1 B4GALT1		251,2	1,13

Tab. 4e

Multivesicular body proteins

MVB				
LMAN2_HUMAN	Vesicular integral-membrane protein VIP36		412.4	1.94
IST1_HUMAN	IST1 homolog / ESCRT associated		249.8	1.23
TS101_HUMAN	Tumor susceptibility gene 101 protein TSG101		131.9	1.04
VP37D_HUMAN	Vacuolar protein sorting-associated protein 37D		143.8	1.09
VTA1_HUMAN	Vacuolar protein sorting-associated protein VTA1		414.5	1.04
VPS28_HUMAN	Vacuolar protein sorting-associated protein 28		161.2	0.96
VPS4B_HUMAN	Vacuolar protein sorting-associated protein 4B		470.5	0.95
VPS4A_HUMAN	Vacuolar protein sorting-associated protein 4A		430.7	0.87
PDC6I_HUMAN	Alix / Programmed cell death 6-interacting protein PDC6IP / interact TSG101		880.5	0.89
CHM4B_HUMAN	Charged multivesicular body protein 4b		134.1	0.74
CHMP3_HUMAN	Charged multivesicular body protein 3 VPS24		80.1	0.68
CHM1B_HUMAN	Charged multivesicular body protein 1b		231.1	0.50
CHMP5_HUMAN	Charged multivesicular body protein 5		515.8	0.45

Tab. 4f

Lysosomal proteins

Lysosome				
ARSA_HUMAN	Arylsulfatase A	N	759.8	3.51
A1AT_HUMAN	Alpha-1-antitrypsin SERPINA1	N	563.6	2.73
LYAG_HUMAN	Lysosomal alpha-glucosidase GAA	N	859.5	2.59
CATD_HUMAN	Cathepsin D CTSD	N	391.7	2.56
ANAG_HUMAN	Alpha-N-acetylglucosaminidase NAGLU	N	792.7	2.65
PPAL_HUMAN	Lysosomal acid phosphatase ACP2	N	175.9	2.60
PPAP_HUMAN	Prostatic acid phosphatase / integral membrane / ineract Flot1	N	254	2.52
GNS_HUMAN	N-acetylglucosamine-6-sulfatase	N	129.3	2.14
CUBN_HUMAN	Cubilin	N	2831.2	1.80
LRP2_HUMAN	Low-density lipoprotein receptor-related protein 2 / cubilin interactor	N	1986.1	1.32
CPVL_HUMAN	Probable serine carboxypeptidase CPVL / May be involved in the digestion of phagocytosed particles in the lysosome	N	142.8	1.17
TPP1_HUMAN	Tripeptidyl-peptidase 1		267.4	1.94
BGAL_HUMAN	Beta-galactosidase GLB1		419.2	1.17
HYAL1_HUMAN	Hyaluronidase-1		128.5	1.61
CLUS_HUMAN	Clusterin CLU		376.8	1.55
MOES_HUMAN	Moesin		398.4	1.39
PPGB_HUMAN	Lysosomal protective protein CTSA		167	1.00
PROX6_HUMAN	Peroxisredoxin-6 / Lysosome / Lipid degradation		113.7	1.20

Tab. 4g

Non classified proteins

inspecific context				
CAD11_HUMAN	Cadherin-11 / Single-pass type I membrane protein / tissue mainly brain	N	81.7	6.16
PEPA_HUMAN	Pepsin A PGA3		213.8	5.47
ITIH4_HUMAN	Inter-alpha-trypsin inhibitor heavy chain H4	N	1098.5	5.08
AACT_HUMAN	Alpha-1-antichymotrypsin SERPINA3	N	244.8	4.74
DNAS1_HUMAN	Deoxyribonuclease-1 DNASE1	N	280.9	4.09
APOD_HUMAN	Apolipoprotein D	N	438.5	4.00
THBG_HUMAN	Thyroxine-binding globulin SERPINA7	N	164.6	3.88
PGRP1_HUMAN	Peptidoglycan recognition protein 1 / bacteriostatic activity	N	290.8	3.25
CEL_HUMAN	Bile salt-activated lipase CEL / O-linked (mucin type)	N,O	159.5	3.11
NTF2_HUMAN	Nuclear transport factor 2		312.6	2.90
SCTM1_HUMAN	Secreted and transmembrane protein 1	N	85.6	2.67
6PGL_HUMAN	6-phosphogluconolactonase PGLS		477.7	2.66
ANGL2_HUMAN	Angiotensin-related protein 2 ANGPTL2		372.6	2.50
CO4B_HUMAN	Complement C4-B	N	522.6	2.48
CERU_HUMAN	Ceruloplasmin CP	N	859	2.41
IBP2_HUMAN	Insulin-like growth factor-binding protein 2 IGFBP2	O	120.3	2.32
IC1_HUMAN	Plasma protease C1 inhibitor SERPING1	N,O	436.6	2.25
VTDB_HUMAN	Vitamin D-binding protein GC / associates with membrane-bound immunoglobulin / complexes with Megalin- Cubilin-Komplex -protein	N	203.2	2.23
HEMO_HUMAN	Hemopexin HPX	N,O	296.9	2.16
DDAH2_HUMAN	N(G),N(G)-dimethylarginine dimethylaminohydrolase 2		143.6	2.16
ABHEB_HUMAN	Abhydrolase domain-containing protein 14B		134.7	2.16
EGF_HUMAN	Pro-epidermal growth factor EGF	N	2104.5	2.04
HPT_HUMAN	Haptoglobin HP	N	142.5	2.07
RET4_HUMAN	Retinol-binding protein 4 RBP4 /complexes with Megalin- Cubilin-Komplex -proteinreabsorption?		223.5	2.06
C1RL_HUMAN	Complement C1r subcomponent-like protein	N	89.8	2.02
NAPSA_HUMAN	Napsin-A	N	128.1	1.95
CP089_HUMAN	UPF0764 protein C16orf89 C16orf89		85.9	1.76
KNG1_HUMAN	Kininogen-1	N	827.5	1.74
ESL2_HUMAN	Epidermal growth factor receptor kinase substrate 8-like protein 2 EPSL2		133.4	1.61

12. Kurzzusammenfassung

Die klassische Galaktosämie wird durch eine defiziente Transferase verursacht, die Glaktose-1-phosphat-Uridyltransferase (GALT). Ursache dieser Defizienz ist eine genetisch vererbte Mutation, die einen Aminosäureaustausch am aktiven Zentrum des Enzyms bewirkt. Die Wechselrate des Enzyms wird hierdurch um mehr als das Tausendfache reduziert. Exogene Galaktoseaufnahme insbesondere aus Milchprodukten induziert eine intrazelluläre Stressantwort. Das Co-Substrat der GALT, Galaktose-1-phosphat akkumuliert in der Zelle, beeinträchtigt den Zuckerstoffwechsel und wahrscheinlich den Leloir-Galaktosestoffwechsel. Der Leloir-Galaktosestoffwechsel stellt UDP-Galaktose und UDP-Glukose für die Glykosylierung von Proteinen und Lipiden bereit. Die UDP-Galaktose wird beispielsweise für die Synthese von N-Glykoproteinen des *Complex*-Typs benötigt. Es wurde angenommen, dass wenn der Leloir-Galaktosestoffwechsel beeinträchtigt ist, dies auch in der Galaktosylierung der *Complex*-Typ Glykane wiederzufinden sein wird. Um diese Veränderungen in Glykosylierungsmustern wiederzufinden, erwies sich die massenspektrometrische Glykananalyse als besonders aussagekräftig. Mithilfe des enzymatischen Verdaus durch PNGaseF konnten die N-Glykane von den Glykoproteinen abgelöst werden und anschließend, nach erfolgter Methylierung, unter Anwendung von *Matrix Assisted Laser Desorption/Ionization* Massenspektrometrie, vermessen werden. Um Veränderungen der Glykosylierungsmuster zu detektieren haben wir Vesikel aus dem Urin von Galaktosemiepatienten isoliert und die N-Glykosylierung der hier lokalisierten Glykoproteine mit denen von gesunden Kontrollpersonen verglichen. Wir konnten zeigen, dass es sich bei den Vesikeln zum größten Teil um Exosomen handelt. Der Vergleich der Massenspektren ergab einen dramatischen N-Glykosylierungsshift von dem in gesunden Personen vorherrschenden *High-mannose*-Typ zum *Complex*-Typ. Der angenäherte Wert des Verhältnisses von *High-mannose*-Typ zu *Complex*-Typ Glykanen bei gesunden Kontrollpersonen betrug 3:1. Insbesondere die N-Glykane, bestehend aus fünf oder sechs Mannosen, waren in auffällig erhöhter Menge zu finden. Im Gegensatz hierzu veränderte sich die Mengenverteilung bei Galaktosämiepatienten in Richtung 1:1 zum *Complex*-Typ. Die meist vorhandene Struktur, die bei Galaktosämiepatienten auf Exovesikeln zu finden war, entsprach einem *Complex*-Typ Glykan mit einer bi-antennaren Struktur, die endständig disialyliert war und keine Kern-Fukose trug. Glykane, die eine höhere Verzweigung aufwiesen, konnten nur in sehr geringen Mengen detektiert werden. Der beobachtete

Glykosylierungsschift ist als neuer Befund einzuordnen, denn bislang konnte eine veränderte Glykosylierung nur unter akutem Stress bei sekretierten Proteinen wie dem Transferrin festgestellt werden. Wenn diese Veränderung wie gezeigt membranäre Proteine betrifft, ist anzunehmen, dass auch glykosylierte Rezeptoren von diesem Ereignis betroffen sind. Veränderungen der Glykosylierungen können für eine Mislokalisierung von Glykoproteinen verantwortlich sein, insbesondere könnte dies zutreffen für Glyko-Rezeptoren, wie dem EGFR (epidermal growth factor receptor), der üblicherweise auf der apikalen Seite von epithelialen Zellen exponiert wird.

Quantitative und qualitative Veränderungen membrangebundener exosomaler Glykoproteine geben indirekt Auskunft über die Veränderungen auf der zellulären Membran. Wir konnten in Westernblots zeigen, dass die erhöhte Menge an EGFR, die in exosomale *lipid rafts* sortiert wird, korreliert, mit einer reduzierten Menge an EGFR in den plasmamembranären *lipid rafts*. Um die Veränderungen des Glykoproteoms insbesondere von Glykorezeptoren in exosomalen *lipid rafts* festzustellen, war eine Quantifizierung durch *Labeling* mit isobarischen Tags zur relativen und absoluten Quantifizierung (iTRAQ) sehr nützlich. Vier einzelne Proben von vier Individuen wurden hierzu ausgewählt: Zwei Proben von Galaktosämiepatienten und zwei gesunde Kontrollpersonen. Die beiden Proben der Galaktosämiepatienten zeigten den typischen Glykosylierungsschift von *High-mannose* zum *Complex*-Typ der vorangegangenen Studie. Die Proben wurden mit den isobaren Tags versehen, danach vereinigt und anschließend über nano-LC MALDI-MS/MS analysiert. Obwohl kein EGFR gefunden werden konnte, wurden erhöhte Mengen an N-Glykoproteinen und einigen Rezeptoren gefunden, die exosomenassoziiert vorlagen: Der Tyrosin-Proteinkinase-Rezeptor UFO, zink-alpha-2-glycoprotein (ZA2G, MHC I-Familie) und Aminopeptidase N (CD13) sind hier zu nennen. Der Cubilin- und Megalin-Rezeptor wurden detektiert. Beide dimerisieren und formen einen Megalin-Cubilin-Komplex der für die Rückresorption von Proteinen aus dem proximalen Tubulus der Nephridien zuständig ist. Dieser Cubilinrezeptor wurde bereits in einem vorangegangenen Experiment als auffälligster Unterschied zwischen Proben von Galaktosämiepatienten und Kontrollpersonen festgestellt. Letztendlich wurde ein weiteres unerwartetes Ergebnis mittels iTRAQ-Methode ausgemacht. Die Proben der Galaktosämiepatienten enthalten stark angereicherte Mengen an Serumproteinen, besonders N-glykosylierte Serumproteine. Eine Vielzahl an Immunglobulinen waren erhöht, desweiteren Albumin, Fetuin, Transferrin und viele mehr. Zusammengenommen weisen diese Ergebnisse auf das Krankheitsbild einer Niereninsuffizienz bei Galaktosämie hin.

Die übliche Methode um diesen Befund festzustellen war in der Vergangenheit die Organbiopsie. Die Untersuchung urinärer Exosomen, könnte in diesem Kontext eine innovative Methode darstellen, um ohne körperlichen Eingriff Nierenversagen feststellen zu können.

13. Erklärung

Ich versichere, dass ich die von mir vorgelegte Dissertation selbständig angefertigt, die benutzten Quellen und Hilfsmittel vollständig angegeben und die Stellen der Arbeit -einschließlich Tabellen und Abbildungen -, die anderen Werke im Wortlaut oder dem Sinn nach entnommen sind, in jedem Einzelfall als Entlehnung kenntlich gemacht habe; dass diese Dissertation noch keiner anderen Fakultät oder Universität zur Prüfung vorgelegen hat; dass sie noch nicht veröffentlicht ist, sowie, dass ich eine Veröffentlichung vor Abschluss des Promotionsverfahrens nicht vornehmen werde. Die Bestimmungen dieser Promotionsordnung sind mir bekannt. Die von mir vorgelegte Dissertation ist von Herrn Prof. Dr. Franz-Georg Hanisch betreut worden.

Simon Staubach